Progressive deformation in monocline, San Rafael Swell, Utah

Tonje Nygaard Sørensen

Master Thesis in Geosciences
Structural Geology and Tectonics
60 Credits

Department of Geosciences
Faculty of Mathematics and Natural Sciences

UNIVERSITY OF OSLO

June 2017

Progressive deformation in monocline, San Rafael Swell, Utah

Tonje Nygaard Sørensen

Master Thesis in Geosciences
Structural Geology and Tectonics
60 Credits

Department of Geosciences
Faculty of Mathematics and Natural Sciences

UNIVERSITY OF OSLO

June 2017

Supervisors: Alvar Braathen and Elin Skurtveit

This work is published digitally through DUO – Digitale Utgivelser ved UiO

http://www.duo.uio.no

It is also catalogued in BIBSYS (http://www.bibsys.no/english)

Acknowledgments

I really want to thank Alvar Braathen and Elin Skurtveit so much for all help during my mater thesis.

And to my family… Thank You!

Abstract

The San Rafael Swell, located in Central Utah, USA, is a regional N-S striking Laramide-style monocline, which likely formed during the latest Cretaceous to Eocene. This structure consists of an east-dipping limb with a dip of about 70-80 degrees.

This study is expanding on work by Zuluaga et al. (2014) on deformation bands and fractures developed during progressive folding of the Navajo Formation sandstones. The Navajo Formation is made up of several hundred meters of highly porous eolian sandstone now situated in the San Rafael Swell. Easily accessible outcrops in Mine Canyon allowed deformational structures to be studied in detail.

Field observations focused on deformation band populations where six populations were reported. The main observations in this study was conjugated sets of deformation bands, bands hosting en-echelon fractures consistent with N-S extension, band swarms progressing into shear fractures and dilation bands with patches of shear-fracture development. Samples were collected to look at microtextural structures in thin-sections.

Table of contents

1. Introduction

The San Rafael Swell is located in Central Utah, USA (Fig. 2.1). This regional N-S structure reflects a kilometer amplitude Laramide-style monocline, which likely formed during the latest Cretaceous to Eocene. The steep part of the east-dipping limb has a dip of about 70-80 degrees, with a gradually more open structure seen both north and southwards, reflecting N and S plunging fold axis, respectively. The monocline is situated east of the Wasatch fault system and south of the Book Cliffs, near and on the western side of the small town named Green River.

The main aim of this study is to describe deformation bands and fractures developed during progressive folding in the monocline of the San Rafael Swell. The Navajo Formation sandstones are the targeted lithology. This detailed analysis is expanding on the more regional work by Zuluaga et al. (2014).

The Navajo Formation is described as several hundred meters of highly porous sandstone, deposited as aeolian sand dunes during the Jurassic. Following subsidence in the Cretaceous and Paleogene formations of the San Rafael Swell caused uplift and erosion in Miocene time, resulting in unroofing and today's outstanding exposures in Mine Canyon. This deep, narrow canyon across the ca 70 degree east-dipping forelimb of the San Rafael Swell is the setting for this detailed study of deformation structures.

The Navajo Sandstones consists of a complex system of deformation bands throughout the formation. This system was divided into six populations based on consistent orientations, common deformation mechanisms, and cross-cutting relationships. There was established a chronology based on observations during fieldwork, photographic- and microtextural analyses, where population 1 is the oldest and population 6 the youngest. Some of these populations show a chronological overlap suggesting conjugated sets of deformation bands.

This study will test three hypotheses:

1. Deformation band sets developed with a given angle to dip of bedding during progressive folding, reflecting fixed stress axes (model of Zuluaga et al., 2014).
2. Conjugate deformation band sets reflect overall horizontal shortening, rather than events of accommodation structures caused by space problems.
3. Deformation band swarms transgressed into slip-surface with accumulated slip within a fixed kinematic system.

2. Regional geology

This chapter is divided into the general geology of Utah and a more specific description of the San Rafael Swell area. The geological evolution of Utah (Fig. 2.1) is long and complex; this summary focuses on the most important events along with geologic features seen throughout the State today.

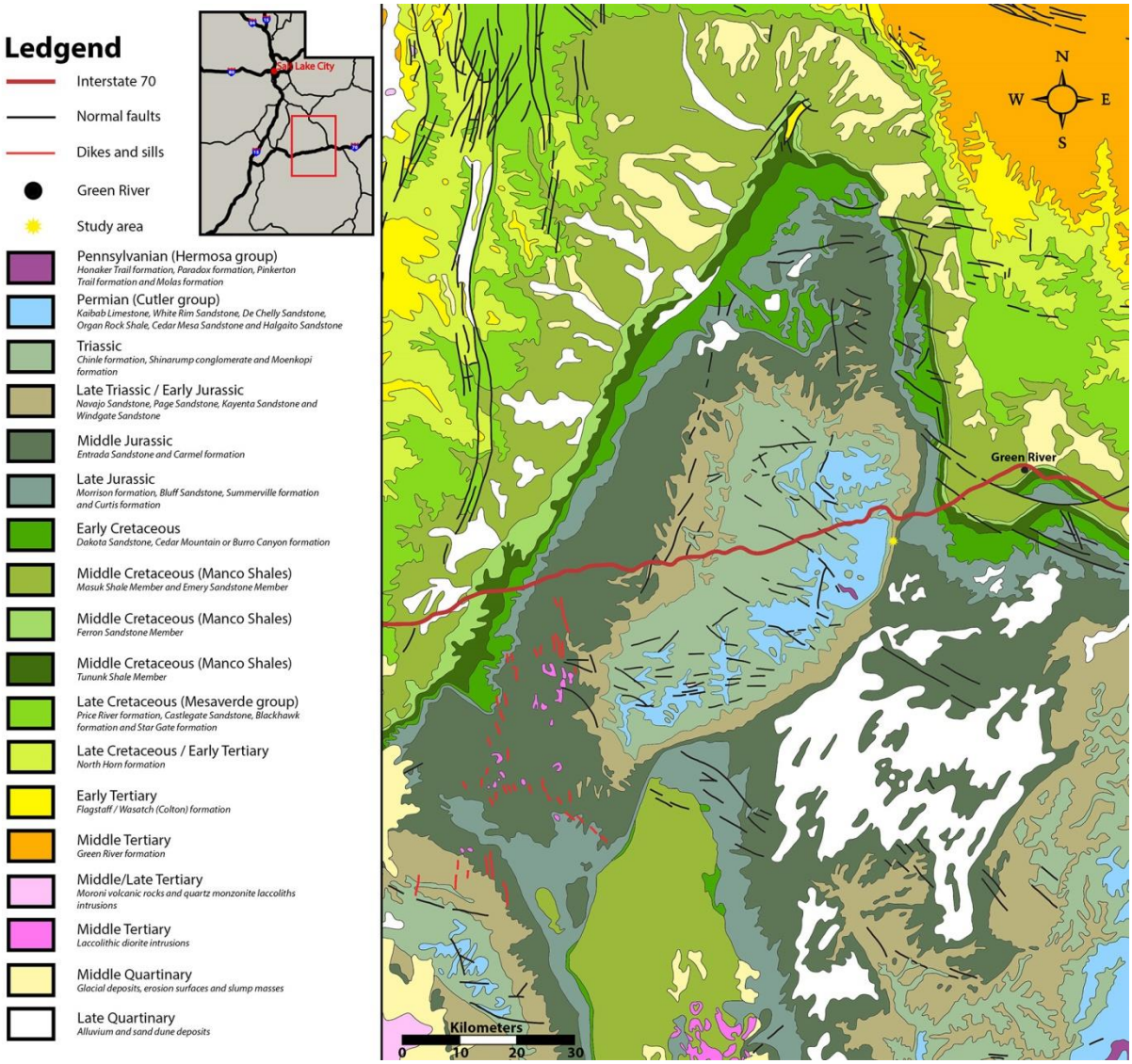

Fig. 2.1: *Bedrock map of the San Rafael Swell region in Central Utah, USA. Map is based on Utah Geologic Highway Map. (Hintze, 1997)*

2.1 Geology of Utah

2.1.1 Cambrian to Devonian (541 – 359 Ma)

In this period, Utah was mostly covered by a large and shallow epicontinental sea that experienced transgressions and regressions over large distances due to the peneplainal conditions of Laurentia at this time (Williams *et al.*, 2014). During Cambrian and Ordovician, Utah was relatively tectonically stable; however, in the Silurian the subduction-related Antler Volcanic Arc began to form west of Utah. The Antler Volcanic Arc was accreted on to the continent in the Devonian in the Antler Orogeny, which caused a western clastic source to sediments deposited in Utah (Williams *et al.*, 2014).

2.1.2 Carboniferous (359 – 299 Ma)

The Oquirrh basin slowly subsided in the beginning of the Mississippian period in the northwestern part of Utah (Williams *et al.*, 2014). This new accumulation space was then filled with volcanic ash and clastic sediments from the Antler Orogeny. In this period Euramerica (Laurentia and Baltica) collided with Gondwana to create the supercontinent Pangea. In Southeastern Utah the Paradox basin subsided at the same time as uplift of the Uncompahgre Mountains in western Colorado took place. The Paradox basin became a sink that was partly filled with sediments from Uncompahgre. However, alternating evaporates and black mud was also deposited due to sea level fluctuations caused mainly by global glacial events.

2.1.3 Permian (299 – 252 Ma)

The Oquirrh and Paradox basins continued to subside and fill throughout the Permian. In the Paradox basin, very restricted conditions caused deposition of salt partly interfingering with sediments from Uncompahgre (Williams *et al.*, 2014). Different and changing sedimentary environments prevailed from frequent sea level fluctuations (shallow-water-, deep-water- and shoreline sediments). For instance, the White Rim Sandstones is interpreted as the upper member of the Cutler Group and was deposited as windblown dunes. These dunes were situated in a coastal dune field which was periodically flooded by sea water.

The Kaibab Sea covered the entirety of San Rafael Swell (Condon, 1997) later in Early Permian (approximately 250 Ma) and the Kaibab Limestones were deposited, this in a shallow marine shelf environment. The Kaibab Limestones are interpreted as a representation

of the Kaibab Seas maximum eastward transgression (Condon, 1997, sed.utah.edu/Kaibab.htm). The Kaibab Sea started to withdraw in Middle Permian and the Uncompahgre Mountains were pretty much worn down by the end of the Permian period, and are from now on referred to as Uncompahgre highlands (Williams *et al*., 2014, sed.utah.edu/WhiteRim.htm, Condon, 1997).

2.1.4 Triassic (252 – 201 Ma)

In the Early Triassic, Utah belonged to the coastal plain to marginal marine environment of Pangea (Williams *et al*., 2014). The Moenkopi Formation where deposited in the southern part of the state in a tidal environment (sed.utah.edu/Moenkopi.htm). Following erosion, the following Chinle Formation is non-marine, and consists of fluvial sandstones and floodplain deposits interfingering with paleosols, marsh deposits, and small lake deposits (Williams *et al*., 2014, sed.utah.edu/Chinle.htm). The supercontinent Pangea was gradually divided into Laurentia north of equator and Gondwana south of equator during the Triassic period (Williams *et al*., 2014), and Utah was located at about 15ºN at this time (sed.utah.edu/Chinle.htm).

2.1.5 Jurassic (201 – 145 Ma)

Utah experienced an arid climate in the Early Jurassic, when a huge desert, like today's Sahara, covered most of the western part of the state (sed.utah.edu/Wingate.htm, sed.utah.edu/Navajo.htm). The Glen Canyon Group, consisting of Wingate, Kayenta and Navajo formations, belongs to the Early Jurassic period (sed.utah.edu/Wingate.htm, sed.utah.edu/Kayenta.htm, sed.utah.edu/Navajo.htm). The Wingate Formation consists of wind-deposited massive sand dunes (Williams *et al*., 2014, sed.utah.edu/Wingate.htm) located at the margin of an erg with a hyper-arid climate during deposition. Wingate is made up of very fine to fine-grained reddish orange sandstone (nps.gov/colm/learn/nature/wingate-sandstone.htm). The Kayenta Formation consists of river-deposits (Williams *et al*., 2014) and has a gradational contacts towards over- and underlying formations (Mathis, 2000). Facies associations are ascribed to seasonal climate variations with rainy summers and dry winters, and with deposition reflecting partly reworking of former aeolian sands (sed.utah.edu/Kayenta.htm).

The climate again became hyper-arid, and an erg returned in Early Jurassic (sed.utah.edu/Navajo.htm, Williams *et al*., 2014). This erg is known as the Navajo sand sea (Kocurek, 2003) with aeolian dunes in eastern Utah deposited in the Navajo Formation today

(Williams *et al*., 2014, Kocurek, 2003). The Navajo Formation and its equivalent formations extend over five states in United States Western Interior (see fig. 18 in Blakey *et al*., 1988), and is known as one of the thickest, best exposed and most widespread aeolian units on Earth (Kocurek, 2003, Allen *et al*., 2000). The Navajo sand sea was in a Ph.D. dissertation (thesis) by J. E. Verlander (1995) divided into a western part with a dry system, and an eastern part consisting of fluvial systems interacting with the margin of the erg (Kocurek, 2003, Allen *et al*., 2000). My thesis deals with the western part of the Navajo sand sea located within current Utah State limits. This part of the Navajo Formation consists of two primary types of deposits, where the first is large massive sand dunes and the second is smaller interdune facies (sed.utah.edu/Navajo.htm). Navajo Formation in the Glen Canyon Group is typically whiteish in color and has a high permeability altered by past fluid flow causing diagenetic bleaching by chemical reduction of iron oxide (sed.utah.edu/Navajo.htm, Beitler *et al*., 2003, Beitler *et al*., 2005). The Navajo Formation is overlain by a small aeolian sandstone package known as the Page Formation. These two formations are separated by the erosional J-2 unconformity (Blakey *et al*., 1988, Mathis, 2000, Allen *et al*., 2000). Page Formation is the lowermost member of the San Rafael Group and has been deposited as a coastal erg system in Middle Jurassic (Mathis, 2000, Blakey *et al*., 1988, Jones and Blakey, 1996). Page Formation found in the study area has been interpreted to be a reworked channelization of Navajo.

The San Rafael Group is made up of the Page, Carmel, Entrada, Curtis, and Summerville formations (Mathis, 2000, Hood and Patterson, 1984). During Middle to Late Jurassic, a long and shallow sea (Sundance Seaway) extended into the western part of Utah from the north. This sea had frequent and short-lived sea level fluctuations causing flooding in the eastern part of Utah (Williams *et al*., 2014). Periodically flooding from the shallow sea caused deposition on the tidal flats in eastern Utah in the Middle to Late Jurassic. This was the foundation of the Carmel Formation, which was deposited on top of the Page Formation during Middle Jurassic. The formation consist of a strata dominated by red-colored siltstone, mudstone and sandstone, alternating with packages of evaporates and limestone in interbedded systems (Mathis, 2000, University of Utah, 2010, Hood and Patterson, 1984, Blakey et al., 1996). The depositional environment of these rocks ranged from fluvial, aeolian and coastal sabkha, to restricted and open marine (Blakey et al., 1996), where these environments was repeated in several cycles throughout deposition.

Sand from dunes near the southeast margin of the shallow sea in the east was deposited as “earthy” facies of the Entrada Formation in eastern Utah during this time period. “Earthy” Entrada is explained as fine-grained massive and aeolian sandstone dunes

interbedded with floodplain and partly tidal flat shaley units (Davis, 1999, Mathis, 2000). Tidal flat as wet aeolian dunes can be ascribed to a high water table caused by sea level fluctuations (Mathis, 2000, University of Utah, 2010, Hood and Patterson, 1984). Entrada is topped by an erosional unconformity, called J3. This unconformity is represented by a non-depositional environment over a period of ca 1 Ma. This is a type 1 sequence boundary. Erosional valleys that cut into the Entrada Formation during J3 were in the lower Curtis Formation filled with tidal channel deposits (Mathis, 2000, University of Utah, 2010). These deposits were almost immediately overlain by marginal marine deposits. The upper part of the Curtis Formation consists of a subtidal to intratidal flat complex (Mathis, 2000). The overlying Summerville Formation reflects a conformable and spatial transition to mainly supratidal deposits (Mathis, 2000, University of Utah, 2010).

2.1.6 Cretaceous (145 – 66 Ma)

During the Cretaceous period the Farallon plate was subducted beneath the North American plate creating the Nevadan-, Sevier-, and Laramide orogenies (Williams et al., 2014). Related uplift was caused by thrusting and folding. During this time the eastern part of Utah was covered by the Western Interior Sea formed primarily as a foredeep basin. It stretched all the way from the Arctic Ocean to the Gulf of Mexico (University of Utah, 2010).

2.1.7 Mesozoic

During the Mesozoic the dip of the subducting slab decreased, with layer subduction coupling causing the sea to retreat and forcing deformation to propagate further inland (Williams et al., 2014). This crustal stress was the reason for block uplifts like the San Rafael Swell. Sediments from the western fold and thrust belt were deposited in the foreland basin, spanning from offshore to prodelta Manco shales (among others) to shallow marine and continental sandstones of the Mesa Verde Group. These sandy sediments are exposed along the Book Cliffs today (University of Utah, 2010).

2.1.8 Faults and deformation

There are two main extensional fault zones in Utah: Wasatch and Moab fault systems. Both of these systems are made of fault segments more or less linked together. The Wasatch fault is still active and is the barrier between the Basin and Range in the west and the Colorado

Plateau in the east. The Moab fault system is located in the southeastern part of Utah, where saltdriven faulting and some anticlinal salt diapirs is seen in the map, like the Salt Wash anticline near Crescent Junction. The Moab fault system has a long evolution but must have been active in the Cretaceous because it truncates rocks in the Book Cliffs. Some of the Moab faults experience fluid mobility, where CO_2 leaks along fractures in some parts of the fault system and surface calcites (travertine) is deposited (Williams et al., 2014, University of Utah, 2010).

2.2 San Rafael Swell

The San Rafael Swell is a Laramide-style anticline often considered a monocline. This section is a short summary of the history behind the San Rafael Swell, which can be explained by looking at Fig. 2.2 below.

Everything started with the Neo-Proterozoic rifting at about 650 Ma, where west-dipping extensional faults originated along with syn-rift deposits (Fig. 2.2a). Sediments filled this accommodation space during Lower Paleozoic with post-rift sediments (Fig. 2.2b). To the east, the Ancestral Rocky Mountain orogeny began to form towards the end of Paleozoic, causing an uplift that the San Rafael Swell has been associated with. This uplift was a gentle shallow marine uplift called the Emery Uplift (Fig. 2.2c), and it limited the influx of sea water at this time. The Emery Uplift was then buried by Mesozoic deposits (Fig. 2.2d) from the inactive Uncompahgre highlands. The lower Jurassic succession is highlighted in Fig. 2.2d. The foreland basin of the Nevadan Orogenic Belt in Mesozoic was located in the east (where the San Rafael Swell now is located). This foreland basin had extremely arid conditions, as seen in Sahara today, which allowed eolian sediments to be deposited in the Lower/middle Jurassic (Fig. 2.2e). Then the San Rafael Swell was uplifted due to the Laramide Orogeny formation (Fig. 2.2f). (Zuluaga et al., 2014).

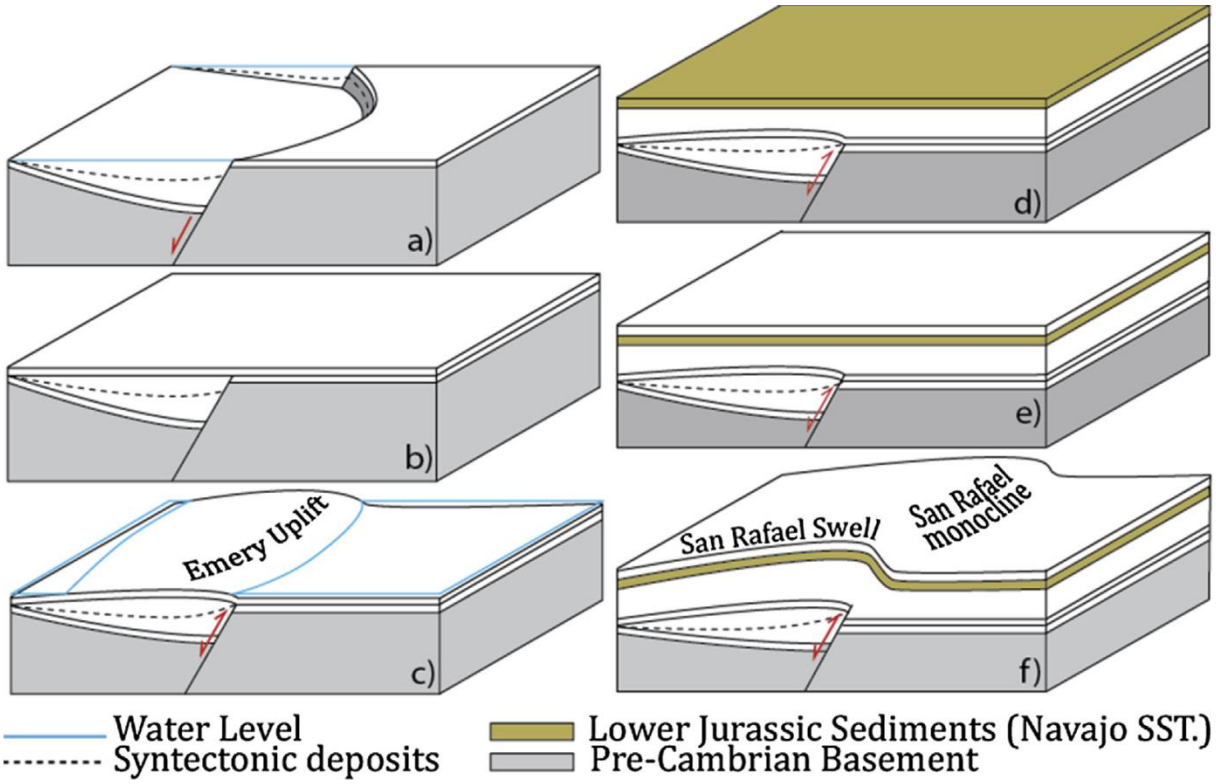

Fig. 2.2: *The tectonic evolution of San Rafael Swell displayed as a block diagram. (a) Precambrian rifting, (b) post-rift sediments from Lower Paleozoic, (c) gentle shallow marine uplift (Emery Uplift), (d) Mesozoic deposits, (e) arid conditions with deposition of eolian units (inkl. Navajo Sandstones), and (f) formation of the San Rafael Swell. Figure is from Zuluaga et al. (2014).*

During the formation of the San Rafael Swell numerous small-scale deformation structures were created, linked to the stress of forced folding and bending. In the Kayenta-, Navajo-, Page-, and Entrada formations, this deformation is seen as deformation bands in porous sandstones, and some smaller thrust faults in the Carmel Formation (Mathis, 2000).

When the San Rafael Swell was folded during the Laramide Orogeny, the whole succession was slowly tilted until what you can see today (layers have an approximately dip of 58 degrees; Fig. 4 in Zuluaga et al., 2014).

3. Terminology, definitions and methods

3.1 Deformation bands and fractures

Brittle structures are the most common deformational structures in the Earth's upper crust. They form in places where the local rupture strength is lower than the maximum stress level the rock can withstand (Fossen, 2010). The type of deformation is largely determined by the amount of pore space available in the stressed rock. Deformation of high-porosity rocks in most cases sediments, in the brittle regimes are often related to formation of deformation bands. Such bands can be divided based on kinematic classifications into dilution bands, compaction bands, and shear bands. By considering deformation mechanisms they classify as disaggregation bands, phyllosilicate bands, cataclastic bands, and solution and cementation bands. Similar deformation in low-porosity rocks is seen as fractures. They divide into extension fractures, shear fractures, and contractional fractures/styloliths (Fossen et al., 2007a).

3.1.1 Deformation bands

Deformation bands have a tabular shape in which strain is localized (Aydin et al., 2006) and are by Fossen et al. (2007a) described as structures formed due to localized strain in rocks and sediments with significant porosity, such as in sandstones. This porosity threshold is approximately 15 percent (Fossen et al., 2007b, Rotevatn et al., 2013, Zuluaga et al., 2014, Fossen and Bale, 2007), herein referred to as high-porosity rocks. This percentage of porosity allows grains to reorganize in the existing pore space. They mainly form in upper-crustal regimes, independent of the tectonism present in the area (Fossen et al., 2007a).

Individual deformation bands can be over 100 meters long, but are seldom wider than about a few millimeters. Some can show shear displacement, this displacement rarely exceeds more than a few millimeters to centimeters (Aydin and Johnson, 1978, Fossen et al., 2007a). Deformation bands can occur as either single bands or clusters/zones of bands (Aydin and Johnson, 1978). Clusters/zones of deformation bands consist of more than one band in the same proximity with overall approximately the same strike and dip. These zones have been recorded to be up to 0.5 meters wide, rarely with a displacement larger than 30 centimeters (Fossen et al., 2007a).

Kinematic classifications

Deformation bands can be divided into different kinematic classifications such as dilation bands, compaction bands, and shear bands (Aydin et al., 2006, Rotevatn et al., 2013). Fig. 3.1 show that deformation bands also form as hybrids of these three types, such as compactional shear bands and dilational shear bands.

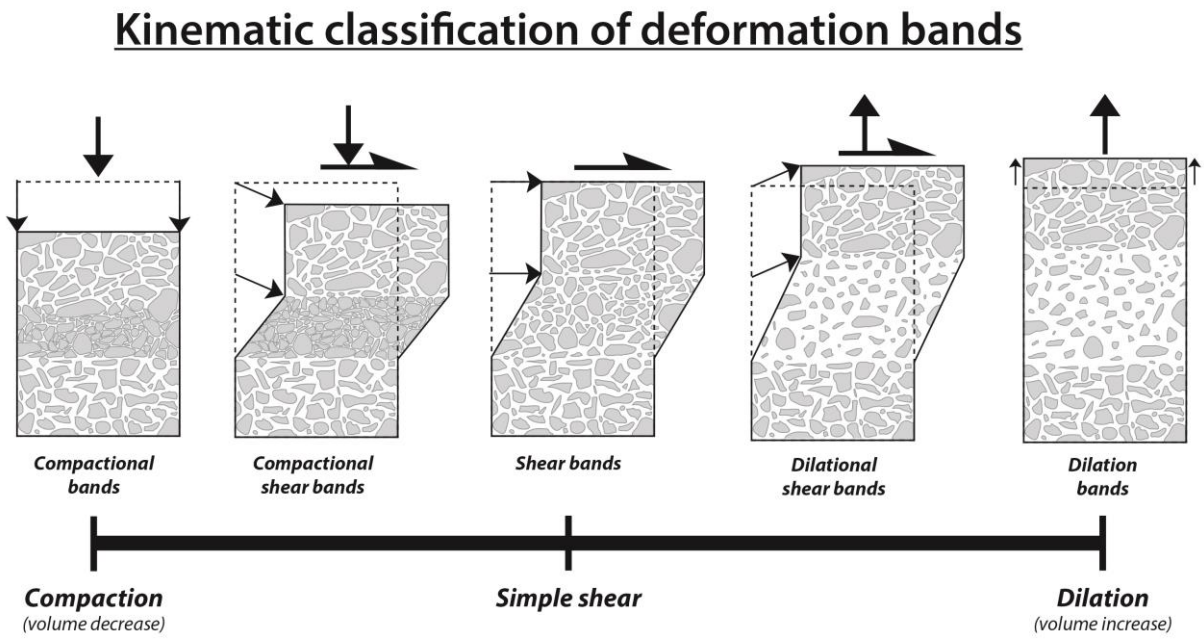

Fig. 3.1: *kinematic classification of deformation bands (modified after Fossen et al., 2007a)*

Dilation bands (Fig. 3.1) have volumetric increase (Du Bernard et al., 2002, Aydin et al., 2006). This increase means that individual bands have a higher porosity compared to the surrounding rock. Dilation bands form perpendicular to the least compressive principal stress direction (σ_3) and in the extensional quadrant of faults. Dilation bands display localized extension where large pores grow from smaller pores due to grain displacement, and pure dilation bands show no shear offset (Du Bernard et al., 2002, Fossen et al., 2007a).

Compaction bands (Fig. 3.1) on the other hand, have volumetric decrease and are described as tabular zones with porosity reduction and no shear offset (Du Bernard et al., 2002, Olsson, 1999). They occur in highly-porous sands and sandstones where the porosity is between 20-30 percent and the grain size is described as fairly coarse; 0.3-0.8 mm (Fossen et al., 2007a, Mollema and Antonellini, 1996). Compaction bands display localized compaction of grains in high-porosity sandstones, where the reduction in pore space and lack of shear offset is not possible to observe neither microscopically nor macroscopically. Mollema and Antonellini (1996) suggested that the formation of these bands is perpendicular to the

maximum compressive principal stress direction (σ_1) and in the compressional quadrant of faults.

The most common deformation bands found in the field are shear bands (Aydin et al., 2006). These bands can again be divided into three different categories (Fig. 3.1); simple shear bands, dilational shear bands, or compactional shear bands. All three of these bands occur in nature, but to different degrees. Simple shear bands, also called isochoric, are bands with shear offset and no to minimal volume change (Aydin et al., 2006). Simple shear bands can rarely be found in the field; most shear bands undergo volumetric changes along with shearing (Aydin et al., 2006, Du Bernard et al., 2002, Fossen et al., 2007a). Also dilational shear bands are described as rare occurrences in both experiments and in the field (Fossen et al. 2007a). Dilational shear bands are explained as a combination of dilation bands and shear bands, where the bands display volumetric increase along with a shear offset. The majority of deformation bands described in literature are the compactional shear bands (Fossen et al., 2007a), which are explained as a combination of compaction bands and shear bands, where the bands display volumetric decrease along with a shear offset. All shear bands usually have a macroscopic shear offset (Aydin et al., 2006) cutting through bedding or older shear bands. Grain fracturing and grain size reduction is very common within shear bands, but are not a necessity for the formation.

Deformational mechanisms

Petrophysical properties such as; mineralogy, grain size, shape, sorting, cementation, porosity and stress state are important to further distinguish between different types of deformation bands. The classifications of deformation bands can also consider the dominant deformational mechanisms. Deformational mechanisms are controlled by internal and external conditions, and can be useful when permeability is important and fluids are present in the rock (Fossen et al., 2007a). Fossen et al. (2007a) describes these dominant mechanisms as; granular flow, cataclasis, phyllosilicate smearing, and dissolution and cementation. This type of classification of deformation bands (Fig. 3.2) is categorized as; disaggregation bands, phyllosilicate bands, cataclastic bands, and solution and cementation bands.

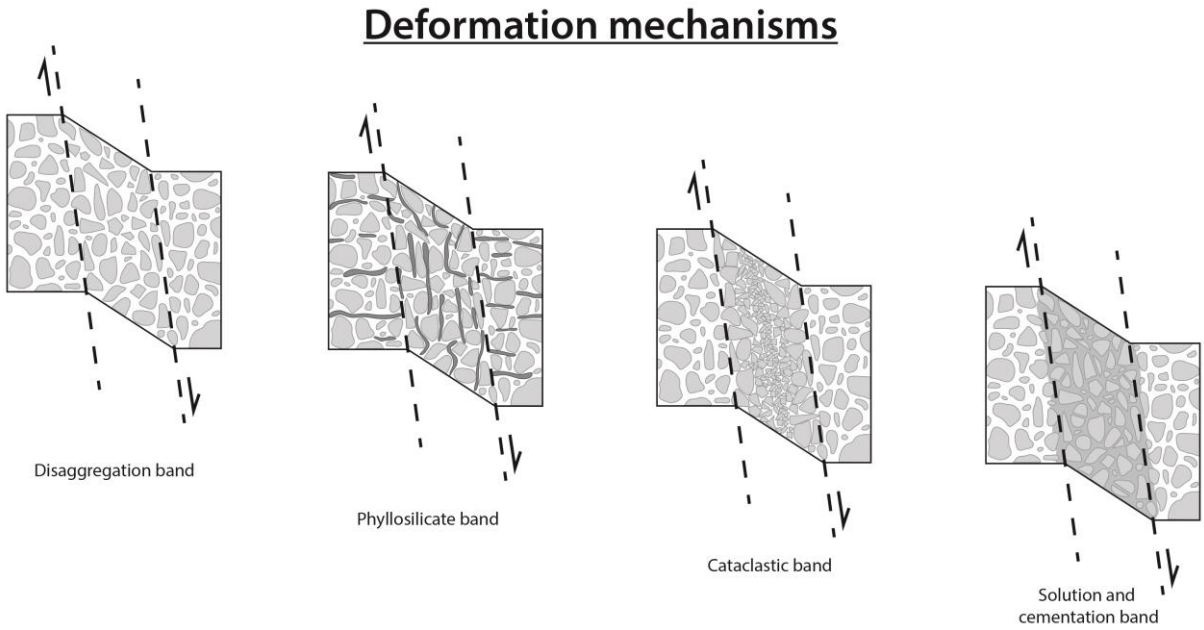

Fig. 3.2: *classification of deformation bands based on deformational mechanisms (modified after Fossen et al., 2007a).*

Disaggregation bands (Fig. 3.2) often form in sands and poorly consolidated sandstones, and are developed by reorganization of grains due to rolling and sliding (Fossen and Bale, 2007, Fossen et al., 2007a). The grains within the band remain intact after the reorganization, which means that the rolling and sliding is due to a non-cataclastic granular flow (Fossen and Bale, 2007). These bands can look almost invisible in sand and sandstones, but becomes distinguishable when they cross and offset other structures, such as the boundary between dunes, bed laminations and pre-existing deformation bands (Fossen, 2010, Fossen et al., 2007a).

Phyllosilicate bands (Fig. 3.2) are considered to be a type of disaggregation band with platy mineral grain sliding. These bands form in sandstones where the amount of platy minerals is above 10-15 percent (Fossen et al., 2007a). Phyllosilicate bands have the largest offset out of all of the different types of deformation bands (Fossen et al., 2007a), and the phyllosilicates in these bands give off a distinct color and/or fabric, making them easy to spot. When the phyllosilicate content of a rock increases, there could be a transition from disaggregation band to a phyllosilicate band.

White colored deformation bands in porous sandstones with grain fracturing and pore collapse are called cataclastic bands (Aydin and Johnson, 1978). The grain fracturing causes a reduction in grain size, a high matrix content, and increased the density within the core of the band. The damage zone of this type of deformation band typically show compaction and mild

fracturing of marginal grains (Aydin and Johnson, 1978, Fossen et al., 2007a). Cataclastic bands (Fig. 3.2) usually have a maximum shear displacement of about 3-4 centimeters, and this is likely reflecting interlocking of the grains, causing strain hardening. Angular grains, absence of pore space, and sharp boundaries between the bands and host rock is really distinct for this type of deformation band (Fossen et al., 2007a, Gibson, 1998).

Solution and cementation bands (Fig. 3.2) are made up of tightly packed grains with little to no cataclasis (Fossen et al., 2007a, Gibson, 1998). The grains in solution bands are usually smaller than the surrounding matrix and have a tendency to align parallel with the direction of the stylolitic seams (Gibson, 1998). Cementation most often occurs in bands with chlorite or illite coating on the grains due to grain crushing and sliding, but can occur during tensile fracturing within the bands. In the latter, minerals such as calcite, anhydrite, salt, hydroxides and quartz may be found within the band (Fossen et al., 2007a).

3.1.2 Fractures

Fractures are low-porosity structures forming in the uppermost few kilometers of Earth's crust (Fossen et al., 2007a). These low-porosity structures usually form where the porosity of the rock is lower than 15 percent (Fossen et al., 2007b, Rotevatn et al., 2013). As mentioned above, fractures belong to the brittle regime and are explained as mechanically weak discontinuities. They have a tendency to reactivate when new stress builds up (Fossen, 2010). Following Pollard and Fletcher (2005, p.371) "Fractures are idealized as two surfaces with mirror image geometry that are in contact in the initial unloaded state and are bounded in extent by a common curve called the tipline".

The Mohr diagram (Fig. 3.3) can be used to describe whether or not a rock is susceptible to fracturing. The strength of a rock depends on the confining pressure the rock is exposed to, but this is not always enough in itself to fracture the rock, the initiation of fracturing needs differential stress that exceeds the rock's strength or cohesion to actually fracture. This confining pressure and differential stress can be explained by using the Mohr diagram and the relationship between normal stress (σ_n) and shear stress (σ_s), and this graphical relationship is called the Mohr-Coulomb fracture criterion. The Mohr-Coulomb fracture criterion is given by this equation (1):

$$\sigma_s = C + \sigma_n \mu \implies \sigma_s = C + \sigma_n tan\phi \qquad \text{Eq. (1)}$$

where C is the cohesive strength of the rock and represents the shear stress for a surface where the normal stress equals to zero, ϕ is the angle of the internal friction, and μ is the coefficient of internal friction. This equation is represented by a straight line (fracture criterion) in the Mohr diagram as shown in Fig. 3.3 as red lines (Allaby, 2013, Fossen, 2010, Schultz, 1996, Underhill and Woodcock, 1987, Labuz and Zang, 2012).

Fractures have a sharp form of deformation localization. They can be divided into different kinematic classifications such as; extensional fractures, shear fractures, and contractional fractures (Fossen et al., 2007a, Mollema and Antonellini, 1996, Fossen, 2010). The green lines in the figure show the critical points of the red failure envelope, where the rock begins to fracture, and the black circle represents the critical state of stress of an unknown rock. The criterion can therefore be described as a tool to find the critical condition where a rock begins to fracture (Fossen, 2010).

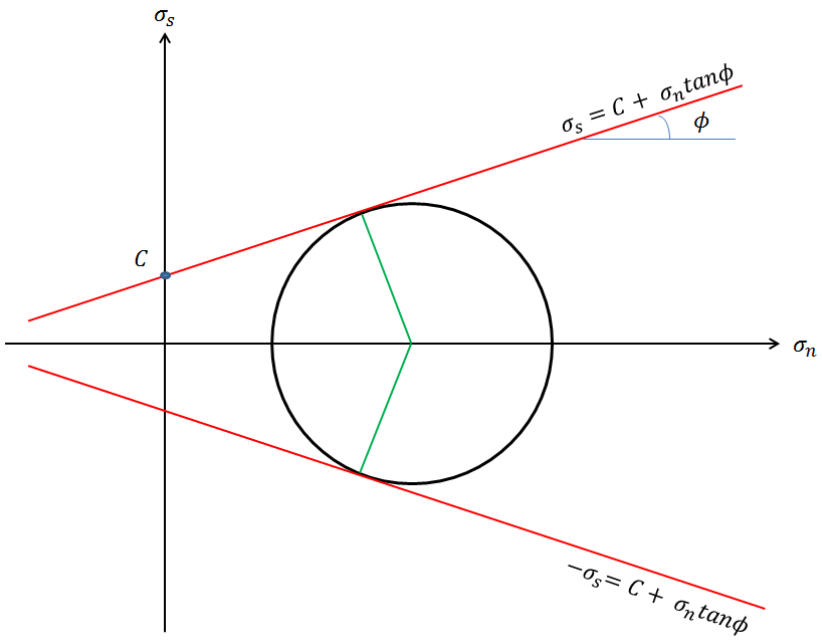

Fig. 3.3: *Mohr-Coulomb diagram with the fracture criterion. Modified from Fossen (2010) and Labuz and Zang (2012).*

Extensional fractures have extension perpendicular to the least compressive principal stress direction (σ_3) (Fossen, 2010, Pollard and Aydin, 1988). Extension fractures can be fissures, veins, dikes, or joints. Fissures are used when the fractures are filled with air or fluid and veins are used for mineral-filled fractures, while dikes are used if the fractures are filled with initially molten rock. Joints as the true extensional fractures are mode I fractures where

there is little to no shear offset. These types of fractures are will often occur perpendicular to the bedding when formed in bedded sedimentary rocks (Fossen, 2010, Narr and Suppe, 1991, Aydin et al., 2006, Fossen et al., 2007a).

Shear fractures, also called slip surface, is a type of fracture where the movement is parallel to the fracture walls (Aydin et al., 2006). Shear fractures have a small shear offset of millimeters to decimeters (Fossen, 2010). These fractures can also be initiated in pre-existing planar weaknesses (Aydin et al., 2006). Shear fractures typically develop as conjugated fractures in bisectors with 20-30 degrees to σ_1 (Fossen, 2010).

Contractional fractures, also called anti-cracks, are filled with remnants of host rock (Fossen, 2010) and links to contraction (Aydin et al., 2006). Stylolites are by some geologists explained as such fractures and are defined as pressure solution surfaces that develop perpendicular to the maximum compressive principal stress direction (σ_1) (Fossen, 2010, Mollema and Antonellini, 1996, Pollard and Aydin, 1988). These types of fractures most commonly occur in carbonates, but can also be observed in sandstones with porosity below 5 percent (Mollema and Antonellini, 1996). Anti-cracks are usually associated with mineral dissolution when there is contact between grains and removal of dissolved material (Aydin et al., 2006).

3.1.3 The Cam cap model

The Cam cap model is a variant of the Mohr diagram giving a more informative and less cumbersome diagram when dealing with the stresses in porous rocks, and it is described in detail by Schultz and Siddharthan (2005). This approach is now widely used in deformation band literature because horizontal axis (p) is the mean stress and the vertical axis is the differential deviatoric stress (q), instead of the normal and shear stress on a particular surface as for the Mohr diagram. The Cam cap model can therefore also be called the q-p diagram. These coordinate axes are a combination of the first two of the three principal-stress invariants (Schultz and Siddharthan, 2005):

$$I_1 = \sigma_1 + \sigma_2 + \sigma_3 \quad \text{Eq. (2)}$$

$$I_2 = \sigma_1\sigma_2 + \sigma_2\sigma_3 + \sigma_1\sigma_3 \quad \text{Eq. (3)}$$

$$I_3 = \sigma_1\sigma_2\sigma_3 \quad \text{Eq. (4)}$$

Eq. (2) is the horizontal axis in the *q-p* diagram (Fig. 3.4) and a combination of Eq. (2) and (3) is the vertical axis (Fig. 3.4) given by:

$$q = \sqrt{I_1^2 - 3I_2} \qquad \text{Eq. (5)}$$

Schultz and Siddharthan (2005, p. 5) describes that "the value of q equals the diameter of the Mohr circle and provides a measure of the shear stress supported in the rock at the given value of mean stress p".

The curve in Fig. 3.4 represents the yield surface, where the deformation goes from elastic to inelastic deformation. The slope of this line is represented by M given in Eq. (6), and it is related to the friction angle for rocks that are sensitive to pressure and the friction coefficient (see μ in section 3.1.2).

$$M = \frac{6sin\phi}{3 - sin\phi} \qquad \text{Eq. (6)}$$

The different numbers in Fig. 3.4 implies the kinematic classifications of the deformation bands in question. Point 1, 3 and 5 represent the three end-members of Fig. 3.1 (dilation, shear and compaction). Point 1 has a low value of p and q=0, and is characterized as pure dilation bands, whereas point 5 has a high value of p and q=0, and is characterized as pure compaction bands. Point 3 lies near the top of the yield surface on the frictional sliding line (e.g., black line in Fig. 3.4), where the curve approaches zero and there is no volume change (Schultz and Siddharthan, 2005). This point is characterized as pure shear bands.

Point 2 lies within the dark shaded area between point 1 and 3, which represents volume increase. Volume increase is indicative to dilational bands (see section 3.1.1, kinematic classifications). Point 2 represents bands with a volumetric increase and shearing (dilational shear bands).

Point 4 lies within the light shaded area between point 3 and 5, which represents volume decrease. Volume decrease is indicative to compactional bands (see section 3.1.1, kinematic classifications). Point 4 represents bands with a volumetric decrease and shearing (compactional shear bands).

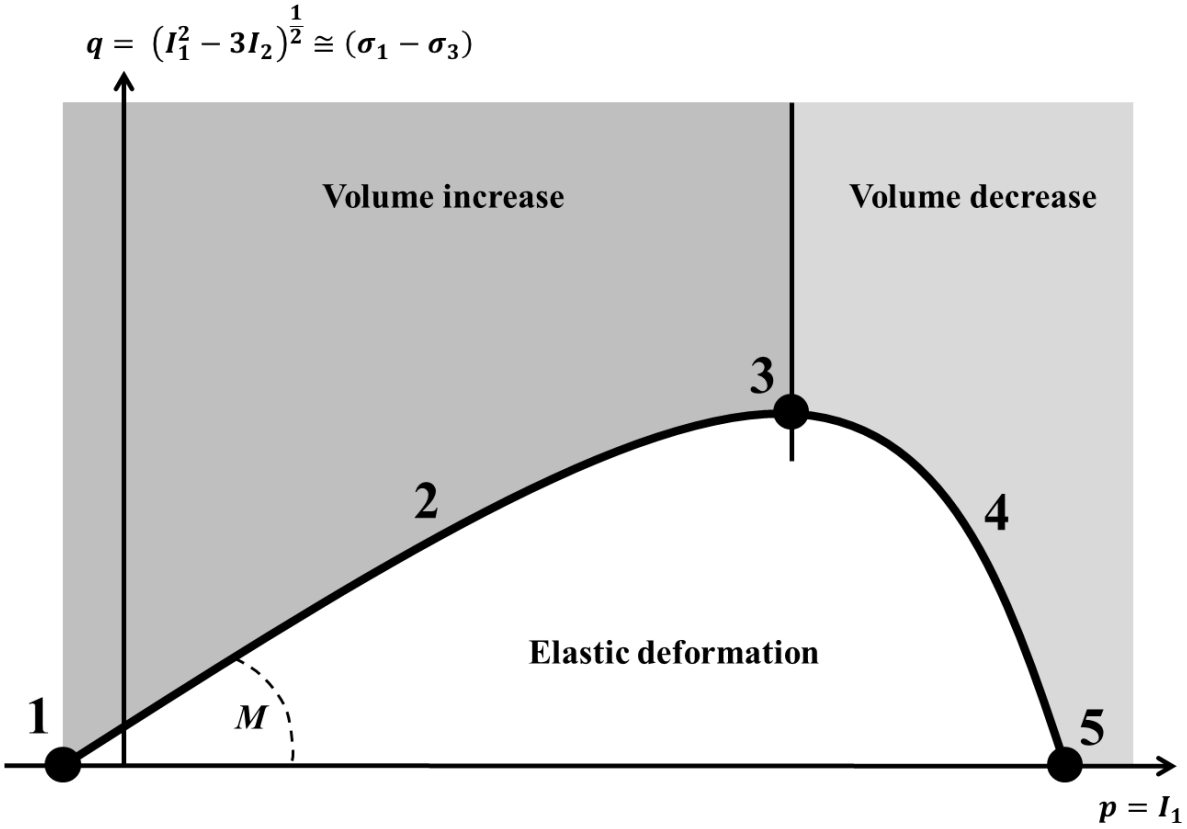

Fig. 3.4: *q-p diagram for porous rocks. M is the slope of the yield surface. (1) dilation bands, (2) dilational shear bands, (3) shear bands, (4) compactional shear bands, and (5) compaction bands. Figure is based on Schultz and Siddharthan (2005).*

3.2 Methods

3.2.1 Fieldwork

The study area (Fig. 2.1) is situated inside the Mine Canyon in the eastern part of the San Rafael Swell in Central Utah, approximately 4.5 kilometers south of I-70. The targeted formation was the Navajo Formation. During fieldwork, several strategies were used; firstly, I distinguished between the different populations of deformation bands to systematize the apparent jumble of bands. The approach was to make detailed sketches of the most important localities within the canyon. Further, strike and dip measurements of the deformation bands, where this was possible, assisted in the grouping. Strike and dip measurements in the field were done manually using a Suunto MC-2 compass and the right hand rule. Other work included scanline and stratigraphic logging, was done in collaboration with, my field assistant, Emil Hagen-Kristiansen. Finally, careful selection of samples by drilling out plugs was undertaken for thin section study (see below).

Scanline and stratigraphic log

The scanline and stratigraphic log follow the same path through the Navajo Formation, but also cover a small part of the underlying Kayenta Formation and the overlying thin Page Formation. This trace was divided into six composite sections (Fig. 3.5) of different length due to the lack of a continuous outcrop through the whole study area. The total length of both the scanline and stratigraphic log is 186 meters, with 178 meters making up the Navajo Formation.

Fig. 3.5: *composite trace making up the scanline and stratigraphic log of the Mine Canyon.*

The scanline was aimed at getting statistical distribution data of the deformation bands throughout the Navajo formation. Deformation bands along this line were recorded for each meter and divided into different populations according to previously defined populations, established earlier during the fieldwork.

A stratigraphic log template with the commonly used horizontal scale (lithology ranging from clay to pebbles) was used for drawing the log, collected in a 1:100 scale. The log was composed to substantiate the thickness and composition of various aeolian features throughout the Navajo formation. Strike and dip measurements were taken for each of the dune-boundaries.

Sample collection

Six samples were collected at four different locations (table 3.1) by using a Makita 18V lithium hand drill with an electric core drill model DE-T3 mounted on it (ASCscientific, 1998). The drill bit used had 1” (25.4 mm) in diameter, and the samples where approximately 5 centimeters long plugs. A type of manually pressurized water pump was used to add water as drilling fluid while collecting the sample. This was done to stabilize both the borehole and

sample, so the porous sandstone would not crumble to sand during the drilling. These samples were later used to make thin sections.

3.2.2 Laboratory

All six samples (table 3.1) collected in the field were handed in to technician Salahalldin Akhavan at University of Oslo, who made thin sections along pre-defined cuts. He saturated the samples with a blue-colored epoxy to fill the pore space prior to cutting. These thin sections were further used in different types of microscopy analysis to confirm observations made during the fieldwork.

Table 3.1: *Overview of the relationship between samples and thin sections, and where they were collected in the field. The location of samples with given numbers are displayed in figure 4.4. The table show where the different thin sections were applied.*

Samples and thin sections				
Sample	*Thin section name*	*Location of sample*	*Analyzed in microscope*	*Porosity calculation*
TNS-01	TNS-01	2	X	X
TNS-02A	TNS-02A	9	X	X
TNS-02B	TNS-02B	9		X
TNS-02C	TNS-02C	9		X
TNS-03	TNS-03	1	X	X
TNS-04	TNS-04	6	X	X

Optical microscope

A Nikon Eclipse Ci-POL microscope was used to preform most of the optical study by using plane-polarized light (PPL). The PPL analysis was used to determine porosity, grain size, directional trends, crushing and mineral fill. The cross-polarized light (XPL) function in a Nikon Labophot-pol microscope was used to confirm some assumptions made during analysis in the Nikon Eclipse Ci-POL microscope.

This microscopy analysis was used to distinguish the different deformation bands found in the field. Further, the work confirm (or disconfirm) what was observed in the field at the four different sample locations, selected based on band populations with distinct characteristics.

Calculation of porosity

The software ImageJ was used as a tool to calculate the porosity of the Navajo sandstone host rock and deformation bands in the thin sections. ImageJ is public open source software running on java, mainly used in processing and analyzation of images in a variety of formats (TIFF, GIF, JPEG, BMP, DICOM and FITS) (Rasband, 2004). By marking a defined area in the picture, the program enables the user to calculate statistics of the area based on pixel values.

In this case, thin sections in this study were, as mentioned, saturated with a blue-colored epoxy. ImageJ was used to find the total pixel area and the pixel area of the blue color. Then, Eq. (7) was then used to calculate the porosity;

$$Porosity = \frac{[Epoxy\ area]}{[Total\ area]} \times 100 \qquad \text{Eq. (7)}$$

where the answer is given in percent of porosity and the areas was given in pixels. This calculation was done for both host rock and deformation band in each of the thin sections.

Stereographic representations

The software OpenStereo was used to create the stereographic illustrations in this study. OpenStereo is a public open source software to create stereographic projections to use in structural geology analysis. The program is written as a cross-platform software in Python with a consistent design regardless of the operating system it is used on (Grohmann and Campanha, 2010). To use this software, all of the data need to be in separated .txt files depending on what you need to do.

In this study the populations needed to be separated into different .txt files for each location to get all of the correct projections. These .txt files were opened as Open Planar Data (Strike/Dip) and plotted in a lower-hemisphere Schmidt net using different colors to distinguish between the six populations.

4. Results

This chapter gives a presentation of the results based in the fieldwork conducted in Mine Canyon, Utah, USA. These data has been analyzed in various ways, including thin-section study.

4.1 Study area

4.1.1 Scanline

Fig. 4.1 shows the graphic representation of the composite scanline, where a total of 6127 deformation bands were recorded along the 186 meters long trace (see appendix 8.1). The scanline plots total number of deformation bands per meters along the trace of the six composite scanlines in Mine Canyon, with basis in the location shown in colors from the trace in Fig. 3.5. There are three gaps in this data set, two in the section between 47 and 49 meters, and one was at 178-179 meters. These gaps reflects a lack of outcrop.

All of these recorded deformation bands are divided into the identified 6 populations and accordingly displayed as individual graphs (Fig. 4.1B-E). Over half of the deformation bands in this scanline were recorded as population 1 (50.34 percent, appendix 8.1). Several large spikes can be observed in Fig. 4.1B in the yellow/light blue area and dark green area, and almost all deformation bands in the dark blue area in this figure is characterized as population 1 deformation bands when compared to Fig. 4.1C-E. Population 2 deformation bands in Fig. 4.1C have a group of large spikes in the dark green area where population 1 were almost non-existent (Fig. 4.1B), in addition to this there were a much smaller amount of population 2 deformation bands in the first 13 meters and a decreasing trend can be observed from about 90 meters and out. Population 3 deformation bands were mostly observed in the yellow and light blue area (Fig. 4.1D), except from some spikes in the dark green area. Most of the deformation bands in the light green area are population 3. Population 5 and 6 deformation bands (Fig. 4.1E) were locally recorded, but combined they only represent 0.24 percent (see appendix 8.1) of the results, and population 4 was not present in the scanline. These bands (populations 4, 5, and 6) are subvertical and subparallel to the scanline and are therefore significantly under-represented.

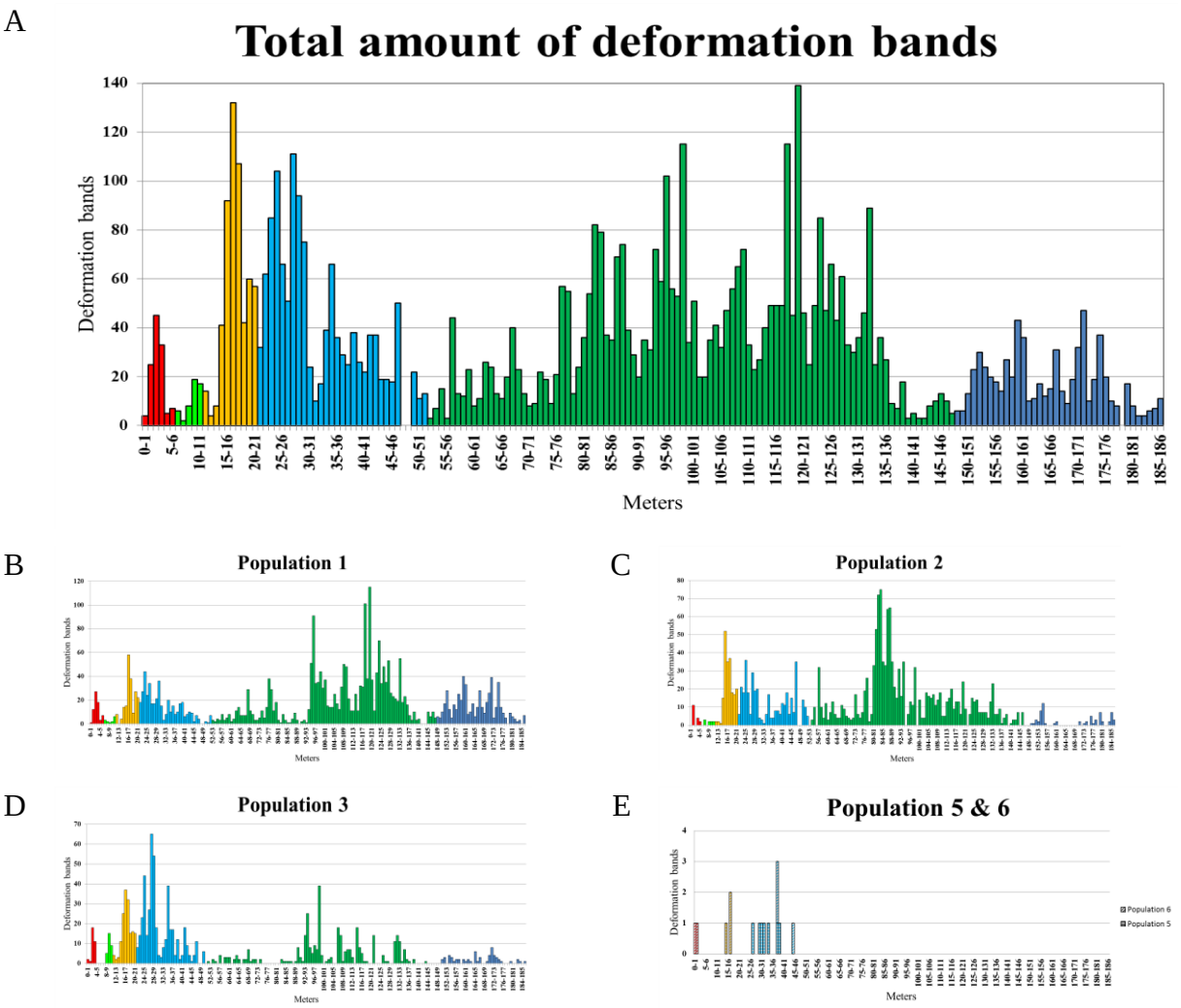

Fig. 4.1: *Graphic representation of the scanline. The color coordination is connected to figure 4.1. (A) total amount of deformation bands shown as a bar chart, and deformation bands characterized as (B) population 1, (C) population 2, (D) population 3, and (E) both population 5 and 6.*

4.1.2 Stereographic representation of locations

Fig. 4.2 shows all of the strike and dip measurements of deformation bands conducted in the field and divided into locations. All of the populations are color coordinated with a legend at the bottom of the figure. Some of the locations were unreachable, so it was not possible to take measurements at all locations. In addition to this, most of the outcrops made it difficult to get completely accurate measurements. So have this in mind when looking at the results of these measurements. Description of the different stereographic representations is found below in the text for each location.

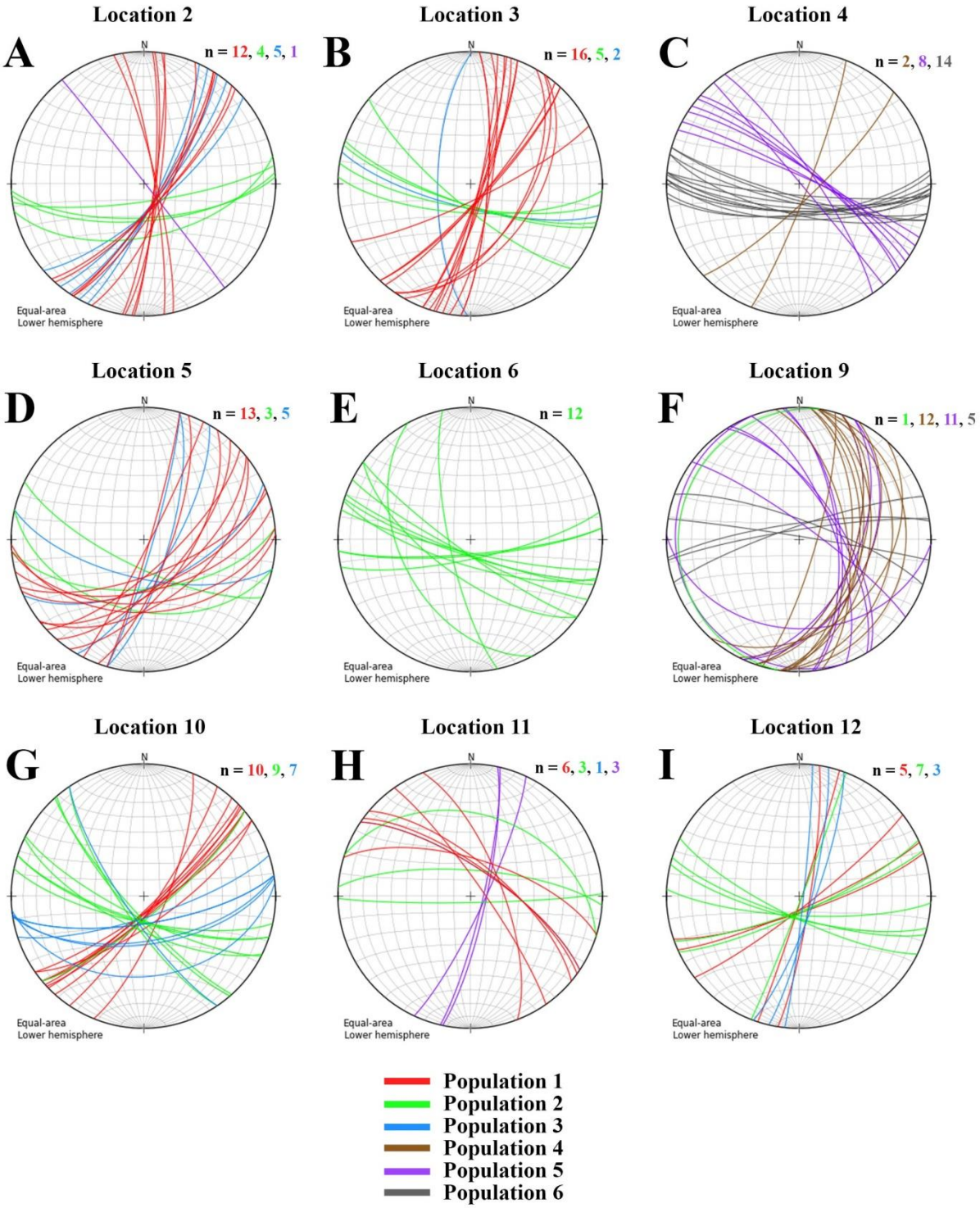

Fig. 4.2: *stereographic representation of the strike and dip measurements from each location in the field. (A) location 2, (B) location 3, (C) location 4, (D) location 5, (E) location 6, (F) location 9, (G) location 10, (H) location 11, and (I) location 12. The populations have been color coordinated and the number of measurements for each population is given per location. The total number of measurements is 185.*

4.1.3 Division and general character of structural populations

The sub-division of deformation structures into populations is based on consistent orientations, common deformation mechanisms, and observations of cross-cutting relationships between deformation band and fracture populations in Mine Canyon. Note that there are chronological transitions that suggest temporal overlap of some structural populations – I will return to these observations below and in the Discussion. For simplicity, population 1 is the oldest population, and population 6 the youngest, generally speaking.

All populations can be related to the east-verging Laramide Orogeny folding of the San Rafael Swell. Population 1 represents west-directed shear structures that follow lamination in the sand dunes and interdunes, hence they are microscopic back-thrusts. On the contrary, the population 2 structures show top-to-the-east (top-E) shear direction of deformation bands, representing microscopic back-thrusts. They have a fanning pattern indicating progressive rotation of bedding in a constant stress field, indicative of formation over a period of time. They have therefore been sub-divided into sub-population 2a to 2c. A similar fanning is seen for population 3; however, these structures show consistent top-W shear direction, opposite to population 2. They have accordingly been sub-divided into populations 3a to 3c. Both population 2 and 3 are locally showing two sets of deformation structures with a nearly 60 degree bisector, suggesting they formed as conjugated sets.

Three populations have nearly vertical orientation, and cut bedding with a high angle. These are populations 4, 5 and 6. Their different orientation suggests they have a different origin to the population 1-3 structures. Population 4-6 structures also consistently cut the other structures. Population 4 structures are isolated deformation bands with a low occurrence. Population 5 and 6 structures from two sets with a nearly 60 degree bisector, which suggest they formed in the same stress field as conjugate structures.

Each population of deformation bands and partly fractures are classified by deformation mechanism and kinematics. These first classifications are based on outcrop observations. By thin-section studies in the following section, these classifications are further substantiated.

The characters, orientations and cross-cutting relationship between different structures will be further summarized in the Discussion. In the following description; however, detailed observations are presented for a number of localities, as shown in Fig. 4.4. Although somewhat repetitive, these observations represent the backbone of the work. A thorough description is therefore required to present a convincing case in the Discussion.

4.1.5 Description of studied succession

Fig. 4.4A shows the eastern succession outside the Mine Canyon, covering formations such as Navajo, Carmel, Entrada, Curtis, Summerville and Morrison. They are outlined with borders between them on the photograph. Page Formation is not visible in this picture, but it is found as a thin layer between the Navajo and Carmel formations.

The study area covers eolian sandstone of the Jurassic Navajo Sandstone (Formation). The succession consists of basically two facies, as shown in the strip-log of Fig. 4.5; (i) 1-20 m thick sand dunes with distinct 30 degree dip of mainly tangential-downlap foreset lamination. The sandstone is made up of very well sorted, highly porous fine to medium sand. There are at places very subtle grain-size variations through the dunes, between various laminae. (ii) Meter-thick interdune successions are sparse. They are made up of either parallel laminated sand or dm-thick tangential-base cross-stratified dunes. The grain-size is the same as for the larger dunes, however slightly more silt seems present in the interdunes. Overall, the Navajo Sandstone represents a dry mega-dune unit, deposited in a sand-sea with very high sand content available for building of sand dunes.

The log (Fig. 4.3) also covers the overlying Page Formation, which is deposited above a hiatus. This unconformity is subtle in outcrops, with a gentle, dm-scale relief. The Page Formation shows meter-thick dunes made up of the same gran-size as the Navajo Sandstone, as suggested by the description in literature highlighting channelization and reworking of the deposits making up the later Page Formation. The unit is interpreted as aeolian dune deposits. The Navajo Sandstone constitutes 178 meters out of the total 186 meters. Most of the succession consists of very-fine to medium sand with some exceptions where there is fine to medium sand (at 37-38 meters and 102-104 meters) or medium to coarse sand (at 171-183 meters).

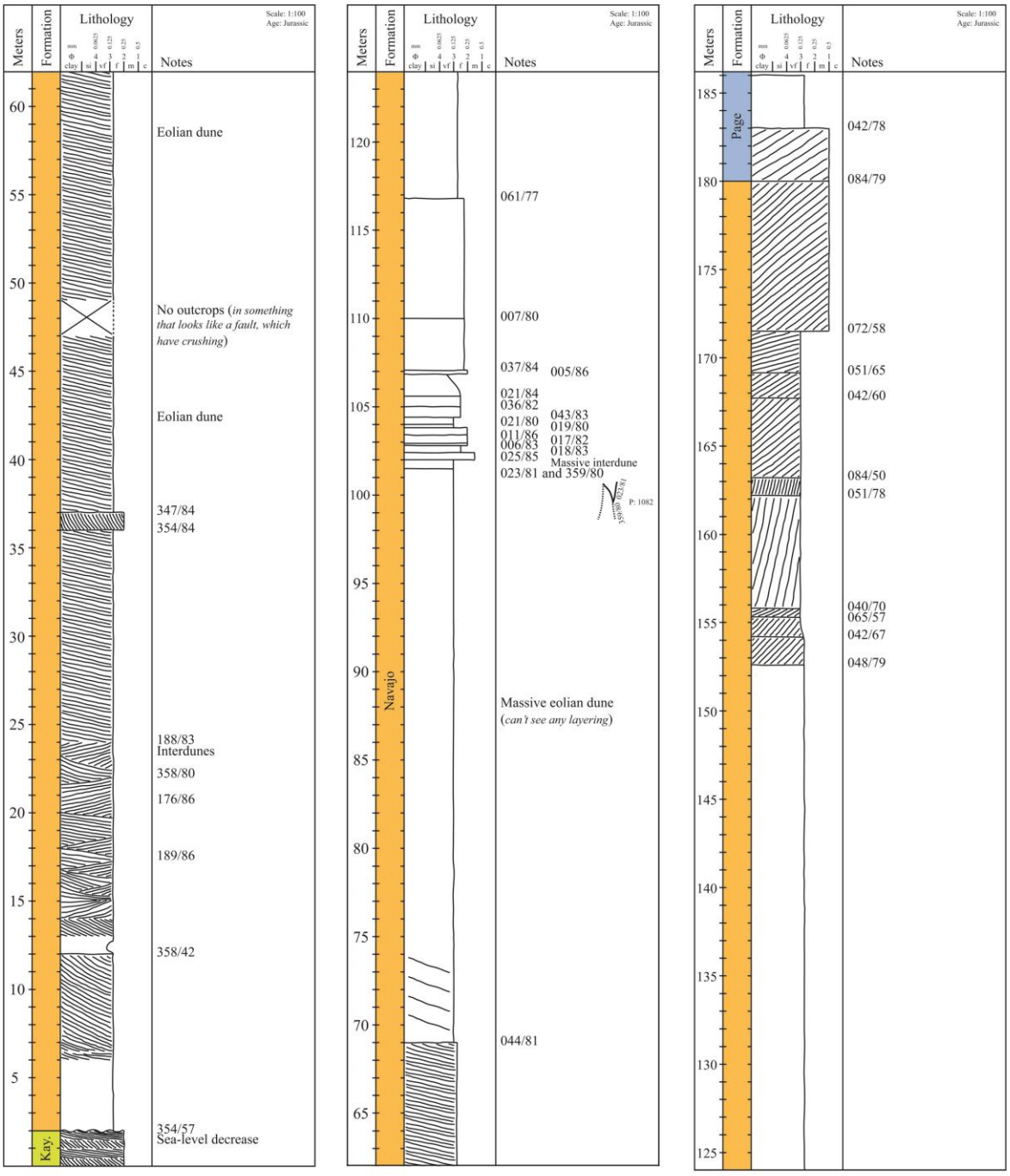

Fig. 4.3: *stratigraphic log with strike and dip measurements of dune boundaries. The log consists of mostly the Navajo Sandstones with large eolian dunes (~20 meters thick) and interdunes.*

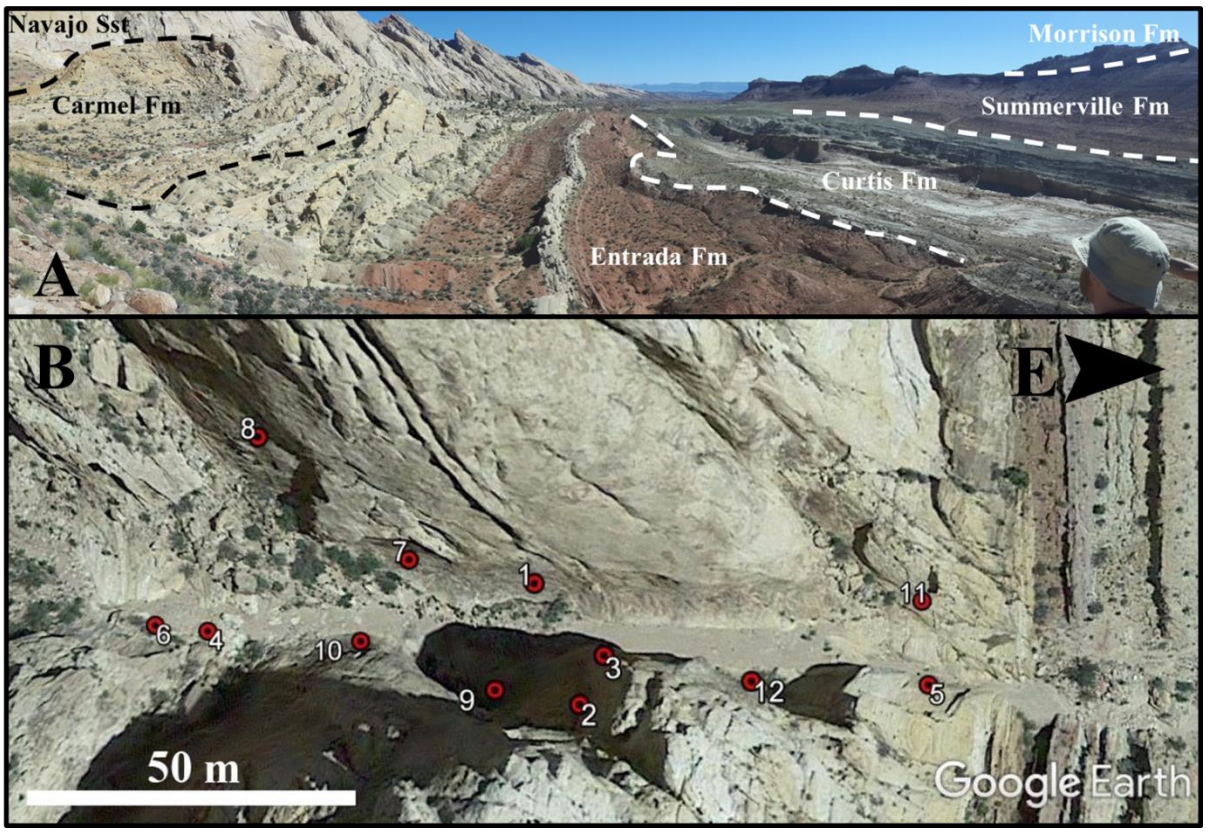

Fig. 4.4: *(A) formations and their boundaries outside Mine Canyon and (B) overview of all the study-locations inside Mine Canyon (collected from Google Earth in 2016).*

4.1.6 Description of structural localities

Fig. 4.4B shows the study-locations inside the Mine Canyon as red dots with a number indicating the different locations described below. The database is from a number of locations, from which deformation was studied in great detail. One location was used as a guide to the chronology, i.e. location 1, which is a cliff-face at the mouth of Mine Canyon. Similarly, locations 7 and 8 are cliff-faces outside reach from the canyon floor. All other locations were easy accessible in the valley floor or in bounding cliff-faces.

Location 1

This location represent the "the main wall" of the study area (Fig. 4.4) as it shows good relationships between deformation band populations 1 to 3. Most of this wall (seen in Fig. 4.5) consists of one thick sand dune with some interdunes in the upper right (east) corner of the figure (outlined in green dotted lines) before it again goes over to be another tick sand dune. Fig. 4.5A shows a series of deformation band swarms. These bands have been outlined as white trace lines in Fig. 4.5B, where the bands can be subdivided into deformation band

populations. Identified bands are from populations 1, 2a-c and 3a-c. Note the cross-cutting relationships, showing the order to be 1, then 2 and finally 3.

Location 2

This location is situated in the middle of the study area in Mine Canyon (Fig. 4.4) and the outcrop is a vertical surface. The outcrop consists mostly of deformation band swarms containing en-echelon R-shear structures with top-E shear direction. There is also a number of dm-long hairline shear-fractures oriented similar to and associated with the en-echelon deformation bands. The white arrows in Fig. 4.6b and c are pointing to fractures.

Fig. 4.6a shows the outcrop from a distance and the more discernible structures are two swarms of cataclastic bands, and some other band orientations. These populations conform to populations 1, 2 and 3 deformation bands. Deformation mechanisms and kinematics for the bands (shear-compaction bands) on microscopic level is further outlined below.

The lowermost population 2 deformation band swarm is truncated by population 3 deformation bands. For detailed documentation, Fig. 4.6b show one of the band swarms of population 1 that can be seen to be drag-folded and cut by the population 2 deformation band swarm with associated fractures.

The circle in Fig. 4.6b locates a sample that was collected from this location - this sample is shown in Fig. 4.6c and 4.6d. Note that also a shear fracture was cored.

The stereographic representation of the strike and dip measurements from this location (Fig. 4.2A) show that populations 1 and 3 are following the approximately same directional trend, while population 2 has a completely different trend. These observations are supported by Fig. 4.6a. There was also reported one population 5 deformation band in this location in Fig. 4.2A.

Location 3

This location is approximately in the middle of the Navajo Sandstone (Fig. 4.4) and it consists of a series of interdune beds with various grain sizes (Fig. 4.7). Dunes have visible layering distinguishing the interdune beds from each other. Here, the sandstone composition is very susceptible to weathering, evident by the spongy appearance of the rock. Fig. 4.7B and 4.8 show population 1 deformation bands following the dune lamination both along dune foresets and along dune interfaces. There is an apparent geomechanical difference between the

different dune-interdune beds. A gentle difference in grain size likely causes the deformation bands following the layering in the dune lamination to change direction at the dune interface (Fig. 5.8). These bands are cut by populations 2 and 3 deformation bands. This is seen in Fig. 4.7C, where the majority of deformation bands are following the lamination of the beds; however, the populations 2 and 3 band is cutting straight through the dunes.

The stereographic representation of the strike and dip measurements from this location (Fig. 4.2B) show two directional trends for the population 1 deformation bands. The first is almost N-S and are representing the bands following the lamination of the interdunes (Fig. 4.7 and 4.8). The second has a NE-SW direction and represents the bands following the dune interface (Fig. 5.8). The population 2 and 3 bands have an E-W direction as seen in both Fig. 4.2B and 4.7.

Location 4

This location is situated in the lower part of the Navajo Formation (Fig. 4.4) and the outcrop makes up a nearly horizontal surface. Fig. 4.9A show obvious layering in the sandstone seen as alternating dark- and light colored lines. Movement on faults/deformation bands in the rock can easily be observed due to offset of the layering. Deformation structures are outlined in the figure as black trace lines in Fig. 4.9B. These lines mostly represent deformation bands, obviously reflecting shear deformation of the rock. The deformation bands can further been divided into three different populations (4-6). Fig. 4.2C is a stereographic representation of the orientation data collected from this location. All strike and dip measurements were separated into different populations and plotted in a lower-hemisphere Schmidt net using different colors.

Two structural trends, populations 5 and 6, have an inconsistent crosscutting relationship suggesting that they have approximately the same age, and reflect conjugated structures. In addition to this, a deformational structure going in an N-S direction was observed throughout this outcrop. This population 4 structure is cut by all the other structures.

The conjugate structures are interpreted as population 5 with an ESE trend and population 6 with an ENE trend (Fig. 4.9), and Fig. 4.2C supports this interpretation. Closer inspection of these deformation bands in this outcrop shows the structures to be disaggregation dilation-shear bands, hosting centimeter long hairline shear fractures. Both bands and fractures are in many cases cemented with MnO.

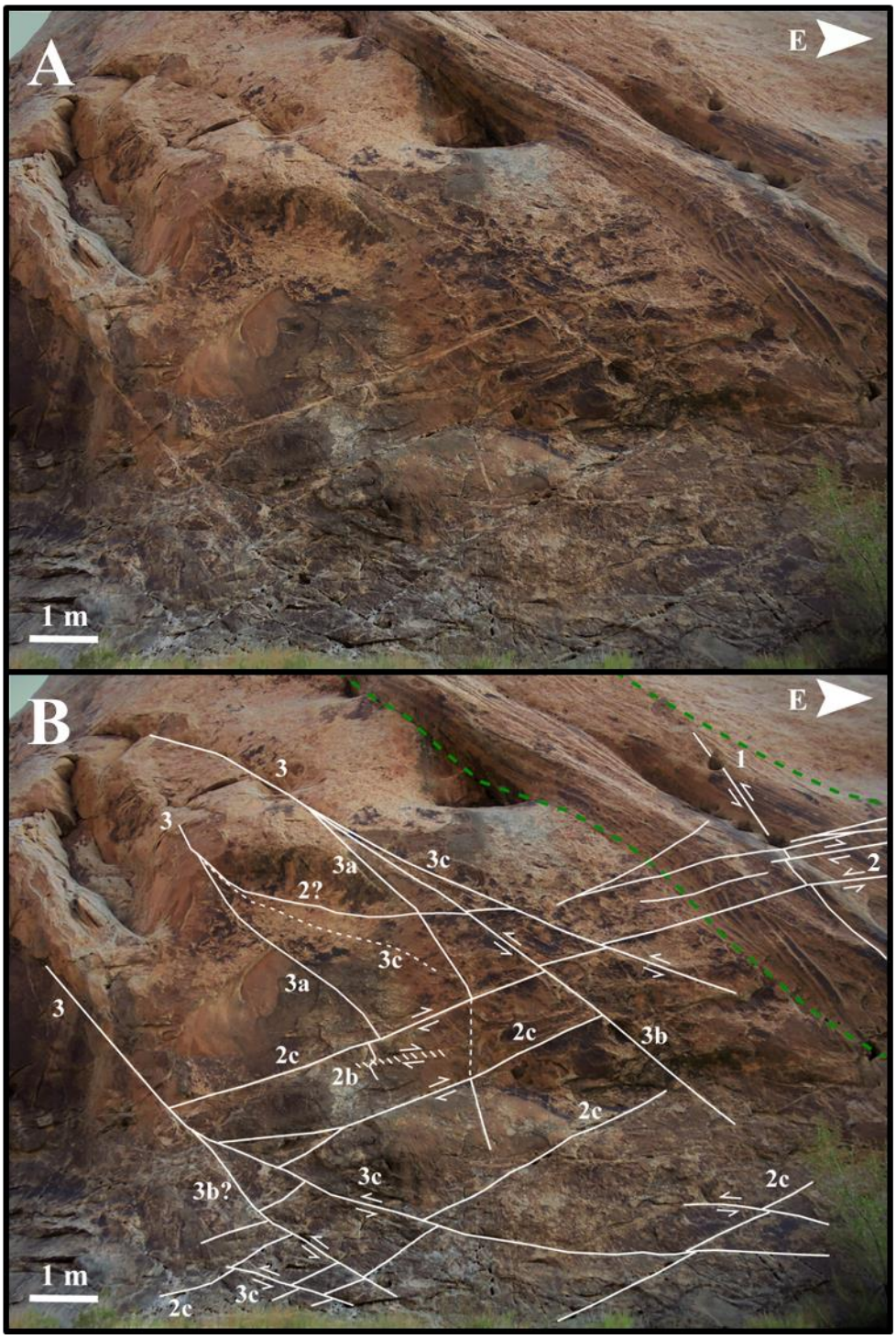

Fig. 4.5: *this wall from location 1 displays all of the different populations in the same location. The upper part of the figure is untouched, while the lower part show the main deformation bands found in the wall. Green dashed lines outline interdunes.*

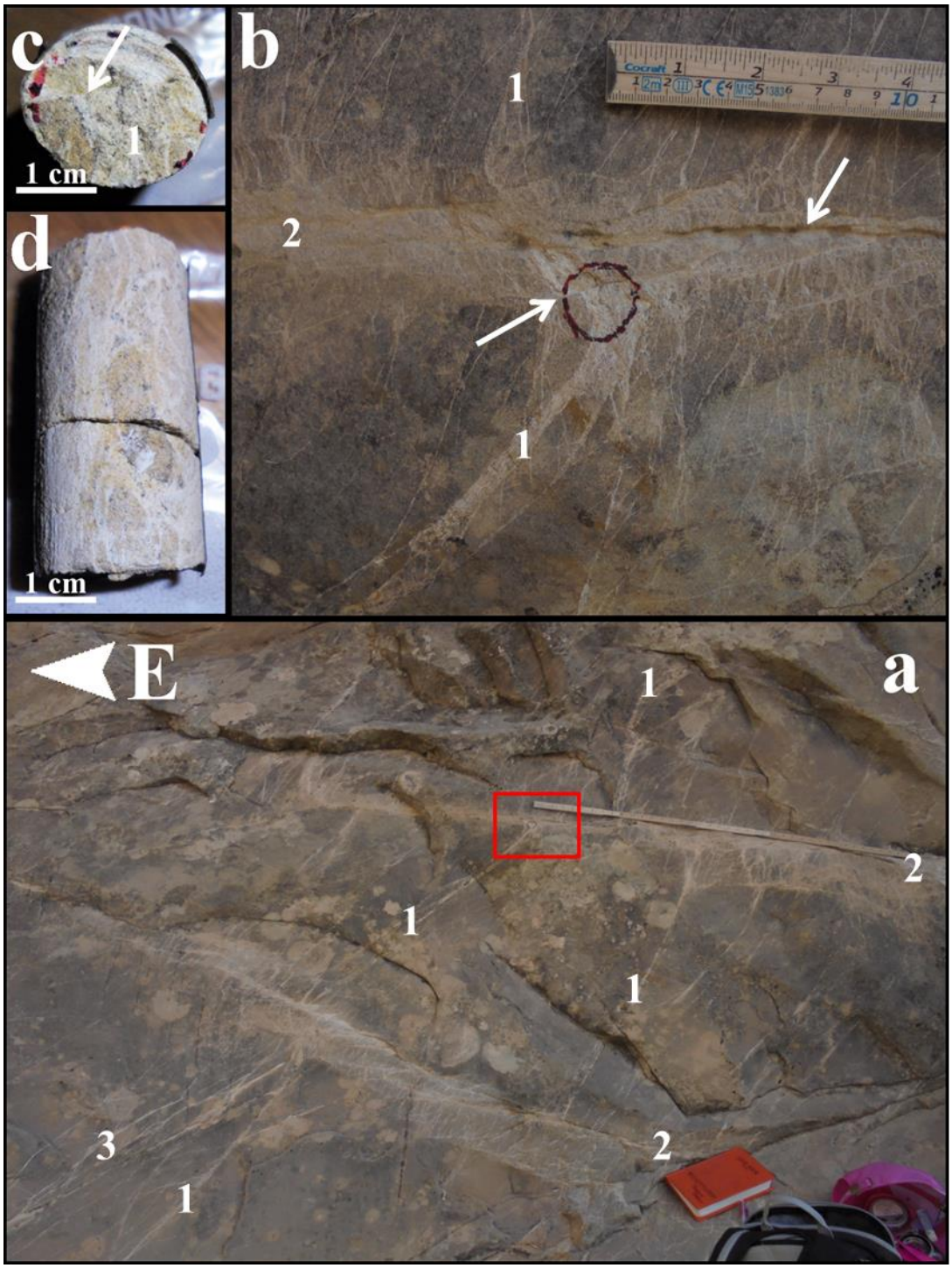

Fig. 4.6: *band populations hosting en-echelon fractures from location 2. (a) Overview of the main part of this location, (b) close-up of the red square with a drill location marked, (c) drill-core from the top, and (d) drill-core from the side. White arrows are pointing to fractures.*

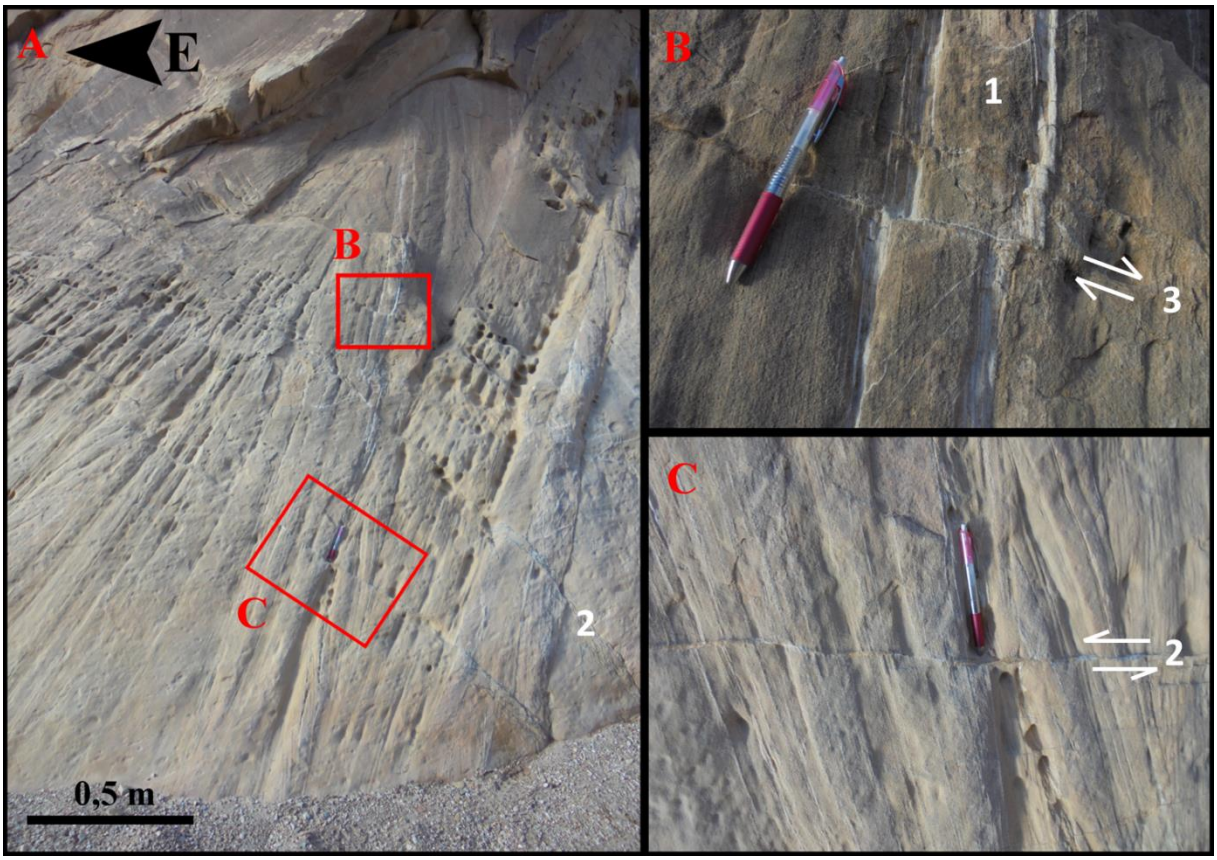

Fig. 4.7: *(A) overview of location 3 with several interdune beds visible, (B) population 1 cut by population 3, and (C) population 1 deformation bands following the lamination of the interdunes being cut by population 2.*

Fig. 4.8: *Population 1 deformation bands following the dune lamination both along dune forests and along dune interfaces.*

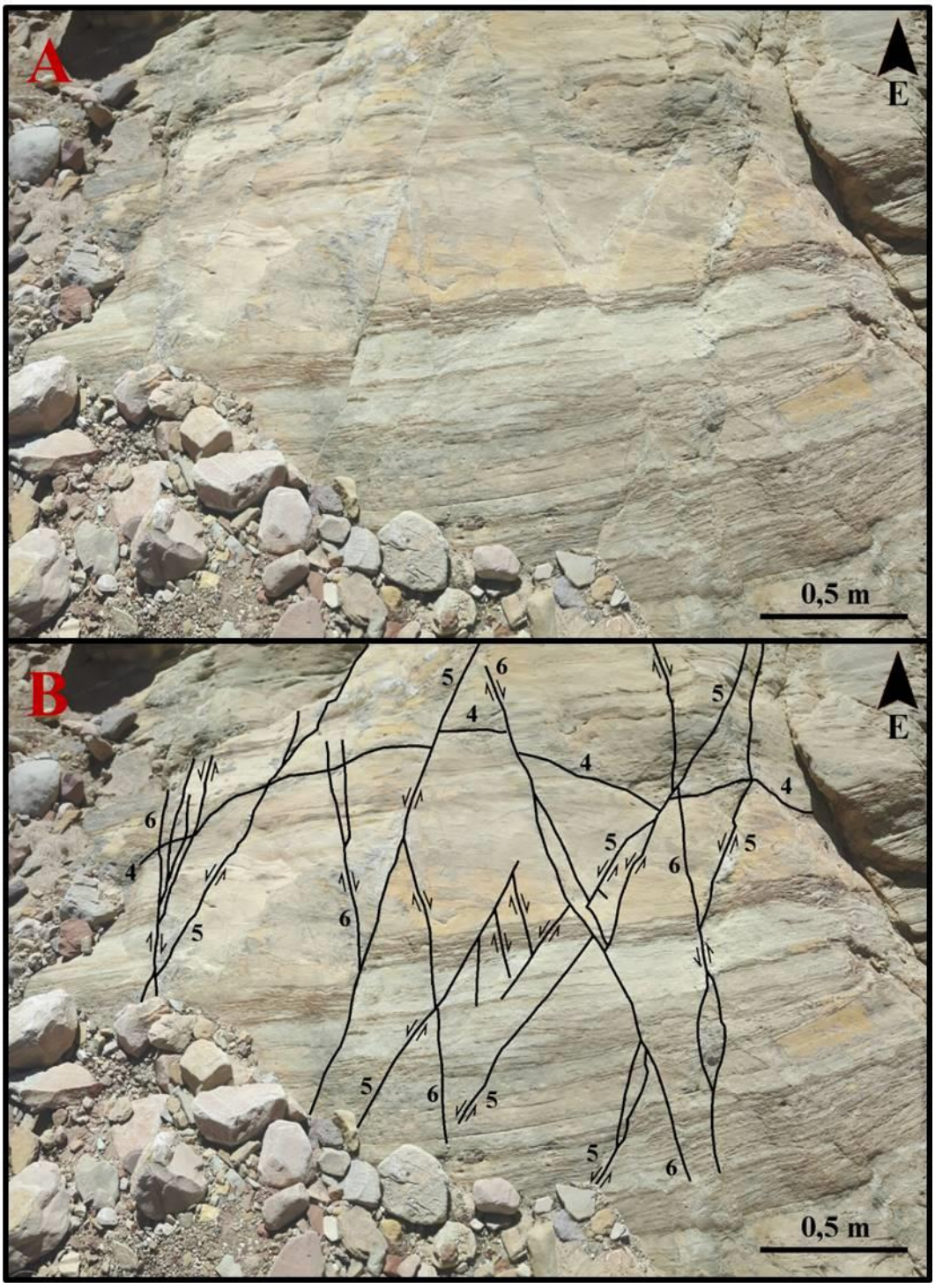

Fig. 4.9: *(A) untouched picture from location 4 and (B) black trend lines where population 4 is cut by conjugated sets of deformation bands (population 5 and 6).*

Location 5

This location is situated in a vertical outcrop in the upper part of Navajo Formation, almost at the mouth of the canyon (Fig. 4.4), and shows similarities to both locations 2 and 3. The outcrop in the field reveals interdunes with population 1 deformation bands following the layering/lamination, just like described for location 3, but does also show other deformation bands crossing the dune. In addition to this, the outcrop offers a deformation band population swarms containing en-echelon R-shear bands and fractures with top-E shear direction, like those described for location 2. These shear bands form ladder-like structures that make up deformation band population 2. Note a vertical deformation band (population 2) swarm that mildly offset a deformation band swarm of population 3.

The stereographic representation of the strike and dip measurements from this location (Fig. 4.2D) show no immediate clear pattern for the deformation bands. The population 2 bands have an approximate NW-SE directional trend and population 3 have more scattered measurements, pointing to fanning of the population in this location.

Location 6

This location is situated in a vertical outcrop in the lower part of the Navajo Formation (Fig. 4.4). This outcrop as shown in Fig. 4.10 has several large white deformation band swarms, with three orientations. There are also smaller deformation bands following the layering of the interdunes, similar to location 3. The bands along lamination are interpreted as population 1 deformation bands. All of the large swarms are population 2a-c deformation bands showing top-E shear movement. The black square (Fig. 4.10B) give a closer look at the deformation band swarms, which are cataclastic deformation bands forming in an en-echelon pattern consistent with R-shear structures. The red square (Fig. 4.10C) show where sample TNS-04 was collected (red circle was plugged) – micro-textures from the core is described below.

The stereographic representation of the strike and dip measurements from this location (Fig. 4.2E) only show population 2 deformation bands. It is possible to observe three slightly different directional trends of bands representing the fanning of population 2.

Location 9

This location is divided into two outcrops situated in horizontal to semi-horizontal surfaces in the middle of the Navajo Formation (Fig. 4.4). The southernmost outcrop in this location contains white zones of subvertical ladder-style population 5 deformation band swarms, revealing dextral shear offset. They are cut by steep fractures and population 6 deformation

bands (Fig. 4.11A) with sinistral shear offset. The population 4 deformation bands are found both between and inside the population 5 bands (Fig. 4.11B).

The northern outcrop in this location contain en-echelon sets of population 6 disaggregation dilation-shear bands with sinistral shear movement and population 5 deformation bands with dextral movement (Fig. 4.12B). Note the population 4 deformation bands are cut by the other populations in Fig. 4.12. The red circle in Fig. 4.12A gives the sample location that was collected at this location.

The stereographic representation of the strike and dip measurements from location 9 (Fig. 4.2F) show both the northern and southern outcrop as one. The population 4 bands have an N-S directional trend, while the population 6 bands have an E-W trend. Population 5 on the other hand does not have a distinct trend. Fig. 4.11 show that the population 5 bands go in at least three different directions, which are fitting well with Fig. 4.2F.

Location 10

This location is situated in the middle of the formation (Fig. 4.4) and consists of interdune sandstone exposed in a vertical surface. The outcrop in Fig. 4.13 displays two main trends of structures offsetting the bedding and lamination of the interdunes, including the population 1 cataclastic deformation bands that mostly follow the lamination of the dunes. The two other populations are 2 and 3 deformation bands, defining cataclastic shear band swarms. There is a crosscutting relationship in this outcrop suggesting population 3 is youngest. Population 2 consistently shows top-E shear and, based on orientation with respect to bedding, is interpreted as the 2c population. Population 3 is seen by top-W shear and, based in bedding, is interpreted as the 3b population. A chronology is suggested by folding of population 2c next to the population 3 bands, the latter of which also cut the population 2 bands. The blue square in the figure (Fig. 4.13C) show a closer look of the relationship between the populations; in this case population 2c is cut by 3b and vice versa suggesting they are temporally related.

The stereographic representation of the strike and dip measurements from this location (Fig. 4.2G) show all of the population 1 bands in an NE-SW trend (following the lamination). Population 2 and 3 has three main directions that occur due to the fanning of both populations.

Location 11

This location is situated in the mouth of the canyon (Fig. 4.4). Fig. 4.14 several interdunes displayed as a 3-dimentional outcrop making it possible to observe all of the populations in

the same outcrop. There are a lot of deformation bands intersecting each other as a systematic network of bands. To get a more complete picture of this network there was constructed trend lines on the lower picture in this figure. Observed the usual trends of the deformation bands as in previous locations; population 1 following the dune lamination, population 2 with top-E shear direction, population 3 with top-W shear direction, population 4 cutting through dune lamination, population 5 with top-E shear direction, and population 6 with top-W shear direction.

The stereographic representation of the strike and dip measurements from this location (Fig. 4.2H) show population 1, 2, 3 and 5. Unfortunately, measurements from the other populations were not collected due to the difficulty of measuring them during the fieldwork.

Location 12

This location is next to location 3 close to the mouth of the canyon (Fig. 4.4). This is a vertical outcrop consisting of one massive looking interdune of several meters, where the lamination was difficult to spot. By using the trend lines in the lower picture of Fig. 4.15, it was possible to distinguish the different population from each other. Deformation bands in this location were found to be population 1, 2 and 3. There are a lot of similarities between the bands in this location and the ones in location 2 and 3 (see above). One of the most interesting features in this location is the population 2 band swarm similar to the one in location 2 (only with another angle).

The stereographic representation of the strike and dip measurements from this location (Fig. 4.2I) show population 1 bands in two directions (N-S and NE-SW) and population 2 in three directions (fanning of the population). Measured population 3 bands are only found in one direction (N-S). The relationship between the population 1 and 3 bands is really similar to the one in location 2.

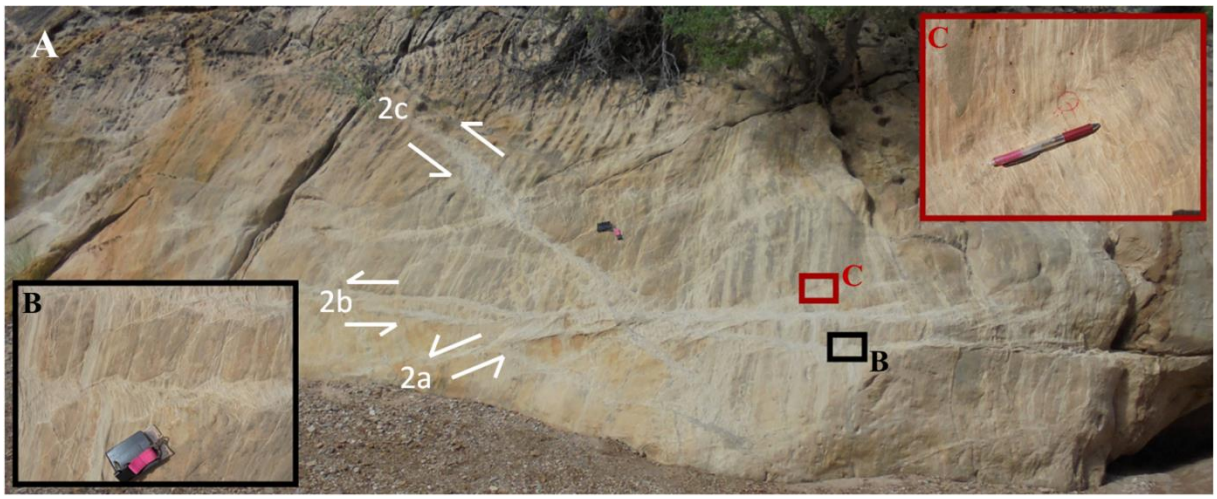

Fig. 4.10: *(A) overview of an outcrop from location 6 with several large white deformation band swarms, (B) deformation band swarm with en-echelon pattern consistent with R-shear structures, and (C) sample location and kink band.*

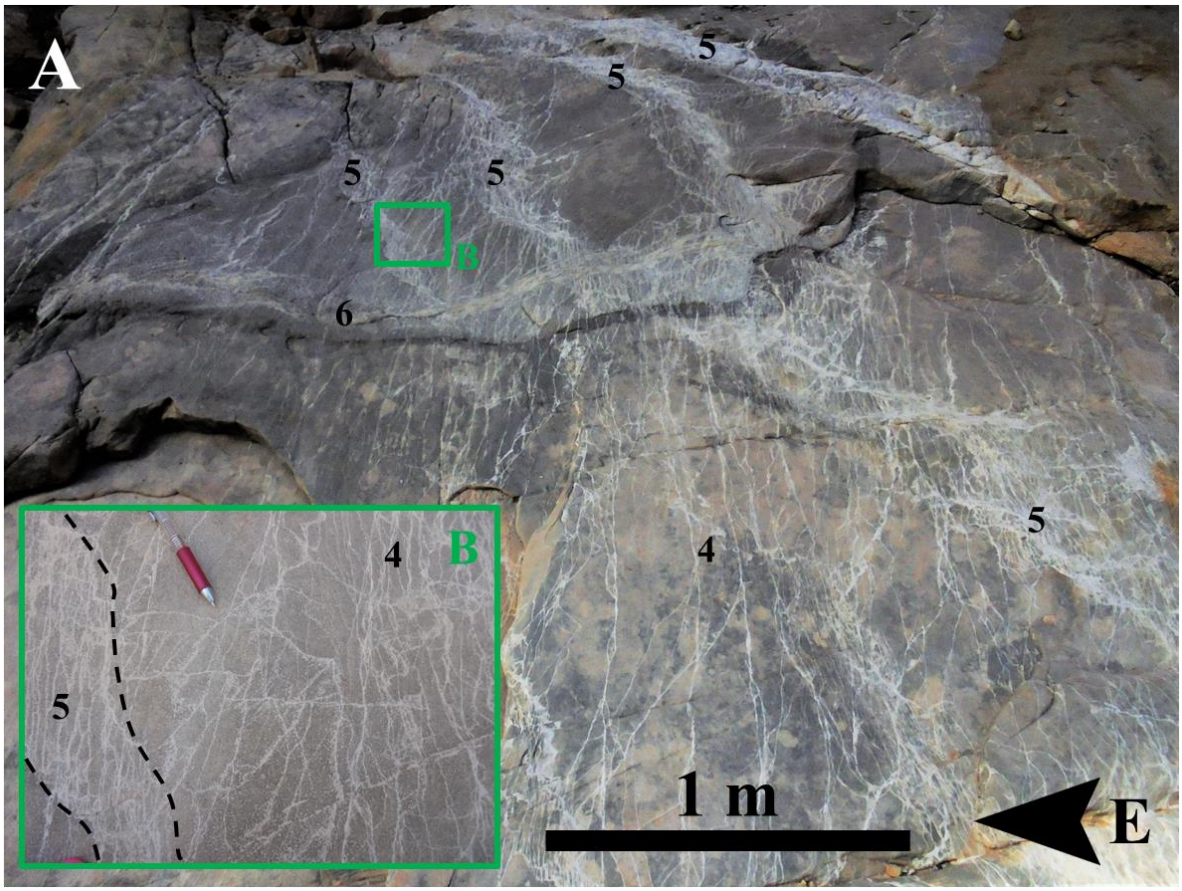

Fig. 4.11: *the southern outcrop of location 9. (A) An overview of the location with numbers indicating which deformation bands are present, and (B) population 4 bands between and inside the population 5 bands.*

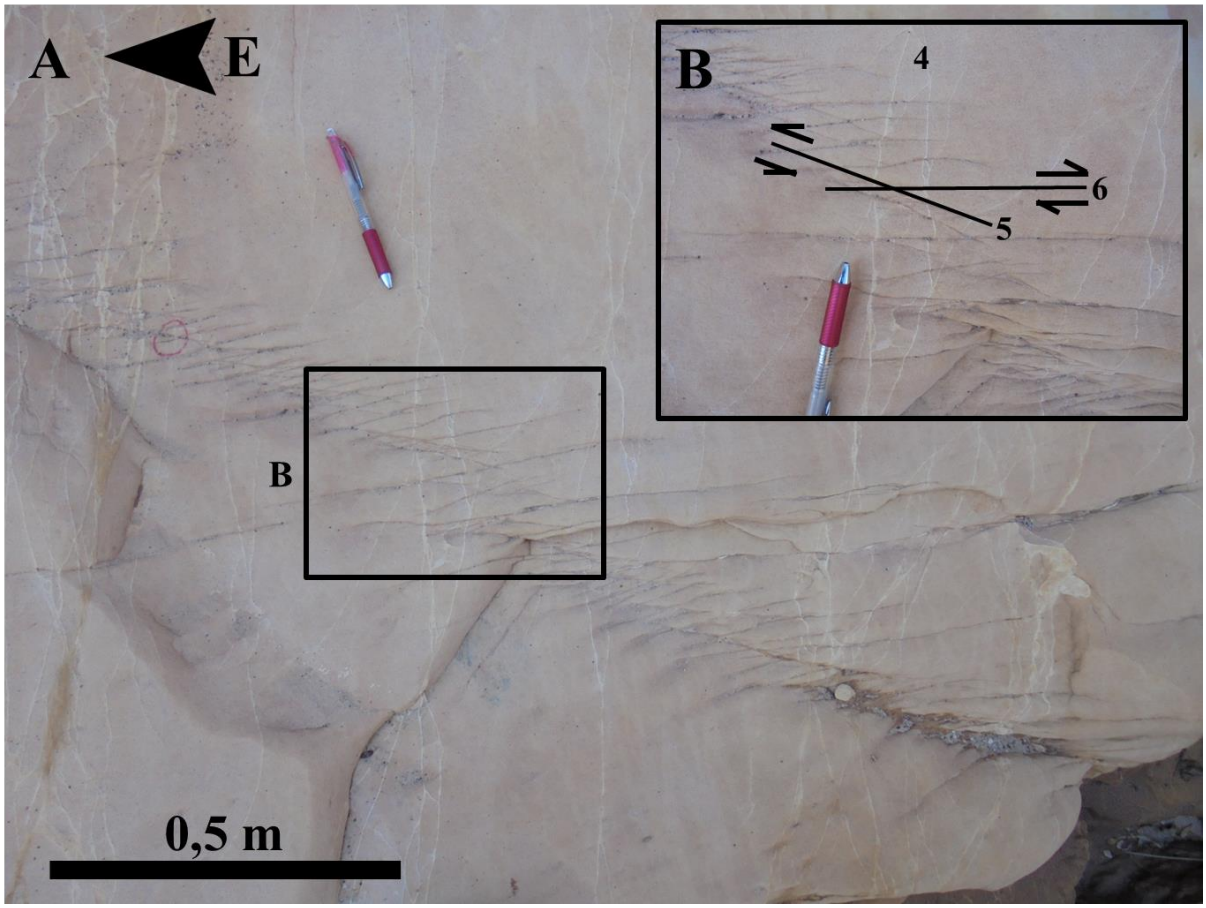

Fig. 4.12: *the northern outcrop of location 9. (A) An overview of the location with the sampling location as a red circle, and (B) a close-up to show the relationship between the present populations. Note that population 4 is cut by the two other.*

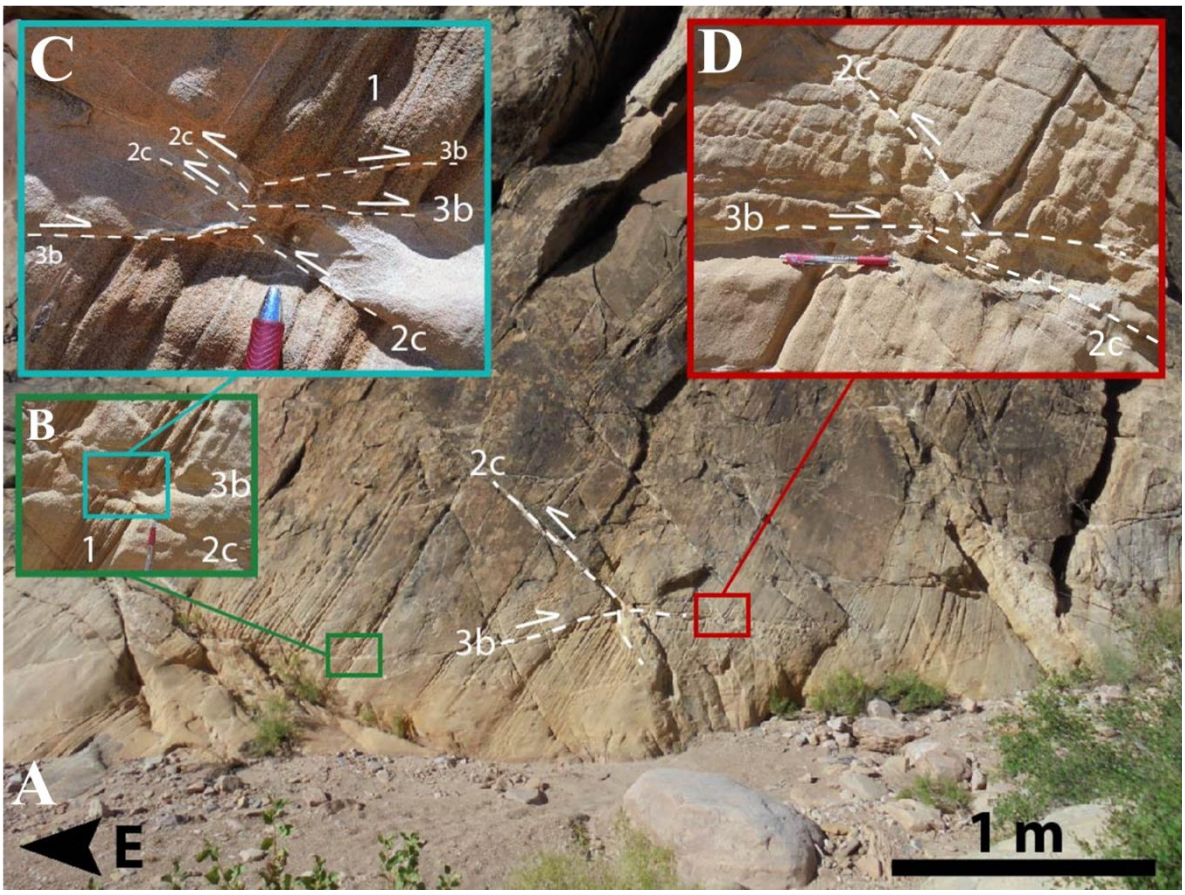

Fig. 4.13: *(A) An overview of location 10, note how population 2c and 3b are interacting (2c is bending instead of being cut). (B) Show an interesting part of the outcrop, (C) shows the cross-cutting relationship between population 2c and 3b, and (D) show population 3b cutting 2c.*

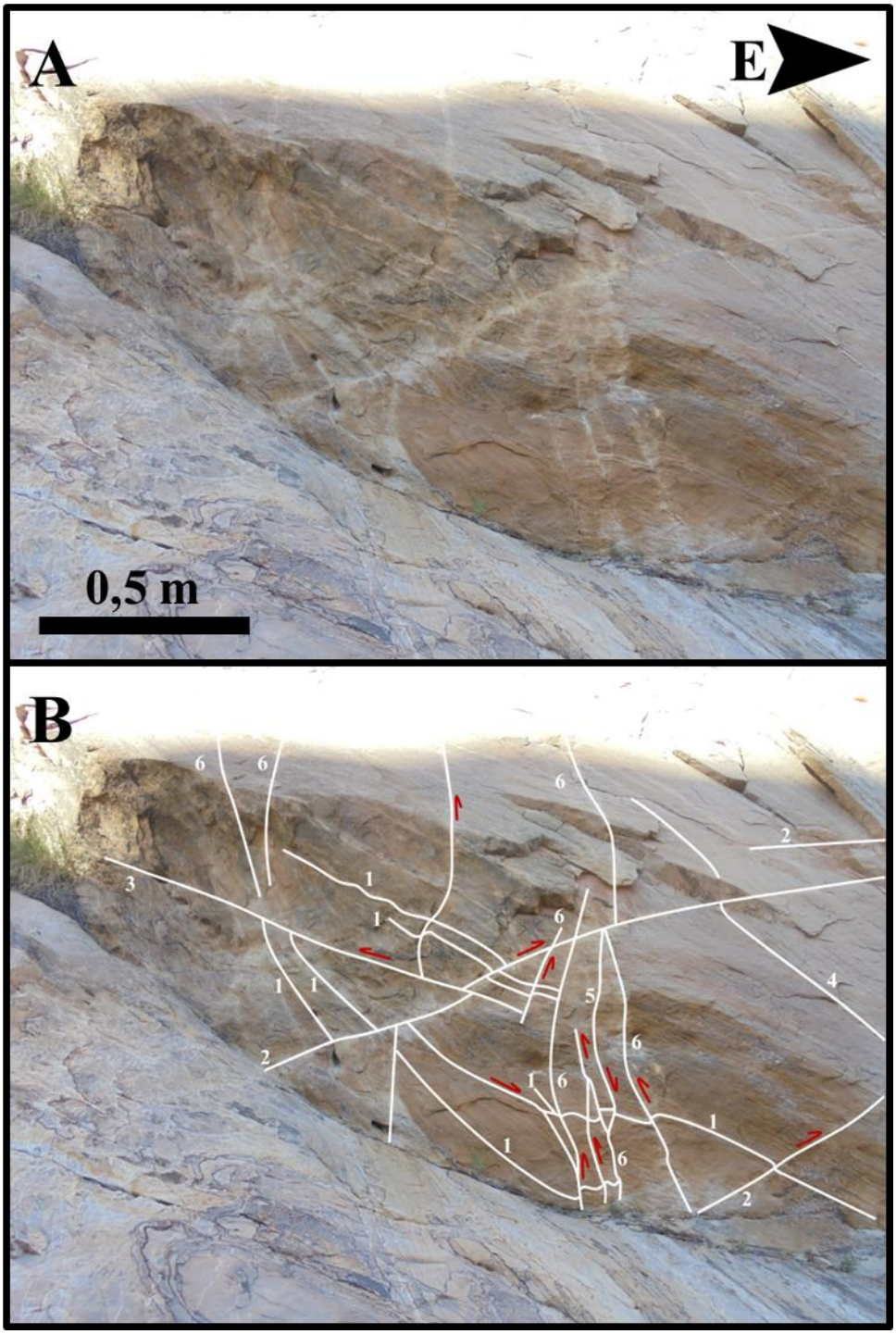

Fig. 4.14: *(A) untouched picture from location 11 showing a 3D outcrop, and (B) white trendlines showing the deformation band relationship.*

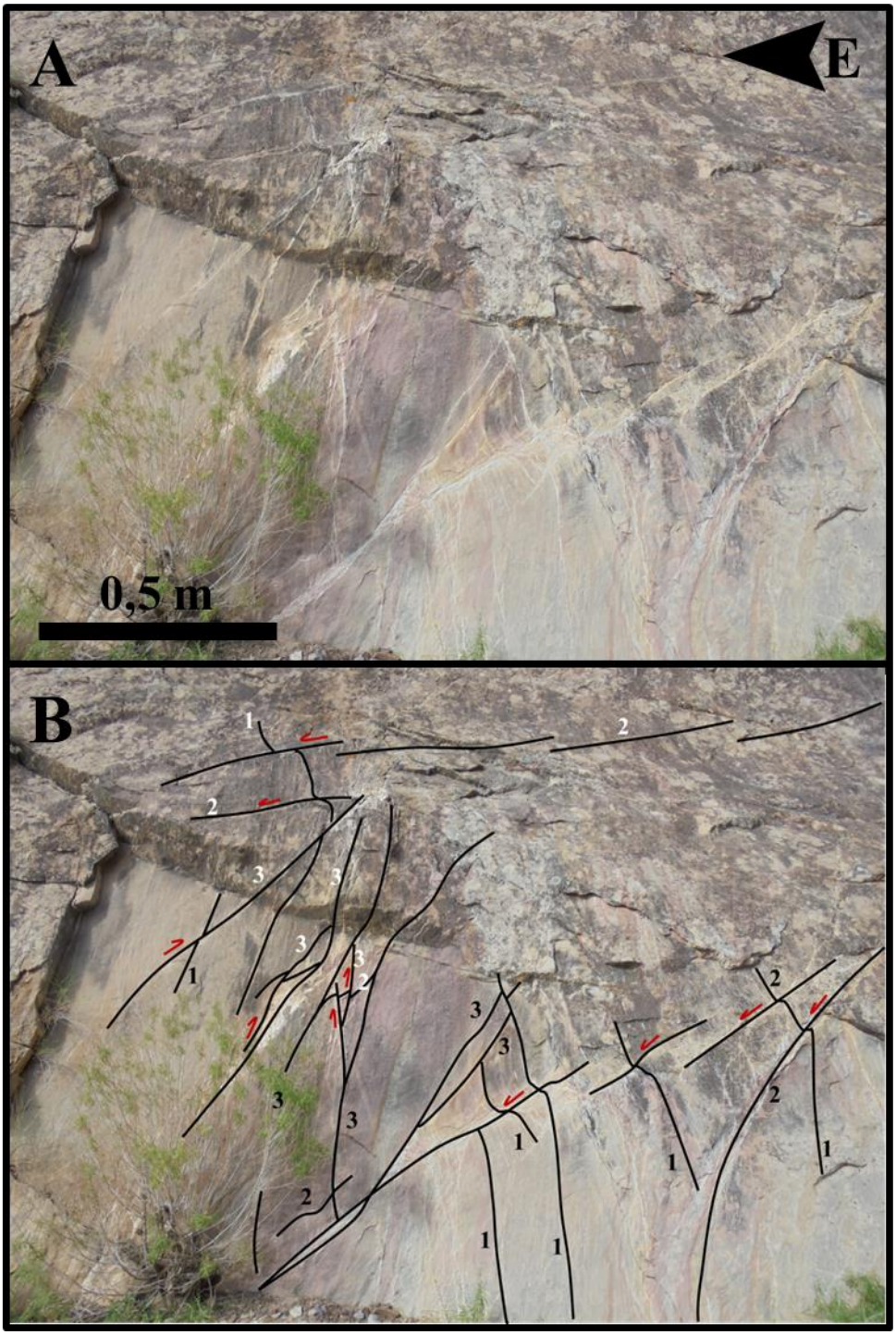

Fig. 4.15: *(A) untouched picture from location 12, and (B) black trendlines showing the deformation band relationships.*

4.2 Microtextural analysis

4.2.1 Host rock characteristics

The mineralogy of the host rock in all the collected samples is quite similar when recorded through the optical microscope, where the main minerals found in the host rock is quartz and feldspar.

Analysis of the thin section from location 2 (TNS-01) showed that the grains in the host rock comprise of moderate to low sphericity with some elongated grains in-between, and that the grains are generally subrounded. There is no obvious directional trend of the grains in this location and the grains in the host rock are moderately to well sorted.

In location 9 there was collected three samples (TNS-02A-C) from the northern outcrop, but only one of these thin sections where studied in closer detail (TNS-02A). Analysis showed that the grains in the host rock mostly have moderate to low sphericity and are poorly sorted. The large grains in the sample are mainly rounded, while the smaller grains have a subrounded to subangular roundness. The directional trend of the grains is not always obvious throughout the thin section, but a subtle SW-NE trend can be observed.

The host rock in the thin section from location 4 (TNS-03) is well sorted, and the grains have a moderate to low sphericity and subangular to angular roundness. A subtle SW-NE directional trend of the grains can be observed in the sample.

The thin section from location 6 (TNS-04) showed a host rock with low to elongated sphericity and subangular to angular roundness. The sample is well sorted and has a SE-NW directional trend of the grains.

The porosity of the host rock was calculated from all of the collected samples (see section 3.2.2 for explanation) and are in table 4.1 summarized and show a host rock porosity variation between 15 – 25 percent.

4.2.2 Sample locations and thin sections

The field area is shown in Fig. 4.4A and table 3.1 explains where the different samples were collected. Here is a short summary of why the different samples were collected during the fieldwork:

- Sample TNS-01 was collected from location 2 (Fig. 4.4) to look at a kinematic bend of population 1 when being cut by population 2, and en-echelon shears (Fig. 4.6b).
- Samples TNS-02A-C was collected from location 9 (Fig. 4.4) to look at the conjugate relationship between population 5 and 6, and the fracture overprinting population 6 (Fig. 4.12).
- Sample TNS-03 was collected from location 4 (Fig. 4.4) to look at the disaggregation dilation-shear band cutting through a cataclastic band (Fig. 5.8).
- Sample TNS-04 was collected at location 6 (Fig. 4.4 and 4.10C) to look at a kink band, which was only observed in this outcrop.

The porosity of the deformation bands was calculated from all of the collected samples and are in table 4.1 displayed with a variation between 8 – 24 percent.

Thin section photograph from sample TNS-01 show significant cataclasis and compaction, rendering it difficult to differentiate between different deformation bands. Fig. 4.16 shows a deformation band crossing the figure in a near horizontal orientation. This population 2 deformation band is cutting several other deformation bands of population 1. The population 2 deformation band have a top-E movement, as seen by the drag-folding of the population 1 deformation bands. The rock experienced dilational reopening after compaction and this is evident in large areas of pore space seen in Fig. 4.16 (large blue areas). The population 2 deformation bands in the figure have a more distinct cataclasis than the surrounding rock, making it possible to distinguish them from the population 1 bands in the sample.

The thin section from sample TNS-02A consists of three main features. Firstly we have a cataclastic compaction band going horizontally through the picture (best seen in Fig. 4.18 as population 4). Then, the cataclastic compactional shear band and the dilational shear bands happened almost simultaneously in an approximately 60 degree angle as conjugate sets of deformation bands (Fig. 4.17A). Some of the dilation bands are filled with a MnO cement and looks black, while others are only dilational. These bands are completely vertical in Fig. 4.17A. The cataclastic compactional shear band is located on the diagonal in the middle of Fig. 4.17A and are missing some blue epoxy (the epoxy did not penetrate the whole deformation band). This band looks like a dilation band due to problems during sample collection, and because it developed into a slip-surface R-shear fracture with some dilation.

Fig. 4.17B is a zoomed picture of the cataclastic wall and you can see grain crushing inside the band.

The thin section from sample TNS-03 consists of mostly cementation bands. The largest band in the thin section is displayed in Fig. 4.19, stretching from top to bottom of the picture, and it is filled with calcite. This band is essentially a population 6 dilational shear band with a dextral movement. The movement direction is evident due to the thin population 4 cataclastic band, visible on the diagonal axis from the top left corner, the population 6 deformation band is cutting through. Originally it looks like the population 6 deformation band is split in two in this figure, but a theory about this figure is discussed in the next chapter. Fig. 4.20 show a clear divide in the core of a cementation band. This is an extensional fracture with secondary calcite filling, where there are some grains residing inside the fracture without any damage. This fracture is created due to reactivation of the band.

The thin section from sample TNS-04 shows the kink seen in the field (see section 5.1.6, location 6). It was difficult/not possible to locate the population 2a deformation band going straight through the kink at a 90 degree angle (as seen in the field). The kink band is a population 1 deformation band with cataclasis through the kink. The kink looks like a wavy cataclastic deformation band stretching from left to right in Fig. 4.21. The population 2 deformation band to the left in this figure is a shear-disaggregation band, and the one to the right seems to be merging with the kink band.

4.2.3 General microtextural observations

A general analysis was done for each thin section (see table 4.1) mainly to find the grain size and porosity of the host rock, porosity of the deformation bands, and give a description of the deformation mechanism observed for populations found in the thin sections. These results are presented in table 4.1, focusing on the detailed results from TNS-01, TNS-02A, TNS-03 and TNS-04. Since TNS-02A, TNS-02B and TNS-02C was collected at the same location, the two latter have been excluded from most of the analysis.

The microtextural analysis of the deformation bands was conducted for populations 1, 2, 4, 5 and 6 using figures 4.16-4.21. Population 3 was not observed in any of the thin sections created and is therefore not a part of this analysis. The host rock in Fig. 4.16 is almost not visible in the image, so a microscope was used to look at the thin section (TNS-01) to find the host rock and do the comparison with the deformation bands.

Population 1

This population was observed in Fig. 4.16 and 4.21. The population 1 deformation band in Fig. 4.16 has a larger variation in grain size than the host rock, where some of the grains are rounded and others more subrounded to angular. There is a high degree of crushing in this band and therefore a low amount of pore space. Black-looking fluid (possibly MnO) has intruded in the residual pore space after the formation of the deformation band. In Fig. 4.21 the population 1 deformation band has reduced grain size and more rounded grains than the host rock. It has a high degree of crushing and a low amount of pore space.

Based on microstructural observations from Fig. 4.16 and 4.21 population 1 is classified as a cataclastic deformation band with a high degree of grain crushing.

Population 2

This population was observed in Fig. 4.16 and 4.21. The population 2 deformation band in Fig. 4.16 has a high degree of crushing with various grain size and visibly rounded grains compared to the host rock. Some of the grains have cracks going through them and the pore space in this band is very low. An oxide fluid (possibly MnO) has intruded the remaining pore space after the deformation band was created, evident by the small black areas in the band.

The two population 2 deformation bands shown in Fig. 4.21 have different appearance in this thin section (sample TNS-04). In both of these population 2 bands, the roundness of the grains is approximately the same as in the host rock. The deformation band to the left have the same grain size, but the pore space is slightly higher than the surrounding host rock. There is no evidence of cataclasis or cementation present in this deformation band and the grains looks exactly as the grains in the host rock. The deformation band to the right in Fig. 4.21 has much less pore space than the host rock. The grain size in this band is partly reduced and a small degree of crushing is evident.

Based on observations population 2 deformation bands can be classified as disaggregation bands with zones of cataclasis depending on location.

Population 4

This population was observed in Fig. 4.18 and 4.19. The population 4 deformation band in Fig. 4.18 has the same roundness of the grains as the host rock. The band has reduced grain size and a higher degree of crushing than the surrounding host rock, and therefore also less pore space.

Fig. 4.19 shows a population 4 deformation band with a high degree of crushing and fractured grains. The grain size and amount of grains in the band is reduced compared to the host rock, and the pore space is almost completely filled in with crushed grains.

Based on the observations in the two thin sections, the band in this population can be classified as a cataclastic deformation band.

Population 5

This population was observed in Fig. 4.17, 4.18 and 4.19. Fig. 4.17 shows two population 5 deformation bands with a slight difference in appearance. The band to the left in the figure has no crushing and a lot of pore space. This pore space is in some small areas filled in with a black fluid (possibly MnO) after the formation of the band. The few grains inside the band have small fractures going through them, and the same roundness as the host rock. The band to the right in Fig. 4.17 and in Fig. 4.18 is the same population 5 deformation band. This band has a lot of fractured grains, but otherwise has the same roundness as the host rock (in the few un-fractured grains). There is no evidence of extensive crushing in this deformation band, and there is observed a high degree of pore space. This pore space has later been almost completely filled in with an oxide fluid (possibly MnO), evident in the black color of the band.

Fig. 4.19 show a population 5 deformation band with a lot of pore space filled with calcite cementation after band formation. The grains are more angular and the grain size is slightly smaller in the deformation band than in the host rock, but there is no obvious evidence of grain crushing.

Based on the pore space observed between the grains population 5 is classified as a dilational band with oxides and cement filling the pore space.

Population 6

This population was observed in Fig. 4.17 and 4.19. The population 6 deformation band in Fig. 4.17 has a lot of crushing along the contact zone on margin of the band. There is difficult to say what the grains were like inside the band before it reactivated and fractured (R-shear fracture). The well-defined and smooth fracture wall might be an indication of formation of a slip surface forming along the deformation band before the fracturing opening. On the margin, the roundness of the grains almost looks like as in the host rock and there is a grain size reduction.

Fig. 4.19 shows a bit different population 6 deformation band. Here, the grains are more angular than in the host rock and a lot of pore space filled up with calcite cement. This calcite cement filled the space after the formation of the band. There is no obvious grain crushing in this deformation band.

Population 6 deformation bands are classified as cataclastic bands that developed slip and fracturing along the band.

Table 4.1: *microtextural overview of the observed populations in each thin-section. This table shows the microtextural properties of all populations found during the analysis. Note that TNS-02B and TNS-02C only has a general porosity analysis of the thin-section as a whole and not for each population, and that porosity was calculated per thin-section for all samples.*

Thin section	Population	Deformation mechanism	Host rock grain size	Host rock porosity	Deformation band porosity
TNS-01	Population 1	Cataclastic	112 µm	25 %	2 %
	Population 2	Cataclastic			7 %
TNS-02A	Population 4	Cataclastic	121 µm	18 %	22 %
	Population 5	Disaggregation			high
	Population 6	Cataclastic/Disaggregation			high
TNS-02B	General analysis	-	-	15 %	17 %
TNS-02C	General analysis	-	-	18 %	24 %
TNS-03	Population 4	Cataclastic	112 µm	15 %	7 %
	Population 5 (?)	Disaggregation (later cementation)			7 %
	Population 6	Disaggregation (later cementation)			7 %
TNS-04	Population 1	Cataclastic	130 µm	19 %	14 %
	Population 2	Disaggregation			14 %
		Cataclastic			14 %

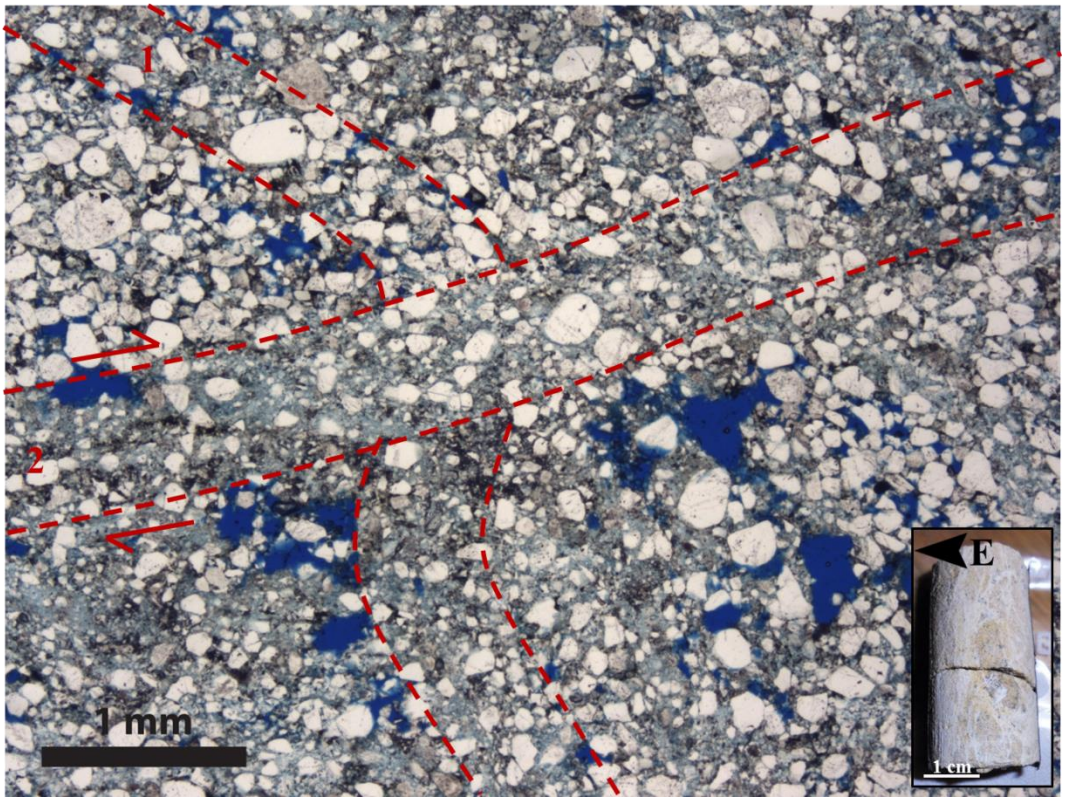

Fig. 4.16: *a population 4 deformation band cutting population 1 deformation band (sample plug TNS-01 in the bottom right corner).*

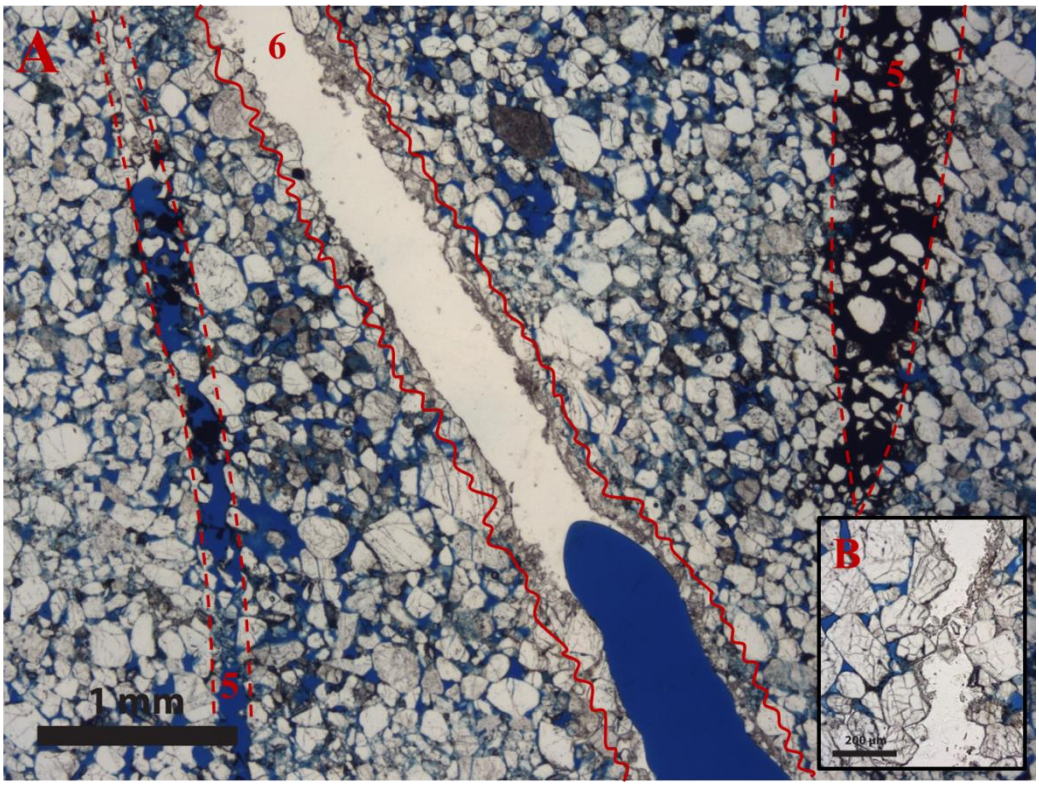

Fig. 4.17: *(A) population 5 deformation band with a cataclastic wall and two population 4 dilation bands, and (B) taken from another location in the thin section to show the cataclastic wall.*

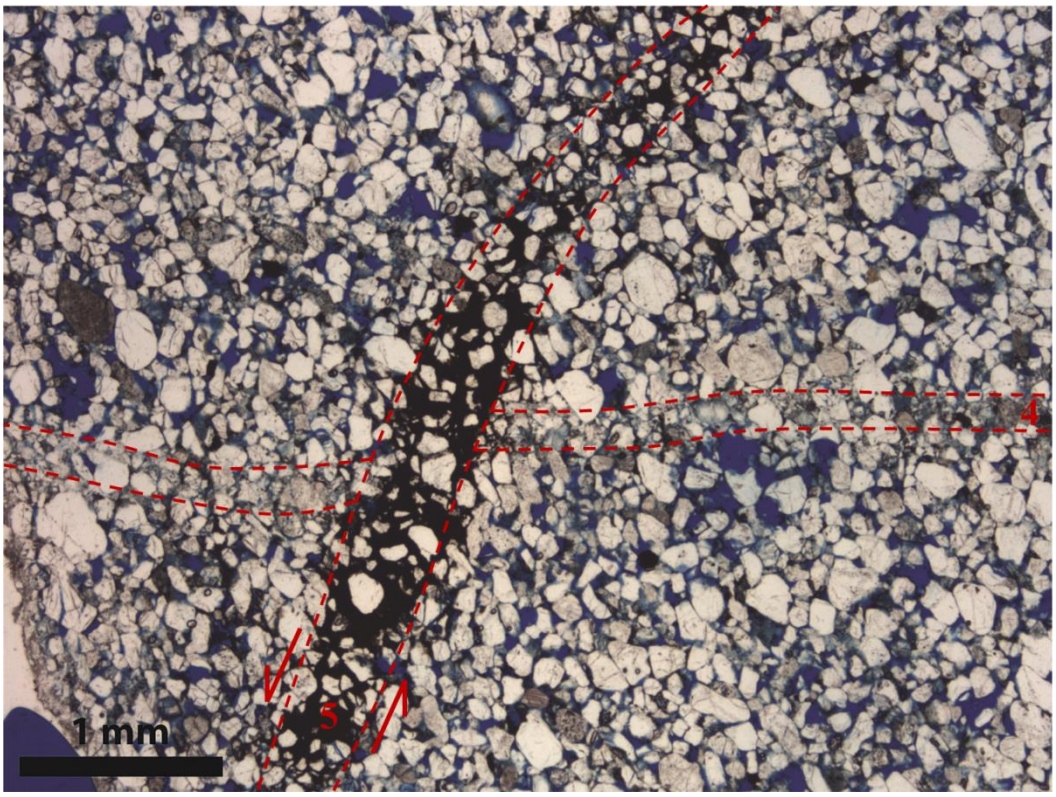

Fig. 4.18: *cataclastic population 1 deformation band cut by MnO filled dilation band.*

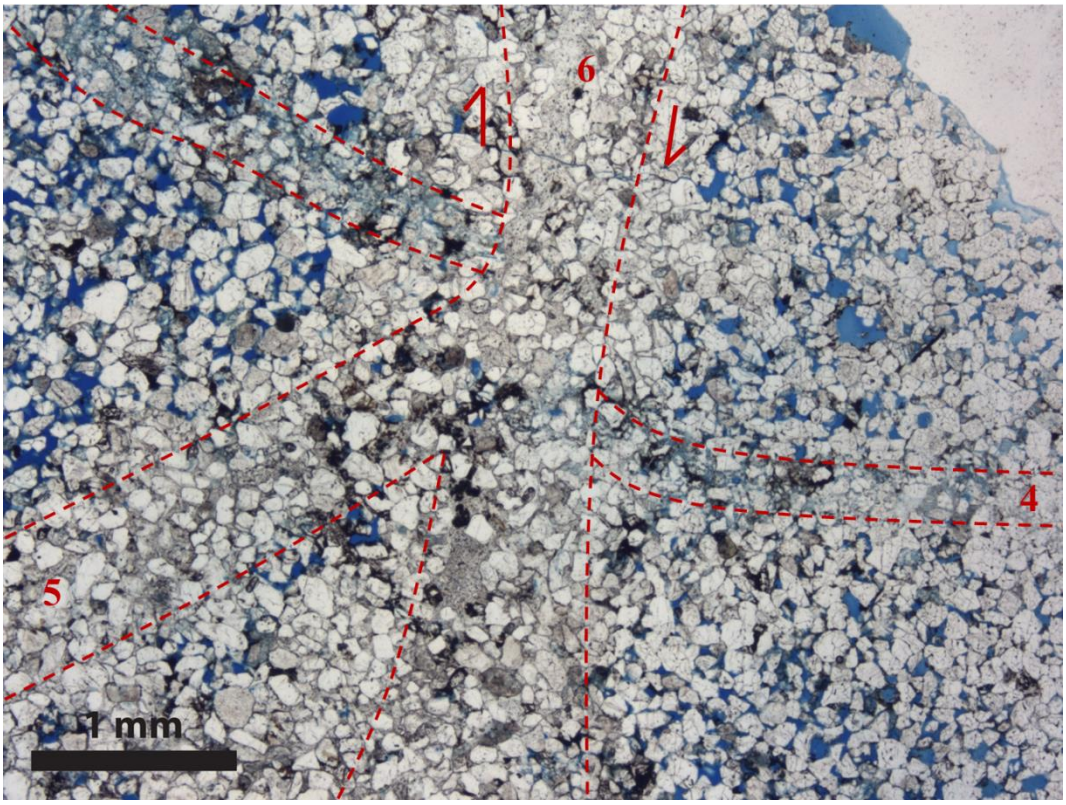

Fig. 4.19: *cataclastic population 1 band cut by a population 5 cementation band*

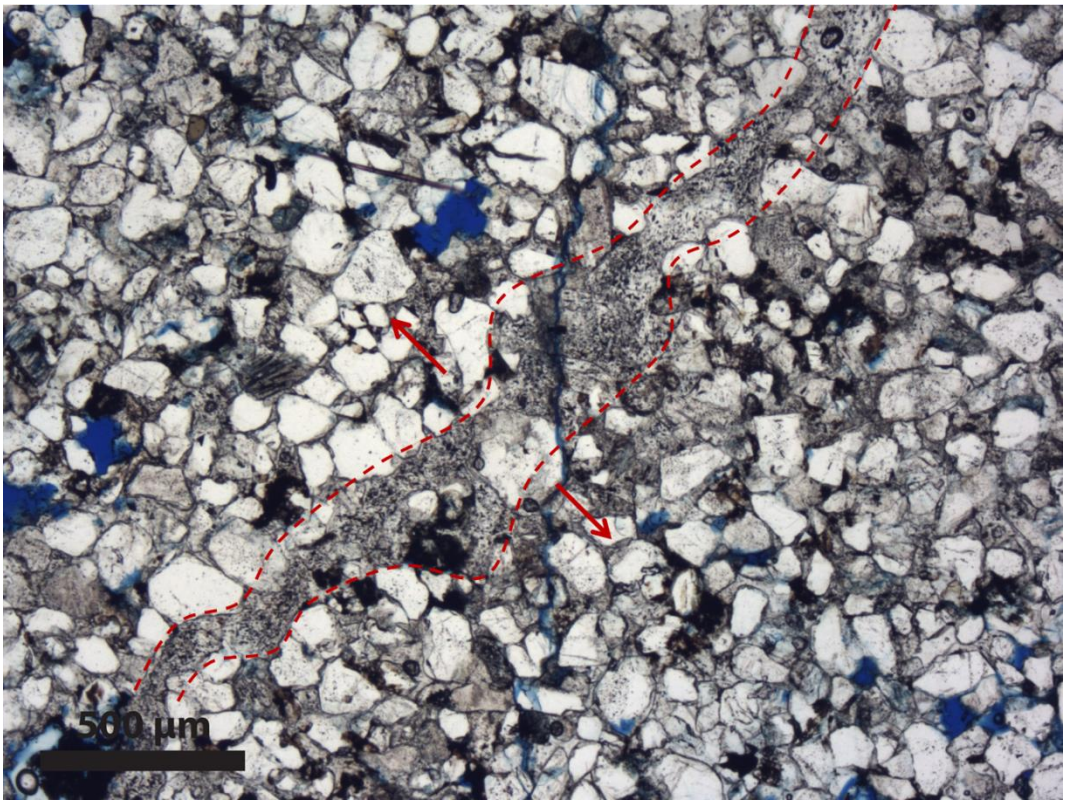

Fig. 4.20: *calcite filled extensional fracture*

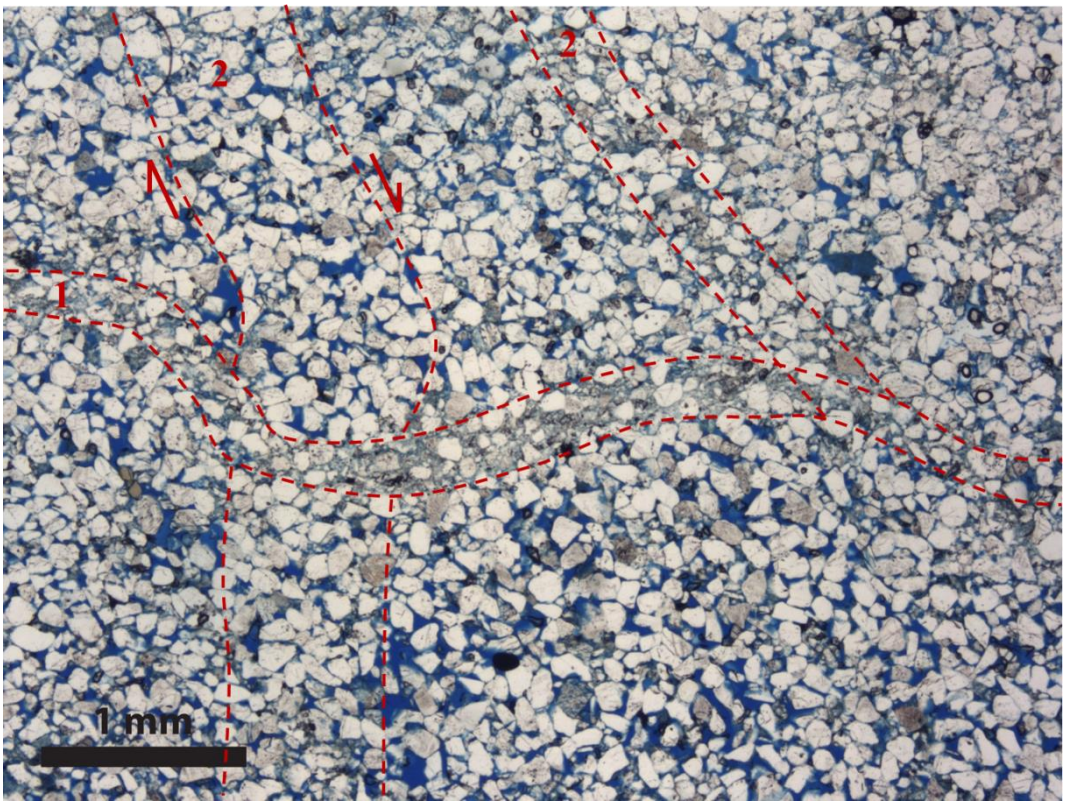

Fig. 4.21: *population 1 cataclastic kink band being moved by a population 2 disaggregation band. The population 2 deformation band to the right in the figure seem to merge into the population 1 deformation band.*

5. Discussion

The study area has been analyzed in detail during fieldwork in Mine Canyon, Utah, and later through laboratory work and data analysis. The main focus of this study was the various deformation bands, some with associated fractures, in the Navajo Sandstones and their relation to each other.

5.1 Deformation band occurrence

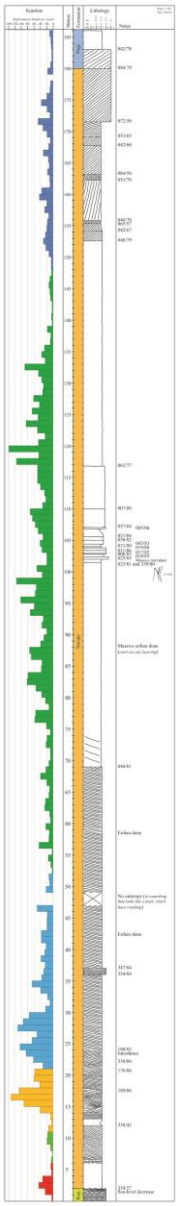

Fig. 5.11: *the scanline and stratigraphic log merged as one figure (Fig. 4.1A and 4.3). Both follow the same composite trace (Fig. 3.5).*

Data for the scanline and stratigraphic log were compiled along the same composite trace (Fig. 3.5), and this fact made it easy to compare the data. Fig. 4.1A and 4.3 has been merged into one figure (Fig. 5.1), where the meters correspond with each of the two previous figures. This new figure (Fig. 5.1) gives a statistical overview of where in the stratigraphy most of the deformation bands are located. This is just a general picture of the distribution of deformation bands throughout the Mine Canyon. Two areas immediately stand out when looking at the deformation band distribution, while the other areas along the composite trace had a lower frequency of deformation bands.

The first striking area is in the lower part of the Navajo Formation (yellow and light blue section of the trace) between 14 and 35 meters. This area mostly consists of inter-dunes with either cross-stratification or lamination. Sample TNS-03 and TNS-04 was collected in this area, and derived thin-sections suggest a host rock porosity of 15 % and 19 %, respectively (table 4.1). The grain size and roundness of the host rock in both samples are fairly similar (section 4.2.1).

The second area with a high amount of deformation bands is between 75 and 135 meters (dark green section of the trace), approximately in the middle of the Navajo Formation. This area has mostly large massive dunes, either with stacked appearance or at

places separated by thin inter-dunes. Sample TNS-01 and TNS-02A was collected in the inter-dunal section, with derived thin-sections showing a host rock porosity of 25 % and 18 %, respectively (table 4.1). The host rock in these two samples is quite different; TNS-01 is a good sorted sample while TNS-02A is less well sorted (section 4.2.1).

5.2 Structural orientations

Fig. 5.2A-F show all of the measured structures, recorded in the field, divided into populations. All the populations are color coded (legend at the bottom of Fig. 5.2). This is a stereographic representation of the same measurements as for individual locations, however, here gathered into populations. Locations are shown in Fig. 4.2.

All of the plots in Fig. 5.2A-F have a relatively obvious gathering of great circles in each stereonet, allowing general orientations to be established for further analyses. Hence, for each population an average strike and dip was extracted. This average great circle for each population was then plotted into the same stereonet (Fig. 5.2G) for easier comparison. Fig. 5.2G was again divided into two stereographic plots containing population 1, 2, and 3 (Fig 5.2H) and populations 4, 5, and 6 (Fig. 5.2I) to distinguish between the bedding systematic populations and the vertical, cross-cutting populations.

Fig. 5.2H shows that the average orientation of populations 1 and 3 has approximately the same strike and dip. This confirms that these two populations have approximately the same orientation and that population 3 is also partly following the lamination of the dunes (at least as an average). Population 2 goes in a completely different direction indicating that the population is cutting straight through the dune lamination.

Population 4 in Fig. 5.2I is, as described in Chapter 4 (section 4.1.3), isolated deformation bands with a low occurrence (n=14 in Fig. 5.2D), showing nearly bedding parallel orientation but the opposite sense of shear (than the populations 1 and 3 structures). The figure also supports the conclusion in section 5.3 about the conjugated sets of deformation bands ascribed to populations 5 and 6. The first conjugated set is population 2b and 3c, where strike and dip measurements unfortunately only were recorded for population 2 and 3 as a whole. By using these measurements; S1 is calculated through a stereographic plot to be 097/03, S2 is 196/74 and S3 is 006/16. The other is populations 5 and 6, where measurements give that S1 is 106/36, S2 is 297/54 and S3 is 200/06.

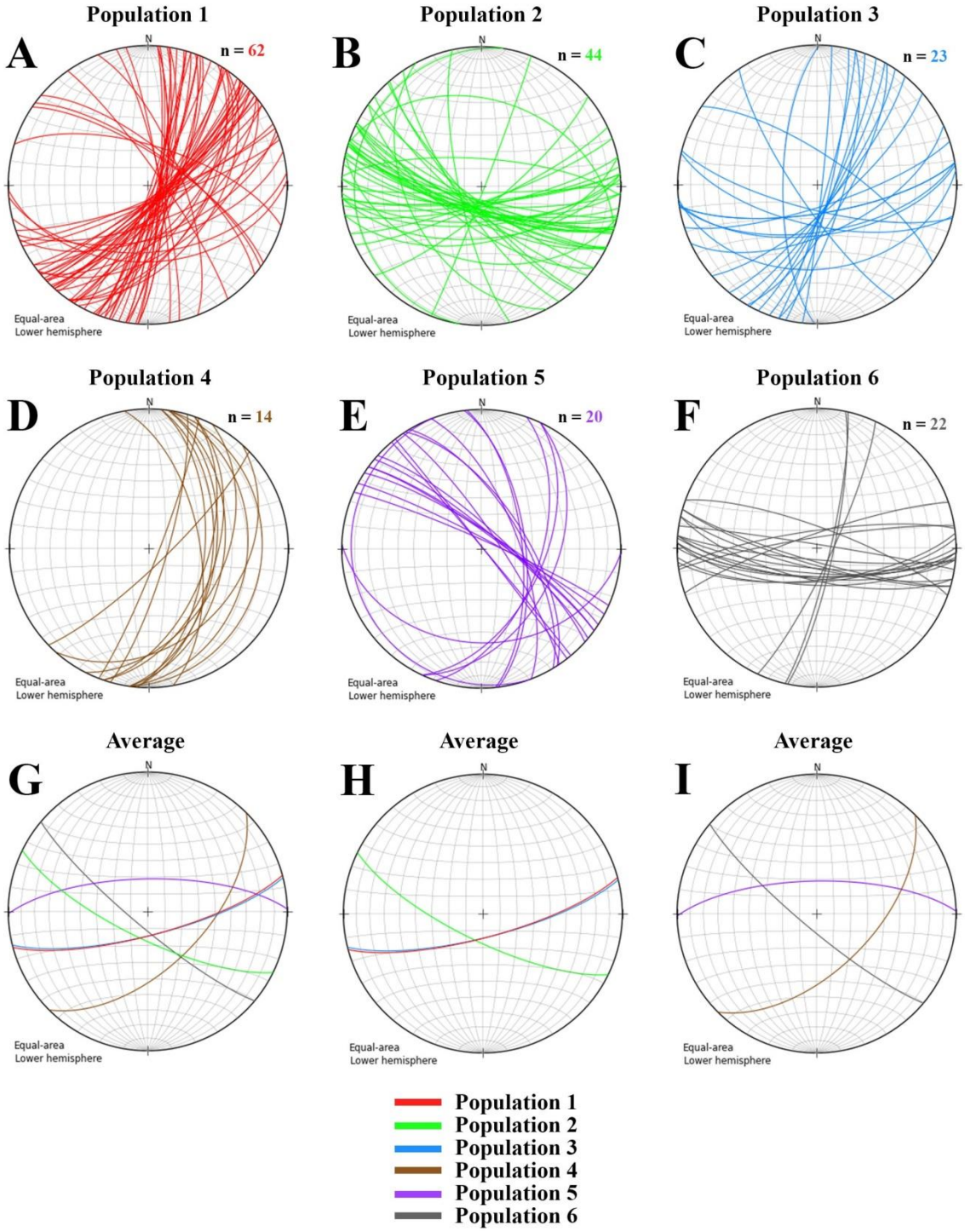

Fig. 5.2: *a revised stereographic representation of the strike and dip measurements based on populations, see Fig. 4.2. (A) population 1, (B) population 2, (C) population 3, (D) population 4, (E) population 5, (F) population 6, (G) average strike and dip for all populations, (H) average strike and dip for population 1 to 3, and (I) average strike and dip for population 4 to 6. The populations have been color coordinated, where the number of measurements for each population is given. The total number of measurements is 185.*

5.3 Chronology

The deformation bands in the study area can be divided into six populations, as described in Chapter 4. As mentioned, chronologically, population 1 is the oldest and population 6 is the youngest. This sequence of deformation is further explored below.

Population 1, 2 and 3 have a strike that parallels the overall N-S bedding orientation in the steep limb of the monocline, hence they have a strike sub-parallel to the San Rafael Swell fold axis in the area. Thereby, they reflect deformation and shear structures with transport normal on the fold axis. As shown in Fig. 4.5 and 4.6, population 1 and in a few cases population 3 is basically following the lamination of the dunes, while population 2 is cutting through the lamination.

Population 1 show down-east transport and isochoric or continental strain, which is suggested to relate to an early stage of Laramide Orogeny contraction, prior to folding of the beds. This match the interpretation of Zuluaga et al. (2014) for similar structures. Population 2 structures truncate population 1 structures as shown in Fig. 5.3, and at many locations. They show displacement of markers conforming to a top-E shear system, hence with a reverse/contractional offset compared to bedding. An overall fanning, ascribed to sub-populations 2a, 2b and 2c, is interpreted as shear-band development conforming to a fixed stress system rather than the orientation of bedding, and with the bedding progressively rotating during folding while new bands formed. Population 2 can be seen as accommodation structures, assisting the fold-limb to rotate towards the east by shearing the upward part of the limb eastward. This is conforming to a geometry and kinematic picture that has been advocated for other Laramide Orogeny monoclines (e.g., Brown, 1994). The kinematics for this population is that of shortening of bedding (contraction) by bands with a steep angle to bedding, and with tectonic transport to the east. A similar fanning as for population 2 is seen for population 3, and ascribed to progressive folding. The population 3 bands can in light of the E-verging monocline, represent back-shear structures, perhaps linked to out-of-the-syncline strain, as described by Brown (1994) for Laramide-style monoclines.

In most cases, population 3 bands cut population 2 bands; however, two observations of the opposite cross-cutting relationship suggest there is a temporal overlap between the two populations (e.g., Fig. 5.3). Hence, forward (eastward) directed shear is replaced by back-ward shear as folding progress. It can be argued from Fig. 4.13 that population 2c and 3b make up a conjugate set of deformation bands, linked to deformation within the same principal stress axes orientations. Fig. 4.13C is a good example of this conjugate set, defining a narrow bisector, by that indicating the location of S1 (sigma 1 stress axis).

Populations 4, 5 and 6 are near vertically oriented and seem consistently oriented with respect to bedding throughout the first order monocline. As they consistently truncate the population 1 to 3 structures, they were formed later in the folding evolution than the former populations. Fig. 4.9 is of a horizontal outcrop in the field and shows that population 4 is cut by both populations 5 and 6. It also shows that population 5 and 6 are cutting each other in a non-consistent fashion; accordingly, there is no obvious answer to which population is the youngest of them by looking at this figure, as seen for other locations as well. Populations 5 and 6 are therefore suggested to have approximately the same age. The most obvious difference between these two populations is the opposite shear offset they display; population 5 shows sinistral and population 6 have dextral offset of markers. Further, there is a nearly 60 degree bisector between the two populations. In sum, this suggests they formed as a conjugate set, with S1 offering a nearly E-W orientation (Fig. 5.4). Most interestingly, they record a shift in stress axes orientation, however, with S1 constant. For populations 1 to 3 S2 is horizontal, whereas for populations 5 and 6 S2 is vertical.

The population 4 bands appear to be really similar to the population 1 deformation bands, in that the bands do not seem to cut any of the other populations and have almost the same orientation. They look to be low-angle back-thrusts formed by contractional shear during late folding, e.g., population band stage 4.

Fractures developed in association with the deformation bands need further consideration. In the case of population 2, a set of en-echelon, dm-long (Riedel-oriented and some connecting Y-oriented fractures; see Hancock, 1983) shear fractures overprints the bands, but show the same orientation and kinematics as the bands. This is seen in Fig. 4.6. This close relationship between the band swarm and fractures suggest the fractures formed by progressive shear during the same event.

Another fracture system is seen in association with population 5 and 6, as documented in Fig. 4.9. These fractures are different from those associated with population 3 in that their association to the deformation bands shows a different evolution. Population 5 and 6 bands are dilational (see below), and change from bands to fracture along strike, making a convincing temporal link between fractures and bands.

The chronology presented in Zuluaga et al. (2014) of the San Rafael Swell do not fit with the populations found during this study, and the article divided the evolution of deformation bands into four stages, shortly summarized here;

- Stage 1 = bedding parallel band formation
- Stage 2 = increased strain developing conjugated sets
- Stage 3 = rotation of preexisting bands creating ladder-zones
- Stage 4 = thick clusters of bands

This evolution could be seen in populations 1 to 3, in what is called early stage of the folding (relative speaking) in this study. The later stage (populations 5 to 6) described above only have Zuluaga et al. (2014)'s second stage.

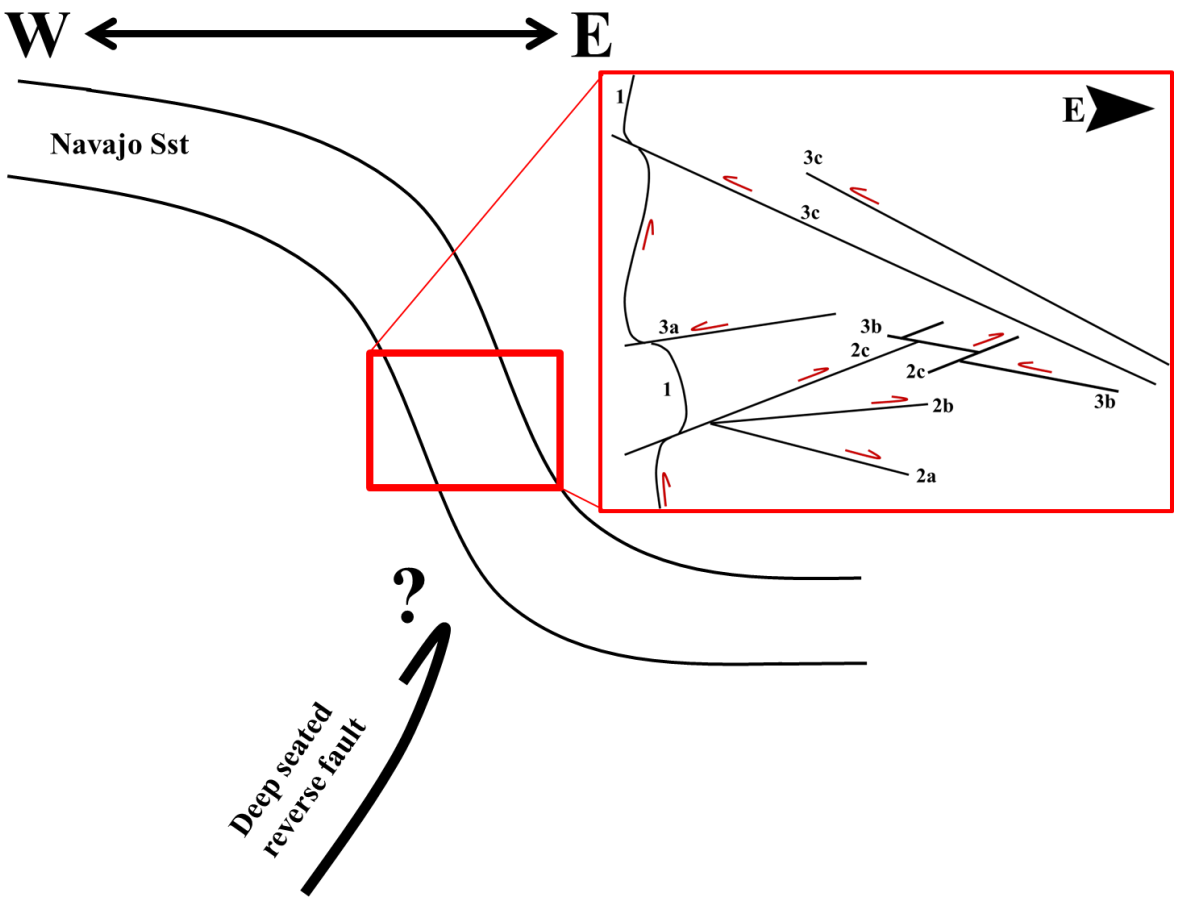

Fig. 5.3: *relationship of populations 1, 2 and 3, and their approximate location in the San Rafael Swell.*

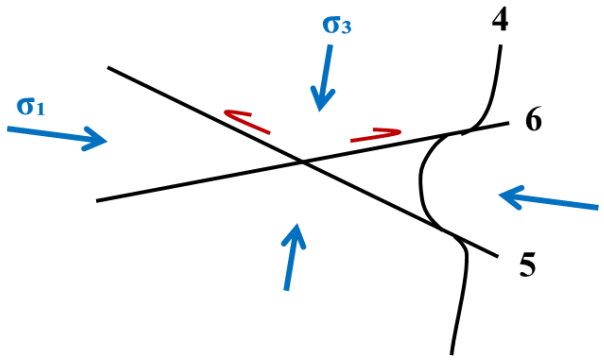

Fig. 5.4: *relationship of populations 4, 5 and 6.*

I took a look at a couple of other folds to correlate if the fracture pattern was similar in other places. The first one I looked at was the Monkshood anticline, Western Canada, another Laramide-style fold. The most common deformation features in this fold is extensional fractures oriented at high angles to bedding, which form in distinct orientation sets (Jamison, 1997). Another was a combination of anticlines in the Zagros fold and thrust belt from Lurestan Province, Zagros Mountains, Iran. Here fractures were represented by either joints or veins (cemented fractures) as both stratabound and non-stratabound, where the veins were filled with calcite. The orientation was perpendicular to bedding, and they were in several locations arranged in en-echelon arrays (Casini et al., 2011).

Both of these folds have fracture systems with similarities to what was seen in Mine Canyon, but more to the deformation bands than the fractures. The fractures in these other locations was in general extensional fractures (Jamison, 1997, Casini et al., 2011), where in Mine Canyon slip-surface fractures is more common, with dilation at the end for the fractures associated with population 5 and 6 (Fig. 4.17).

5.4 Structural kinematics and deformation mechanisms

All the six populations were studied thoroughly to determine the different kinematic classifications and deformational mechanisms ascribed to each population. This documentation is covered in Chapter 4, and summarized below.

Population 1

The population 1 deformation bands are described in Fig. 4.16 and 4.21, and offer a complete picture of the population. In both these locations, deformation bands show significant grain crushing (cataclasis) and a low porosity compared to the host rock, but there is limited

evidence of shearing. A few observations of population 1 bands with shear offset of lamination, especially in the inter-dunes, suggest a minor shear element on the structures. This element could be suppressed by the bands nearly exclusively following lamination and dune interfaces. The total dataset points to deformation bands being cataclastic compaction mild-shear bands, as summarized in Fig. 5.5.

On the contrary to the overall impression of the bands outlined above, the interpretation of the population 1 band in Fig. 4.16 is that the band has undergone dilation. This extensional strain seems to reflect orientation of dune lamination which, when dipping down in the direction of tectonic transport, was reactivated as a dilation structure. As most dune forest laminae face the tectonic transport, the most common structures experienced compaction and some shear.

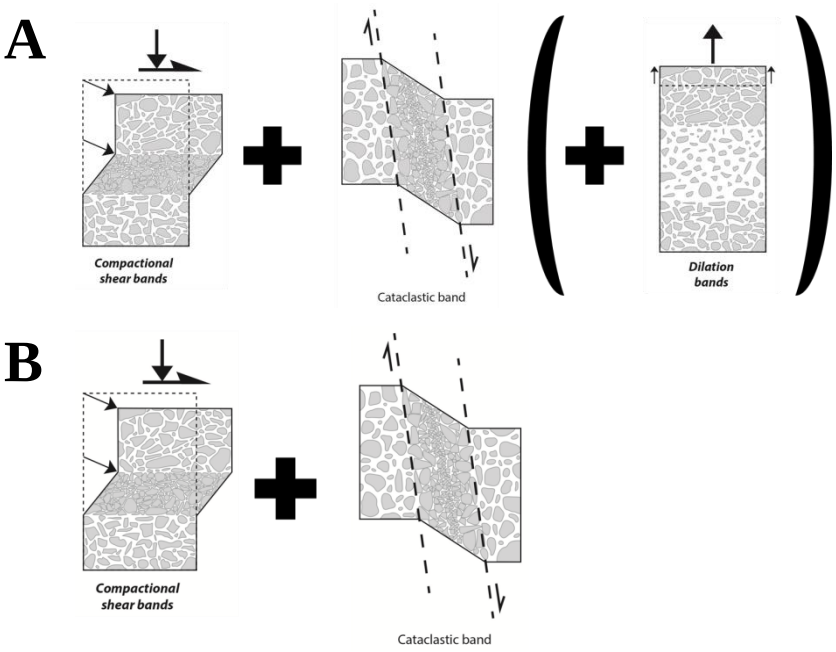

Fig. 5.5: *the population 1 deformation bands found in Mine Canyon where (A) is cataclastic compactional-shear bands with reactivation as a dilational structure, and (B) is cataclastic compactional-shear bands.*

Population 2

As outlined in Figs. 4.16 and 4.21, the classification of the population 2 deformation bands found in the study area is a bit difficult to pinpoint, as they do not fit one specific kinematic classification and deformational mechanism.

The first population 2 deformation band studied (Fig. 5.6A) was the one in Fig. 4.16. This band was earlier described with a high degree of crushing, conforming to a cataclastic band. There seem to be compaction involved during the creation of the band, and based on

this (and the obvious shear in Fig. 4.16) the population 2 band in Fig. 4.16 can be interpreted as a cataclastic compactional-shear band (Fig. 5.6A).

Fig. 5.6B and C is two completely different population 2 deformation bands, both found in Fig. 4.21. They both conforms to population 2 bands due to the east-verging tectonic transport. Description of the bands based in thin-section (Fig. 4.21) shows that the population 2 deformation band here has a slightly higher porosity than the surrounding host rock, and that grains within the band are basically intact. This, accompanied with the evident shear in Fig. 4.21, gives reason to classify the band as a dilational-shear disaggregation band (Fig. 5.6B). The population 2 band to the right in Fig. 4.21, on the other hand, has reduced pore space and grain crushing, but show no obvious evidence for shear. This band is therefore described as a cataclastic compaction band that could have a shear element in Fig. 5.6C.

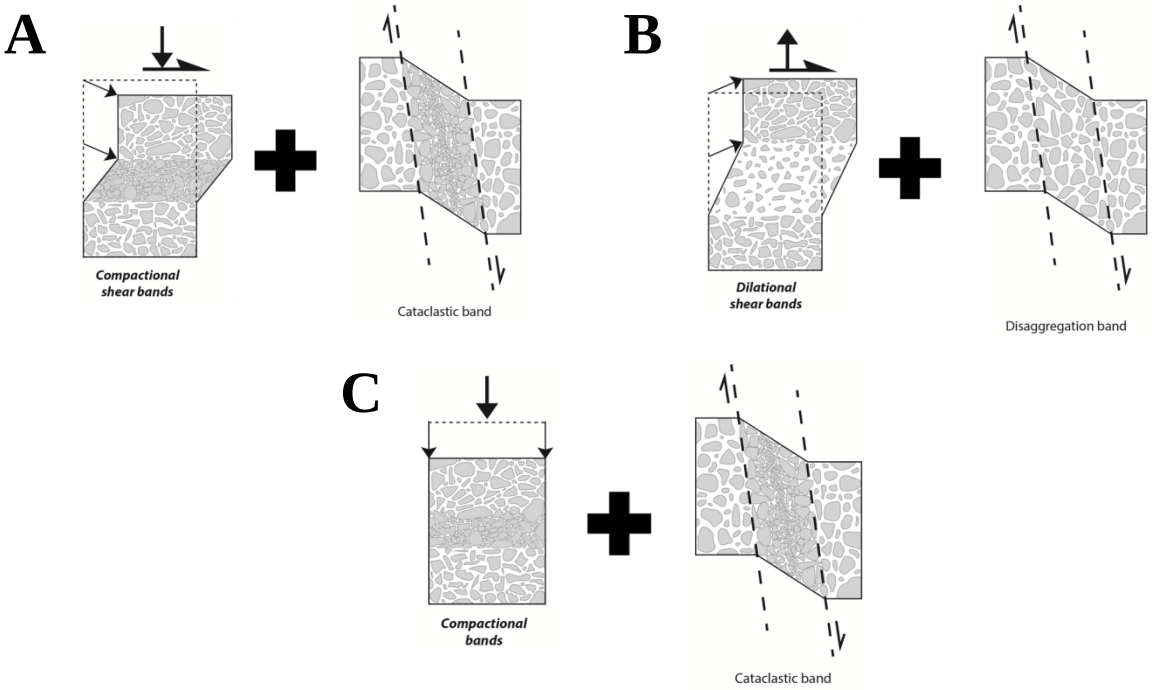

Fig. 5.6: *the population 2 deformation bands found in Mine Canyon, where (A)is cataclastic compactional-shear bands, (B) is dilational-shear disaggregation bands, and (C) is cataclastic compaction bands.*

Population 3

The analysis of the population 3 deformation band was only observed during fieldwork and by studying photographs from the field; no thin-section was available. The analysis is therefore less complete than for other populations. However, the white, very fine grained bands appear similar to other cataclastic compactional-shear bands (Fig. 5.7).

This conclusion is based in the following facts: Population 3 bands studied closer are found in Fig. 4.7B and 4.13. The white color inside the bands and a very fine grained matrix under hand-lens gives an indication of cataclasis in the deformation bands. It is a bit more complicated to determine the kinematic classification of the bands, but in these figures it seems that the bands have volumetric decrease coupled with top-W shear.

For the mentioned shear fractures closely associated with the bands, the mechanism would be that of shear related compaction, in which porosity was lost during band formation. At a threshold porosity (<12-15 %; e.g., Fossen et al., 2007a), when the rock is saturated with bands, the fractures start to form. Noticeably, they record a shift from compaction by band to dilation by fracturing.

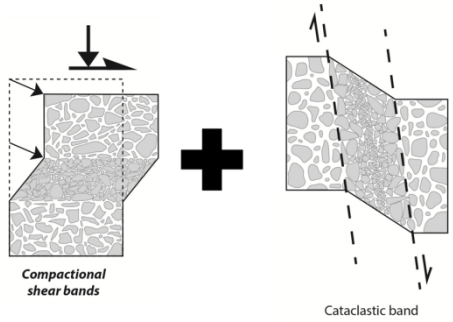

Fig. 5.7: *the population 3 deformation bands in Mine Canyon were found to be cataclastic compactional-shear bands.*

Population 4

The population 4 deformation bands were studied in Fig. 4.18 and 4.19. This population is really similar to the population 1 bands described above, but are treated separately as they appear to have up-to-the-west and low-angle-to-bedding shear. They show significant crushing and very little pore space within them, and limited evidence of shear. This population is in Fig. 5.8 interpreted as cataclastic compactional (-shear) bands.

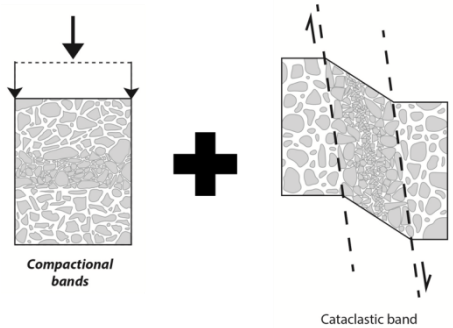

Fig. 5.8: *the population 4 deformation bands in Mine Canyon were found to be cataclastic compactional (-shear) bands.*

Population 5

The population 5 deformation bands were studied using Fig. 4.17, 4.18 and 4.19. Both of the analyzed bands in Fig. 4.17 and 4.18 display some degree of shearing. There was no obvious shearing in Fig. 4.19, but fieldwork and other figures (seen in section 4.1.6) show a clear shear direction. All of these bands showed significant volumetric increase, as described earlier. There was on the other hand no evidence of crushing within the bands in any of the figures, but there was observable fracturing (possibly secondary) of the grains in the bands. This information gives reason to conclude that the population 5 deformation bands are dilation shear disaggregation bands (Fig. 5.9A).

Population 5 and 6 bands show fracture patches along strike, suggesting they are of the same age. The considered deformation mechanisms for this development is that dilation of the sandstone during deformation caused short fractures to form together with dilation bands, probably related to mild differences in cohesion of the rock.

Secondary filling (Fig. 5.9B, secondary filling displayed by the parenthesis) is observed in two of the population 5 bands, suggesting granular substances were able to fill the pore space in an already formed deformation band and/or fracture, likely linked to the volumetric increase. This increase of volume opens up for secondary cementation, as seen in Fig. 4.19, consistent with precipitation from fluids filling the accumulated space (Fig. 4.18). In the case of Fig. 4.18, the population 5 band is filled with MnO, and the pore space in the band in Fig. 4.19 is cemented with calcite.

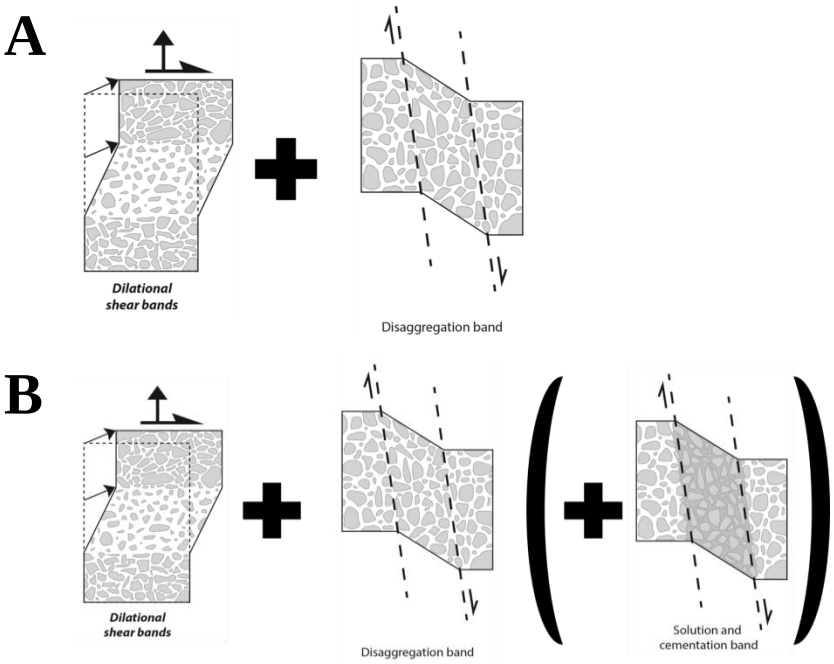

Fig. 5.9: *the population 5 deformation bands found in Mine Canyon where (A) is dilational-shear disaggregation bands, and (B) is dilational-shear disaggregation bands with secondary calcite cementation.*

The plug in the lower right corner of Fig. 5.10 show the deformation band populations outlined. The population 5 band is not visible above the crack in the sample, but that is as would be expected for a disaggregation band, whereas the lower part of the plug has deformation bands filled with cement. One theory is that the crack seen in the plug is a fracture and that the calcite has only seeped in on one side of this fracture, making the deformation bands on the other side indistinguishable to the naked eye. Fig. 4.19 shows what looks like a deformation band being slit down the middle into two bands by a populations 5 and 6 structures. As seen on the right part of the population 4 band, the cataclastic band here is almost not distinguishable from the broken-up host rock, which is saturated with deformation.

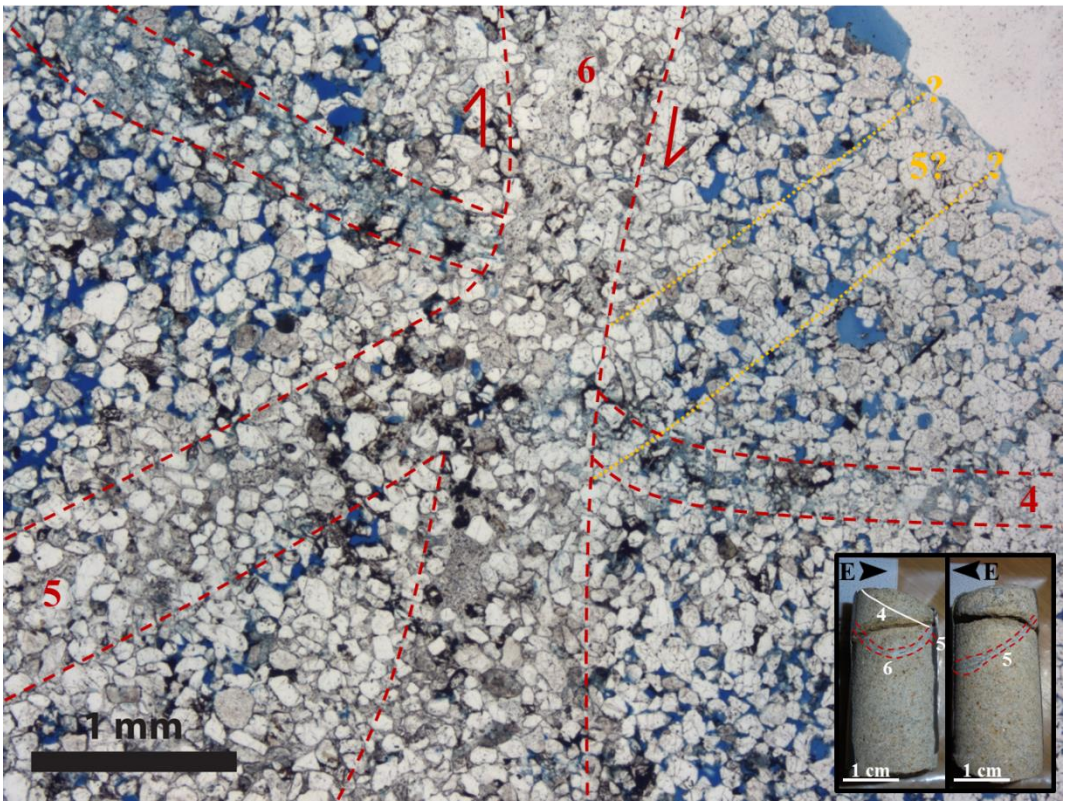

Fig. 5.10: *based on Fig. 4.19. The yellow dashed lines show the possible other side of the population 5 deformation band. The plug in the lower right corner shows the intersection of the bands.*

Population 6

The studied population 6 structures, as shown in Figs. 4.17 and 4.19, show a close relationship to population 5 structures. In outcrops, the dilational nature and close association with shear-fracture formation is well established. Observations from thin-section complicate

however this picture. Accordingly, this population was difficult to classify by one specific kinematic style and deformational mechanism due to the different appearance of the two bands found in the thin-sections. However, most bands show a dilational component, despite also showing signs of grain crushing.

The band in Fig. 4.17 has previously been described as a band with a lot of crushing along the margin. As it hosts a fracture, a shear fracture formed along the deformation band. Fracture walls suggest there was a cataclastic compactional-shear band in place prior to fracturing. Alternatively, the initiation of the shear fracture caused grain crushing prior to mild dilation opening. The increase of volume by fracturing suggests this is a type of shear-dilation structure, as shown in Fig. 5.11A (displayed by the parenthesis).

The other studied population 6 band is shown in Fig. 4.19. This band shows no evidence of grain crushing and instead suggests an overall volumetric increase. It displays a clear shear offset of lamination. The band experienced infill of calcite cement after formation, and is therefore described as a dilational shear disaggregation band with secondary cementation (Fig. 5.11B) filling the residual pore space.

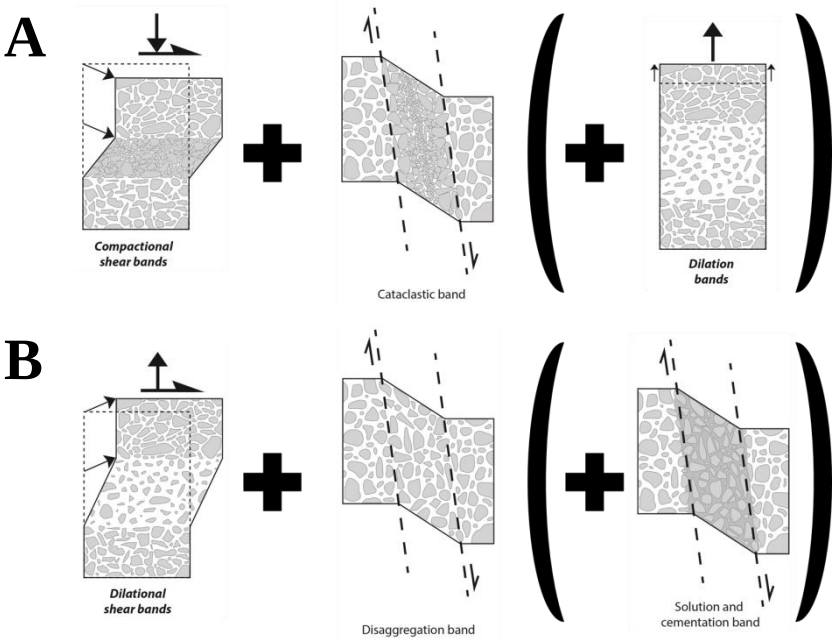

Fig. 5.11: *the population 6 deformation bands found in Mine Canyon where (A) is cataclastic compactional-shear bands prior to dilational fracturing, and (B) is dilational-shear disaggregation bands with secondary calcite cementation.*

Comparison to previous studies

Mostly literature refers to compactional-shear bands as the most common deformation bands to form (Fossen et al., 2007a, Du Bernard et al., 2002, Fossen, 2010, Ballas et al., 2012, Rotevatn et al., 2013). This makes most of the deformation bands found in my study area unusual, since at least half of the populations categorized during this study have been classified as dilational-shear bands.

Davatzes and Aydin (2003) proposed that fractures can overprint existing deformation bands due to the already present physical discontinuity. This approach is a two stage evolution where for example en-echelon fractures are forming first, and then at a later stage these fractures will be connected be a joint (see stage 3 in Fig. 1; Davatzes and Aydin, 2003). Another approach is Rotevatn et al. (2008) proposing that cataclastic deformation bands can have a central discrete slip surface with intense cataclasis, higher offsets, lower permeability, but higher porosity than the normally described cataclastic deformation bands. These new bands are referred to as "slipped deformation bands" or Sinai bands, and they show minimal compaction during simple shear due to strain softening in their evolution. The Sinai bands do not have a compaction zone along the margin of the band, but instead have a sharp transition between the core of the band and the host rock.

Population 2 shows en-echelon fracturing within the deformation band in Fig. 4.6b (as mentioned above). Fig. 4.16 on the other hand tell another story, as explained in Chapter 4, the thin-section show a lot of cataclasis with the population 2 band cutting population 1. It also shows large areas of pore space within the cataclasis, and that is an indication of this being a Sinai band (explained above). It is possible to observe the transition between the band and the host rock in this thin-section (Fig. 4.16), but the other indications of this type of band can be observed in the sample. This population can therefore be explained as a band in a gradual transition to become a fracture. This transition from bands to fractures is unusual, and not covered in literature, with the exception of Rotevatn et al. (2008).

The population 6 deformation band, explained above, (seen in Fig. 4.17) are known as a faulted deformation band (Fossen et al., 2007a) due to the formation of a slip surface with late dilation inside the already existing deformation band. The population 3 deformation bands also display fracturing after band formation, but this is a compaction experiencing dilational fracturing.

Dissolution or cementation bands, according to Fossen et al. (2007a), occur commonly after deformation band formation. This fit well with the results gathered for populations 5 and 6, which have experienced infill of either calcite or MnO after volumetric increase, creating

cementation bands. Du Bernard et al. (2002) proposed that dilation and shear bands typically are susceptible to infill of pore space (preferentially by clay, kaolinite, chlorite, iron oxides or organic matter). This infiltration will prevent pore collapse after seized formation, and Fig. 4.17 is a great example of this. The figure show two dilation bands of population 5 where one of them are filled with MnO as a secondary oxide and the other band have no infill. The band with MnO is significantly thicker than the one without infill, which can indicate that the second band has experienced pore collapse after formation.

Fig. 5.12 show a modified figure from Zuluaga et al. (2014) where the populations in this study has been compared to with this figure. Fig. 5.12A show bands formed when the bedding was completely horizontal (0 degree angle). The population 1 bands found in this study are following the lamination with a top-W shear direction. This is the same finding as Zuluaga et al. (2014).

Fig. 5.12B show the bedding with a 25 degree dip in Zuluaga et al. (2014)'s figure. At this time the deformation bands enter stage 1 of Zuluaga et al. (2014)'s evolution, which is bedding parallel band formation (see section 5.3). The deformation bands I observed were formed in a fanning fashion with top-E contraction-to-bedding and about 10 degrees between the three sub-populations and were characterized as population 2a-c deformation bands. The bedding is assumed to have an angle of 20-30 degrees during this formation.

Fig. 5.12C show the bedding with a 50 degree dip in Zuluaga et al. (2014)'s figure and the deformation bands entered stage 2 of Zuluaga et al. (2014)'s evolution, which is increased strain developing conjugated sets (see section 5.3). In this study the deformation bands are described as top-W extensional-to-bedding and formed in a fanning fashion with about 10 degrees between the three sub-populations. These bands are characterized as population 3a-c deformation bands and the bedding is assumed to have an angle of 45-55 degrees during this formation.

Fig. 5.12D show the bedding with a 65 degree dip in Zuluaga et al. (2014)'s figure. At this time the deformation bands enter stage 3 of the evolution, which is rotation of preexisting bands creating ladder-zones (see section 5.3). The deformation bands formed during this angle of dip was the population 4 bands with a top-W shear direction.

Fig. 5.12E is displayed in mapview due to the vertical formation of the bands. The dip angle of bedding was at this time above 65 degrees and population 5 and 6 formed as conjugated sets of deformation bands with lateral extrusion.

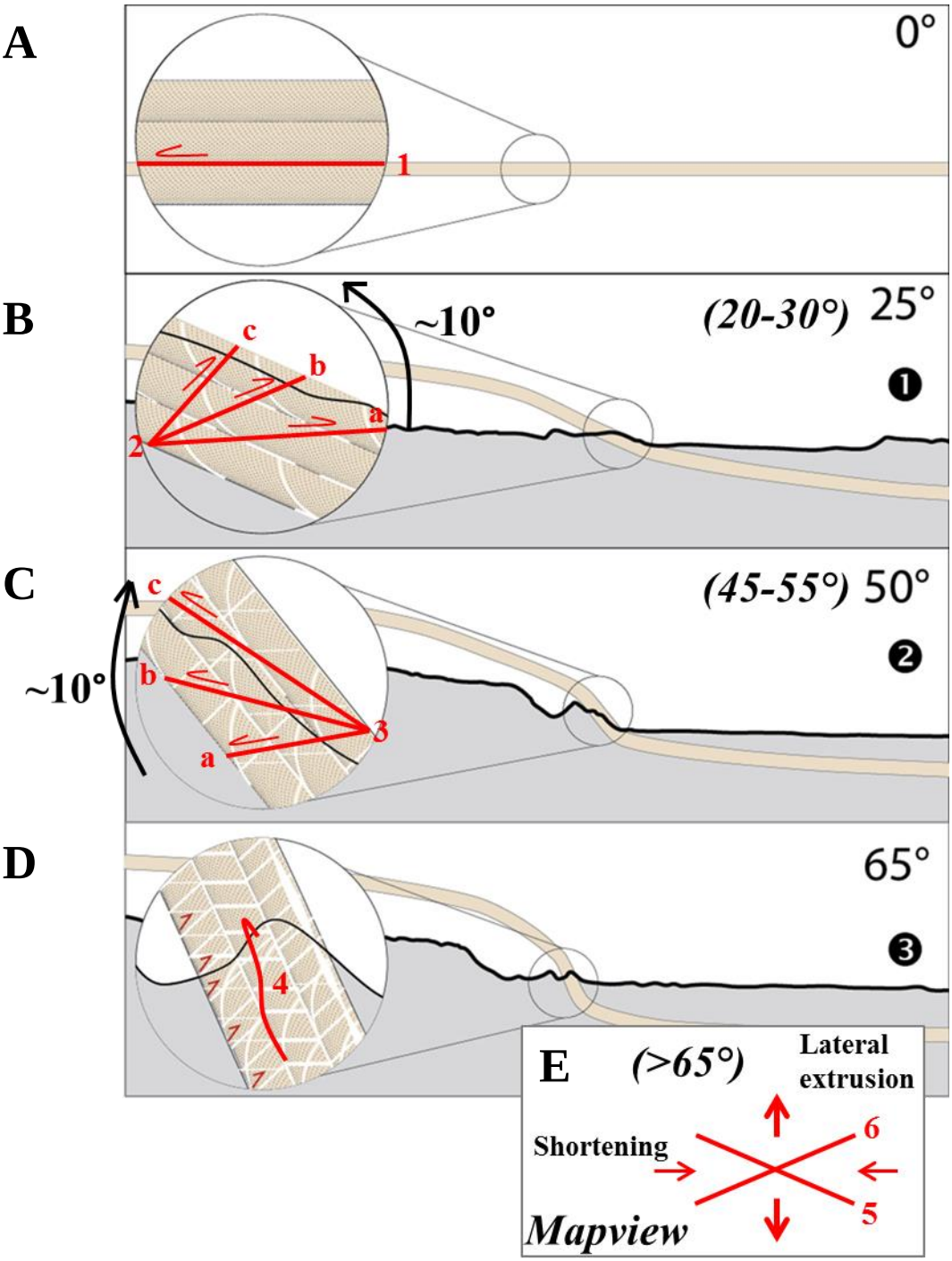

Fig. 5.12: *comparison between the populations I found in the Min Canyon versus what Zuluaga et al. (2014) found and documented. Modified from Zuluaga et al., 2014.*

5.6 q-p diagram

This section is based on section 5.4; here I am placing the different populations into the q-p diagram (commonly known as the Cam-cap curve, see section 3.1.3). For further reading on this type of plot, the reader is referenced to Schultz and Siddharthan (2005), and Fossen et al. (2007a). The populations are renamed to P1 to P6 for the simplicity of fitting in the diagram. In this diagram only the initial kinematic classification described in section 5.4 is taken into account, which is a simplification but confirms to the overall observations.

Population 1 (P1 in Fig. 5.13) was classified as compactional shear bands. The shear mentioned above was not that extensive; hence P1 has a volume decrease (compaction) and a small amount of shearing (close to the p-axis).

Population 2 ($P2_1$ and $P2_2$ in Fig. 5.13) shows two types of kinematics on different locations in the field. $P2_1$ was classified as compactional shear bands, while $P2_2$ classify as dilational shear bands. The $P2_1$ bands had extensive volume decrease, but displayed more shearing than the P1 bands. They are therefore placed right above P1 in the diagram (Fig. 5.13). $P2_2$ on the other hand is classified as dilational shear bands. These bands displayed more shearing than the other dilational bands in the analysis but with a moderately amount of shearing. They are accordingly placed approximately in the middle of the volume increase half of Fig. 5.13 due to the combination of shear and dilation.

Population 3 (P3 in Fig. 5.13) was classified as compactional shear bands based on field observations. The bands display significant shear, but the amount of volume decrease is difficult to determine without thin-sections. These bands were therefore placed closest to the pure shear-line in the diagram.

Population 4 (P4 in Fig. 5.13) was classified as compaction bands; however, there is a question around possible shearing, which was never resolved due to low occurrence of this population in the field. These bands cut straight through the bedding in a vertical direction (see sections 4.1.3 and 5.3). Anyhow, P4 was categorized as pure compaction bands and placed on the p-axis.

Population 5 (P5 in Fig. 5.13) was classified as dilational shear bands. These bands had a small amount of shearing and significant volume increase. They are therefore placed closest to pure dilation (at the p-axis) out of all of the populations.

Population 6 ($P6_1$ and $P6_2$ in Fig. 5.13) had two types of kinematics on different locations in the field. $P6_1$ was classified as compactional shear bands, while $P6_2$ classified as dilational shear bands. The $P6_1$ bands displayed volume decrease with a lot of shearing and was placed right below P3 in the diagram (Fig. 5.13). $P6_2$ on the other hand showed

significant volume increase and extensive shearing. They were placed right below $P2_2$ because $P6_2$ showed more dilation than the P2 bands.

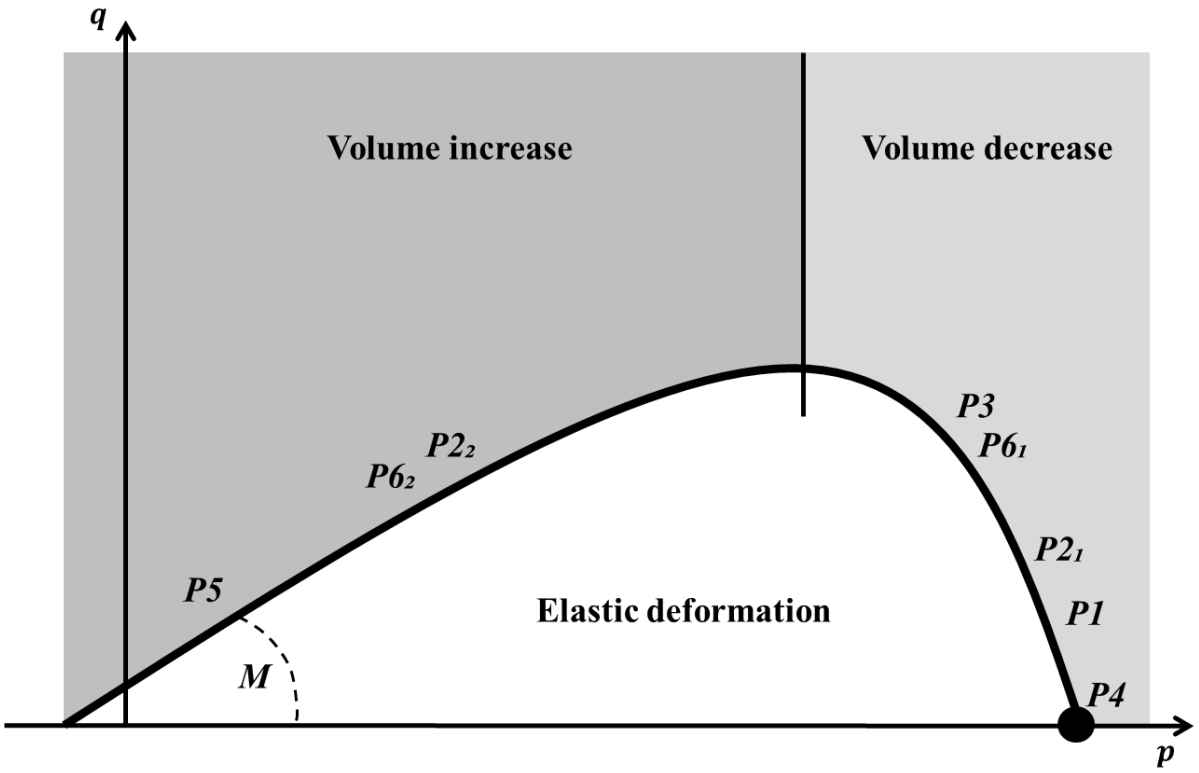

Fig. 5.13: *q-p diagram applied to the deformation bands found in the study area. P1-P6 is explained in the text above. Figure is modified from Schultz and Siddharthan (2005).*

6. Conclusion

1) San Rafael Swell, Laramide monocline
2) Deformation related to folding of the Navajo Sandstones
3) Six populations, reflecting forward (E) and backward (W) directed shear kinematics in the east-verging monocline at various stages of folding.
4) Overall deformation mechanisms is by shear-related cataclastic deformation bands, but significant variability exist, with band swarms progressing into shear fractures and dilation bands showing patches of shear-fracture development. Many of the transitions from bands to fractures have not been fully explored in the literature, and thereby offer new learning on such deformation systems.

Three hypotheses were suggested in Chapter 1:

4. *Deformation band sets developed with a given angle to dip of bedding during progressive folding, reflecting fixed stress axes (model of Zuluaga et al., 2014).*
   - **confirmed**
5. *Conjugate deformation band sets reflect overall horizontal shortening, rather than events of accommodation structures caused by space problems.*
   - **confirmed**
6. *Deformation band swarms transgressed into slip-surface with accumulated slip within a fixed kinematic system.*
   - **Deformation band swarms developed into both dip-slip fractures and as gradual transition to fractures due to the close relationship between band swarms and fractures, and was formed by progressive shear during the same event.**

Further studies are suggested on the population 3 deformation bands to conform observations reported during this study. Studies are also suggested on these unusual dilational deformation bands to uncover all of their secrets, and last but not least to dive further into the kinematics and mechanisms of these Sinai bands (deformation bands gradually transitioning to fractures).

7. References

Allen, P.A. & Dublin, T.C., 1996. Jurassic giant erg deposits , flexure of the United States continental interior , and timing of the onset of Cordilleran shortening. , pp.2–5.

ASCscientific, 1998. Portable Rock Core Drills & Core Orienting Fixtures. Available at: http://www.ascscientific.com/drills.html [Accessed January 23, 2017].

Aydin, A., Borja, R.I. & Eichhubl, P., 2006. Geological and mathematical framework for failure modes in granular rock. *Journal of Structural Geology*, 28(1), pp.83–98.

Aydin, A. & Johnson, A.M., 1978. Development of faults as zones of deformation bands and as slip surfaces in sandstone. *Pure and Applied Geophysics PAGEOPH*, 116(4–5), pp.931–942.

Ballas, G. et al., 2013. Shear-enhanced compaction bands formed at shallow burial conditions; implications for fluid flow (Provence, France). *Journal of Structural Geology*, 47, pp.3–15. Available at: http://dx.doi.org/10.1016/j.jsg.2012.11.008.

Beitler, B., Parry, W.T. & Chan, M.A., 2005. Fingerprints of Fluid Flow: Chemical Diagenetic History of the Jurassic Navajo Sandstone, Southern Utah, U.S.A. *Journal of Sedimentary Research*, 75(4), pp.547–561.

Beitler, B., Chan, M.A. & Parry, W.T., 2003. Bleaching of Jurassic Navajo Sandstone on Colorado Plateau Laramide highs: Evidence of exhumed hydrocarbon supergiants? *Geology*, 31(12), pp.1041–1044.

Blakey, R.C., Peterson, F. & Kocurek, G., 1988. Synthesis of late Paleozoic and Mesozoic eolian deposits of the Western Interior of the United States. , 56.

Brown, W.G., 1993. Structural style of Laramide basement-cored uplifts and associated folds. In *Geolofy of Wyoming*.

Casini, G. et al., 2017. Sub-seismic fractures in foreland fold and thrust belts : insight from the Lurestan Province , Zagros Mountains , Iran.

Condon, S.M., 1997. Geology of the Pennsylvanian and Permian Cutler Group and Permian Kaibab Limestone in the Paradox Basin, Southeastern Utah and Southwestern Colorado. *U.S. Geological Survey Bulletin*, p.46. Available at: http://pubs.usgs.gov/bul/b2000p/b2000p.pdf.

Davatzes, N.C. & Aydin, A., 2003. Overprinting faulting mechanisms in high porosity sandstones of SE Utah. *Journal of Structural Geology*, 25(11), pp.1795–1813.

Du Bernard, X., Eichhubl, P. & Aydin, A., 2002. Dilation bands: A new form of localized failure in granular media. *Geophysical Research Letters*, 29(24), pp.21–29. Available at: http://www.scopus.com/inward/record.url?eid=2-s2.0-0038066524&partnerID=40&md5=d864961e5dc1e96a1a4e1b89954e82f3.

Fossen, H. et al., 2007. Deformation bands in sandstone: a review. *Journal of the Geological Society*, 164, pp.755–769.

Fossen, H., 2010. Chapter 7: Fracture and brittle deformation. In *Structural Geology*. Cambridge University Press, pp. 119–149.

Fossen, H. & Bale, A., 2007. Deformation bands and their influence on fluid flow. *AAPG Bulletin*, 91(12), pp.1685–1700.

Fossen, H. et al., 2007. Deformation Bands: Strain Localization Structures in Highly Porous Sandstone. *American Geophysical Union, Fall Meeting 2007, abstract #T33C-1502*. Available at: http://adsabs.harvard.edu/abs/2007AGUFM.T33C1502F [Accessed November 2, 2016].

Gibson, R.G., 1998. Physical character and fluid-flow properties of sandstone-derived fault zones. *Geological Society, London, Special Publications*, 127(Table 1), pp.83–97.

Grohmann, C.H. & Campanha, G.A., 2010. TI : OpenStereo : Open Source , Cross-Platform Software for. *Abstract presented at AGU 2010 Fall Meeting*. Available at: http://www.igc.usp.br/openstereo.

Hancock, P.L., 1985. Brittle microtectonics: principles and practice. , 7.

Hood, J.W. & Patterson, D.J., 1984. Bedrock aquifers in the northern San Rafael Swell area, Utah, with special emphasis on the Navajo Sandstone. *State of Utah, Department of Natural Resources, Technical Publication No. 78*.

Jamison, W.R., 1997. Quantitative Evaluation of Fractures on Monkshood Anticline , a Detachment Fold in the Foothills of Western Canada 1. , pp.1110–1132.

Jones, L.S. & Blakey, R.C., 1997. Eolian-fluvial interaction in the Page Sandstone (Middle Jurassic) in south-central Utah, USA — a case study of erg-margin processes. , 109, pp.181–198.

Kocurek, G., 2003. Limits on extreme eolian systems: Sahara of Mauritania and Jurassic Navajo Sandstone examples. *Special Paper 370: Extreme depositional environments: mega end members in geologic time*, pp.43–52. Available at: http://specialpapers.gsapubs.org/cgi/doi/10.1130/0-8137-2370-1.43.

Labuz, J.F. & Zang, A., 2012. Mohr-Coulomb failure criterion. *Rock Mechanics and Rock Engineering*, 45(6), pp.975–979.

Mathis, A.C., 2000. Capitol Reef National Park and Vicinity Geologic Road Logs , Utah. *Geologic Road, Trail, and Lake Guides to Utah's Parks and Monuments 2000*.

Mollema, P.N. & Antonellini, M.A., 1996. Compaction bands: A structural analog for anti-mode I cracks in aeolian sandstone. *Tectonophysics*, 267(1–4), pp.209–228.

Narr, W. & Suppe, J., 1991. Joint spacing in sedimentary rocks. *Journal of Structural Geology*, 13(9), pp.1037–1048.

Olsson, W.A., 1999. Theoretical and experimental investigation of compaction bands in porous rock. , 104(B4), pp.7219–7228.

Pollard, D.D. & Fletcher, R.C., 2005. *Fundamentals of Structural Geology* 1. Edition., Cambridge University Press.

Pollard, D.D. & Aydin, A., 1988. Progress in understanding jointing over the past century Progress in understanding jointing over the past century. *Geological Society of America Bulletin*, 100(8), pp.1181–1204.

Rasband, W., 2004. ImageJ website. *National Institutes of Health, USA*. Available at: https://imagej.nih.gov/ij/docs/index.html [Accessed January 15, 2017].

Rotevatn, A. et al., 2013. Deformation bands and their impact on fluid flow in sandstone reservoirs: The role of natural thickness variations. *Geofluids*, 13(3), pp.359–371.

Rotevatn, A. et al., 2008. Slipped deformation bands : A new type of cataclastic deformation bands in Western Sinai , Suez rift , Egypt. *Journal of Structural Geology*, 30(11), pp.1317–1331. Available at: http://dx.doi.org/10.1016/j.jsg.2008.06.010.

Roznovsky, T.A. & Aydin, A., 2001. Concentration of shearing deformation related to changes in strike of monoclinal fold axes : the Waterpocket monocline , Utah. , 23, pp.1567–1579.

Schultz, R.A. & Siddharthan, R., 2005. A general framework for the occurrence and faulting of deformation bands in porous granular rocks. , 411, pp.1–18.

Schultz, R.A., 1996. Relative scale and the strength and deformability of rock masses. *Journal of Structural Geology*, 18(9), pp.1139–1149.

Underhill, J.R. & Woodcock, N.H., 1987. Faulting mechanisms in high-porosity sandstones; New Red Sandstone, Arran, Scotland. *Geological Society, London, Special Publications*, 29(1), pp.91–105. Available at: http://sp.lyellcollection.org/cgi/doi/10.1144/GSL.SP.1987.029.01.09.

Williams, F., Chronic, L. & Chronic, H., 2014. *Roadside Geology of Utah* 2nd Ed., Mountain Press Publishing Company.

Zuluaga, L.F., Fossen, H. & Rotevatn, A., 2014. Progressive evolution of deformation band populations during laramide fault-propagation folding: Navajo Sandstone, san rafael monocline, Utah, U.S.A. *Journal of Structural Geology*, 68(PA), pp.66–81. Available at: http://dx.doi.org/10.1016/j.jsg.2014.09.008.

University of Utah, 2010: (online)

sed.utah.edu/Carmel.htm

sed.utah.edu/Geology.htm

sed.utah.edu/Moenkopi.htm

sed.utah.edu/Chinle.htm

sed.utah.edu/Wingate.htm

nps.gov/colm/learn/nature/wingate-sandstone.htm

sed.utah.edu/Kayenta.htm

sed.utah.edu/WhiteRim.htm

sed.utah.edu/Kaibab.htm

Hintze, L, 1997, Utah Geologic Highway Map

9. Appendices

9.1 Appendix 1

Locality: Mine Canyon, Utah, USA
Scale: Measurements each meter (1:100)
Geologist(s): Tonje Nygaard Sørensen with assistance from Emil Hagen-Kristiansen
Formation: Mainly Navajo, but also Kayenta and Page
Age: Jurassic
Meters: Total amount of meters are 186

Table 9.1: Total amount of deformation bands recorded during the fieldwork for this study.

	Deformation bands divided by populations					
Meters	*Popul. 1*	*Popul. 2*	*Popul. 3*	*Popul. 4*	*Popul. 5*	*Total*
0-1	1		2		1	4
1-2	12	11	1		1	25
2-3	27		18			45
3-4	18	4	11			33
4-5	3	2				5
5-6	7					7
6-7	3	3				6
7-8	2					2
8-9	1	2	5			8
9-10	2	2	15			19
10-11	6	2	9			17
11-12	8	2	4			14
12-13		2	2			4
13-14	4	1	3			8
14-15	14	15	11	1		41
15-16	15	52	25			92
16-17	58	35	37		2	132
17-18	38	37	32			107
18-19	9	18	15			42
19-20	27	17	16			60
20-21	22	20	15			57
21-22	18	6	8			32
22-23	27	21	14			62
23-24	44	18	23			85
24-25	24	36	44			104
25-26	34	18	14			66
26-27	17	6	27	1		51
27-28	17	29	65			111
28-29	21	19	54			94
29-30	36	20	18	1		75
30-31	15	4	4	1		24
31-32	3	3	3	1		10
32-33	8	1	8			17
33-34	20	6	12	1		39
34-35	10	17	39			66
35-36	15	4	17			36

36-37	8	4	17			29
37-38	10	8	4	1	2	25
38-39	17	8	12	1		38
39-40	18	6	2			26
40-41	6	12	4			22
41-42	8	11	18			37
42-43	10	18	9			37
43-44	9	6	4			19
44-45	2	15	1		1	19
45-46	7	7	4			18
46-47	4	35	11			50
47-48	No outcrops					0
48-49	No outcrops					0
49-50	2	14	6			22
50-51	1	10				11
51-52	7	5	1			13
52-53	3					3
53-54	2	3	2			7
54-55	4	10	1			15
55-56	3					3
56-57	8	32	4			44
57-58	3	10				13
58-59	5	4	3			12
59-60	8	12	3			23
60-61	2	3	3			8
61-62	4	7				11
62-63	11	13	2			26
63-64	14	6	4			24
64-65	7	4	2			13
65-66	7	4				11
66-67	7	11	2			20
67-68	29	9	2			40
68-69	11	5	7			23
69-70	8	4	1			13
70-71	3	3	2			8
71-72	3	4	2			9
72-73	5	17				22
73-74	11	6	2			19
74-75	5	4				9
75-76	14	7				21
76-77	38	19				57
77-78	29	26				55
78-79	11	2				13
79-80	18	6				24
80-81	3	33				36
81-82	1	53				54
82-83	8	72	2			82
83-84	3	75	1			79
84-85	1	35	1			37
85-86	1	33	1			35
86-87	4	64	1			69
87-88	9	65				74
88-89	3	35	1			39

89-90		21	8			29
90-91	2	15	3			20
91-92	3	31	1			35
92-93	1	16	14			31
93-94	12	35	25			72
94-95	51		8			59
95-96	91	6	5			102
96-97	34	13	9			56
97-98	35	11	7			53
98-99	44	32	39			115
99-100	30		4			34
100-101	37	14				51
101-102	15	4	1			20
102-103	14	4	2			20
103-104	14	18	3			35
104-105	25	16				41
105-106	17	15				32
106-107	12	17	18			47
107-108	31	11	14			56
108-109	50	14	1			65
109-110	48	18	6			72
110-111	21	5	7			33
111-112	11	5	7			23
112-113	11	13	3			27
113-114	25	15				40
114-115	11	20	18			49
115-116	32	9	8			49
116-117	31	13	5			49
117-118	101	13	1			115
118-119	38	6	1			45
119-120	115	24				139
120-121	37	9				46
121-122	11		14			25
122-123	43	6				49
123-124	70	15				85
124-125	34	13				47
125-126	48	14	4			66
126-127	35	7	1			43
127-128	53	7	1			61
128-129	26	7				33
129-130	23	7				30
130-131	21	4	11			36
131-132	19	13	14			46
132-133	55	23	11			89
133-134	18	6	1			25
134-135	23	6	7			36
135-136	16	9	2			27
136-137	7	1	1			9
137-138	3	4				7
138-139	10	6	2			18
139-140	3					3
140-141	4	1				5
141-142		3				3

142-143		3				3
143-144		7	1			8
144-145	10					10
145-146	6	7				13
146-147	10					10
147-148	5					5
148-149	6					6
149-150	5	1				6
150-151	10	1	2			13
151-152	17	3	3			23
152-153	28	2				30
153-154	12	8	4			24
154-155	5	12	3			20
155-156	16	1	1			18
156-157	12		2			14
157-158	25		2			27
158-159	20					20
159-160	40	1	2			43
160-161	33	2	1			36
161-162	8		2			10
162-163	10		1			11
163-164	17					17
164-165	6		6			12
165-166	14		1			15
166-167	28		3			31
167-168	14					14
168-169	9					9
169-170	18		1			19
170-171	26	2	4			32
171-172	39		8			47
172-173	5	1	4			10
173-174	14	2	3			19
174-175	35		2			37
175-176	14	5	1			20
176-177	9	1				10
177-178	5	3				8
178-179						0 *slickensides*
179-180	9	7	1			17
180-181	6	2				8
181-182	4					4
182-183	2		2			4
183-184	3	2	1			6
184-185		7				7
185-186	7	3	1			11
Total:	3084	1966	1062	8	7	6127
Percent:	*50,34 %*	*32,09 %*	*17,33 %*	*0,13 %*	*0,11 %*	*100 %*